TABLE OF CONTENTS

Page

LIST OF TABLES

Page

LIST OF FIGURES

Page

LIST OF ABREVIATIONS

ATC	Applied technology council
C1L	Concrete moment frame low rise
CSM	Capacity spectrum method
DCM	Displacement coefficient method
DF	Damage factor
DS	Damage state
ELER	Earthquake loss estimation routine
ESDOF	Equivalent single degree of freedom
GMPE	Ground motion prediction equation
HAZUS	Hazards United States loss estimation method
IM	Intensity measure
MDF	Mean damage factor
MDOF	Multi-degree of freedom
NLSA	Nonlinear static analysis
NLTHA	Nonlinear time history analysis
PGA	Peak ground acceleration
S1L	Steel moment frame low rise
S2L	Steel braced frames low rise
S5L	Steel frames with URM infill low rise
URM	Unreinforced masonry
URMB	Unreinforced brick masonry
URMS	Unreinforced stone masonry
W1L	Wood light frame low rise
UHS	Uniform hazard spectrum
NBCC	National building code of Canada

LIST OF SYMBOLS

S_d	Spectral displacement
S_a	Spectral acceleration
S_{ay}	Spectral acceleration at the yield point of a capacity curve
k	Degradation factor
λ	Median value
β	Log-Standard deviation
λ_{ds}	Median value for a specific damage state
β_{ds}	Logarithmic standard deviation of a specific damage state
Φ	Cumulative standard normal distribution function
ξ_e	Elastic damping ratio
ξ_{eff}	Effective damping ratio
H	Total height of the building
h_s	Height of the first story
V_r	Shear strength corresponding to the flexural rocking failure
V_{dt}	Shear strength corresponding to diagonal cracking failure
L	Masonry wall length
t	Masonry wall thickness
T	Period of vibration
T_y	Yield period of vibration
θ	Inter-story drift
θ_{DS}	Inter-story drift at the threshold of a specific damage state
Δ	Displacement at the top of a wall
EI_{eff}	Effective flexural stiffness
GA_{eff}	Effective shear stiffness
f_m	Masonry compression strength
f_{dt}	Masonry shear strength corresponding to diagonal cracking
E_m	Masonry elastic modulus
G_m	Masonry shear modulus
Γ	Modal participation factor

M	Earthquake scenario magnitude
R	Earthquake scenario epicentral distance
F_a	Soil-site amplification factor for the constant-acceleration portion
F_v	Soil-site amplification factor for the constant-velocity portion
R_A	Damping reduction factor for damping ratios more than 5% for constant-acceleration portion
R_V	Damping reduction factor for damping ratios more than 5% for constant-velocity portion
T_{AVD}	The period at the intersection of the constant-acceleration and constant-velocity portions of the demand spectrum
g	Gravitational acceleration

INTRODUCTION

Context

Earthquakes represent a major natural hazard that regularly impact the built environment in seismic prone areas worldwide and cause social and economic losses. Recent earthquakes, e.g., 2009 L'Aquila earthquake in Italy and 2010 Christchurch earthquake in New Zealand, showed that most of the damage and economic losses are related to old vulnerable masonry buildings (Ingham and Griffith, 2011). The high losses incurred due to destructive earthquakes promoted the need for assessment of the performance of existing buildings under potential future earthquake events. This requires improved seismic vulnerability and risk assessment tools to assist informed decision making with the objective to minimize potential risks and to develop emergency response and recovery strategies.

In Eastern Canada, most of the existing buildings were constructed before the introduction of the seismic provisions in building codes. In particular, pre-code masonry buildings types are predominant in dense urban centers such as Quebec City and Montreal in the Province of Quebec. The potential economic and social losses due to strong earthquake events can thus be extensive. On the other hand, although masonry buildings represent major and most vulnerable part of the existing building stock, less research was devoted to study the seismic vulnerability of this type of buildings compared to other structural types, e.g. reinforced concrete and steel buildings.

Typical regional seismic risk assessment studies consist of three major components: hazard, exposure, and vulnerability of the exposure with respect to the seismic hazard (Coburn and Spence, 2002). Seismic hazard defines the intensity of the expected earthquake motion at a particular location over a given time period; exposure identifies the built environment (buildings and infrastructures) in the area affected by the earthquake; and vulnerability refers to the exposure susceptibility to earthquake impacts defined by the expected degree of damage and loss that would result under different levels of seismic loading. The key among

these components is the vulnerability modelling. The vulnerability is typically presented with sets of fragility functions describing the expected physical damage whereas economic losses are given by vulnerability functions (Porter, 2002). The typical results of risk assessment comprise estimates of the potential physical damage and direct economic losses.

Problem statement

Many historic buildings in the old urban centers in Eastern Canada such as Old Quebec City are built of stone masonry and represent un-measurable architectural and cultural heritage. These buildings were built to resist gravity loads only and generally offer poor resistance to lateral seismic loads. Damage to stone masonry buildings from past earthquakes around the world is generally attributed to inadequate structural integrity and resistance which results in typical shear cracking and disintegration of stone walls and their partial or total collapse (Tomaževic and Lutman, 2007). The high seismic risk related to stone masonry buildings is even more aggravated due to their location in densely populated urban centers in a way that the consequences of failure of these structures tend to be severe with regards to human casualties, damage and economic losses (Chidiac et al., 2000). Seismic risk assessment of stone masonry buildings is therefore the first necessary step in developing seismic retrofitting and pre-disaster mitigation plans.

Recent developments in seismic risk assessment identified the vulnerability modelling as a key component in regional seismic risk assessment (Coburn and Spence, 2002). Performed over a large population of structures with similar characteristics such as material, structural type, height, it leads to the estimation of earthquake damage within a specified geographical area.

Existing vulnerability modelling methods rely on damage data derived from post-earthquake surveys, expert opinion, analytical simulations of structural models, or combinations of these respectively (Jeong and Elnashai, 2006). In regions with high seismicity, such as Western United States, the considerable amount of strong ground motion and respective damage

records have been used to build observational and expert opinion based vulnerability modelling tools. In regions with scarcity of recorded damage data, such as Eastern Canada, risk assessment relies mainly on analytical vulnerability modelling. The analytical methods consist of structural modeling and evaluation of the likelihood for a given building to experience damage from earthquake of a given intensity.

Existing analytical vulnerability models for unreinforced masonry structures were focused on brick masonry buildings due to availability of experimental data and mechanical models. Currently, the most widely used North American regional seismic risk assessment tool, Hazus (FEMA, 2003), reflects the vulnerability information of the construction types present in the United States. It considers only one structural class for unreinforced masonry buildings (URM), brick masonry structures with vulnerability information based mainly on expert judgment and observational data (Kircher et al., 1997a). It has been shown, however, that Hazus vulnerability model for URM do not adequately represent the response of stone masonry structures to earthquake loading (Lefebvre, 2004; Abo-El-Ezz et al., 2011b). On the other hand, only few analytical vulnerability studies of stone masonry buildings are available in the literature and mainly focused on European building types (Rota et al. 2010; Borzi et al., 2008). The earthquake loss estimation routine ELER (Erdik et al., 2010), which is mainly used in Europe, considers stone masonry buildings with vulnerability information mainly derived based on observed damage data collected from Italian earthquakes and expert judgment (Giovinazzi, 2005).

Another important issue which merits particular attention are the uncertainties related to the various parameters used in the in the vulnerability modelling that may have considerable impact on the risk assessment results. These include: uncertainties due to variability of the ground motions, uncertainties in seismic demand and capacity of structures due to variations of their geometry and material properties, and uncertainties in the definition of the damage states (Choun and Elnashai, 2010). All these uncertainties should be systematically quantified in the vulnerability modelling in order to provide confidence in the estimated risk and identify the model sensitivity to input parameters.

Objectives and methodology

The main objective of this study is to develop a set of probability-based analytical methods and tools for efficient analysis of seismic vulnerability of stone masonry buildings with systematic treatment of respective uncertainties. The specific objectives are focused on the : (1) development of fragility and vulnerability functions for stone masonry buildings; (2) quantification of the uncertainties in the vulnerability modelling and (3) application of the developed tools for the evaluation of seismic vulnerability and risk assessment study of existing buildings including stone masonry buildings in Old Quebec City.

The methodology applied to achieve the above objectives comprises the following steps:

1) inventory and characterisation of existing stone masonry building in Old Quebec City;
2) identification of a probabilistic framework for the development of capacity curves and displacement based fragility functions for stone masonry buildings;
3) development of a framework for generation of seismic hazard compatible fragility and vulnerability functions for stone masonry buildings in Quebec City in terms of a structure-independent intensity measure (e.g. spectral acceleration at specific period);
4) sensitivity analysis of the seismic vulnerability to major input parameters for stone masonry buildings;
5) application of developed methodology for vulnerability modelling to other buildings types present in Old Quebec City;
6) application of the developed methodology through a scenario based seismic risk assessment of existing building in Old Quebec City.

Thesis originality and contributions

The main original contribution of this thesis is the development of a simplified analytical methodology for vulnerability modelling of stone masonry building with systematic treatment of uncertainties which can be adapted to other building types. The application of the methodology resulted in the following contributions:

1) development of sets of capacity curves and displacement fragility functions for stone masonry buildings. These functions represent effective tools for rational seismic vulnerability assessment of stone masonry buildings through consideration of their nonlinear deformation behaviour;

2) development of sets of hazard compatible fragility functions for stone masonry buildings and representative building classes of existing buildings inventory in Old Quebec City susceptible to Eastern Canada ground motions. These functions can be directly integrated with seismic hazard analysis output typically presented in terms of a structure-independent intensity measure. These functions are effective for conducting rapid regional scale vulnerability assessment of building classes to estimate potential damage for a given earthquake scenario. The probabilistic framework for these functions allows identification and quantification of significant uncertain parameters affecting vulnerability assessment;

3) development of a seismic damage assessment scenario for existing buildings in Old Quebec City. This scenario includes ground motion input that is compatible with the seismo-tectonic settings of the study region and fragility functions specific for the building classes in the inventory. The results of this scenario provide a quantitative evaluation of the seismic risk that serves the decision making process for risk reduction strategies and planning.

The thesis contributions have been presented in the following scientific publications:

Journal articles:

1) Abo-El-Ezz A., Nollet M.J, and Nastev M. 2013a. « Seismic fragility assessment of low-rise stone masonry buildings ». Accepted for publication in the *Journal of Earthquake Engineering and Engineering Vibrations*, Vol.12 No.1, 2013;

2) Abo-El-Ezz A., Nollet M.J, and Nastev M. 2012a. « Seismic hazard compatible vulnerability modelling: method development and application». *Manuscript submitted to the Journal of Earthquakes and Structures.*

Conference proceedings articles:

1) Abo-El-Ezz A., Nollet M.J, and Nastev M. 2011a. « Analytical displacement-based seismic fragility analysis of stone masonry buildings». *Proceedings of the 3rd International Conference on Computational Methods in Structural Dynamics and Earthquake Engineering*, Corfu, Greece, Paper No.679;

2) Abo-El-Ezz A., Nollet M.J, and Nastev M. 2011b. « Characterization of historic stone masonry buildings for seismic risk assessment: a case study at Old Quebec City ». *Proceedings of the Canadian Society of Civil Engineering General Conference*, Ottawa, Canada, Paper No. GC-223;

3) Abo-El-Ezz A., Nollet M.J, and Nastev M. 2012b. « Development of seismic hazard compatible vulnerability functions for stone masonry buildings». *Proceedings of the Canadian Society of Civil Engineering 3rd Structural Specialty Conference*, Edmonton, Canada, Paper No. STR-1030;

4) Abo-El-Ezz A., Nollet M.J, and Nastev M. 2012c. « Regional seismic risk assessment of existing building at Old Quebec City, Canada ». *Proceedings of the 15th World Conference on Earthquake Engineering*, Lisbon, Portugal, Paper No. 1543;

5) Abo-El-Ezz A., Nollet M.J, and Nastev M. 2013b. « A methodology for rapid earthquake damage assessment of existing buildings ». *Submitted to the 3rd Specialty Conference on Disaster Prevention and Mitigation, Canadian Society of Civil Engineering*, Montreal, Paper No. DIS-16.

Thesis organization

Chapter 1 presents a literature review of seismic fragility and vulnerability functions and regional scale seismic vulnerability modelling components with emphasis on masonry buildings including: methods of seismic response and structural analysis of masonry buildings, damage analysis and uncertainty quantification. Chapter 2 gives details of the inventory and the structural characterisation of existing stone masonry buildings in Old Quebec City. It also introduces the simplified analytical methodology for vulnerability modelling of stone masonry building with systematic treatment of uncertainties and depicts the obtained sets of capacity curves and displacement fragility functions. Chapter 3 details the methodology for the development of seismic hazard compatible fragility and vulnerability functions and its application to stone masonry buildings for different scenario earthquakes. Chapter 4 presents the conducted sensitivity analysis to major input parameters in the seismic vulnerability modelling of stone masonry buildings. The results of the validation of the developed methodology and its application of vulnerability modelling of existing building types in Old Quebec City and respective scenario-based risk assessment are given in Chapter 5. The final chapter of this thesis presents the summary, conclusions and recommendations for future research.

Five Appendices are given at the end of the thesis as follows: Appendix-I presents the displacement based fragility analysis results, Appendix-II presents the detailed computations and a spreadsheet implementation of the procedure presented in Chapter 3 for the development of seismic hazard compatible fragility and vulnerability functions; Appendix-III presents the fragility functions developed for existing building in Old Quebec City that were used to conduct the risk scenario presented in Chapter 5; Appendix-IV presents the details of the Atkinson and Boore (2006) ground motion prediction equations used in this thesis and Appendix-V presents the details of the comparison of damage estimation using the developed methodology in this thesis and Hazus software.

CHAPTER 1

LITERATURE REVIEW

1.1 Introduction

The physical damage; social and economic losses incurred during the past destructive earthquakes emphasize the need to reasonable prediction of potential risk in seismic prone areas. A standard definition of seismic risk considers a combination of the seismic hazard, exposure, and vulnerability. The seismic hazard is a measure of the probability of a given intensity of earthquake shaking at the studied location over a given time period; exposure refers to elements at risk, i.e, built environment in that area; and vulnerability introduces the susceptibility to earthquake impacts, generally defined by the potential for damage and subsequent economic loss as result of intensity of seismic loading. Vulnerability modelling is the key element within the general seismic risk framework. The physical damage is generally represented through a set of *fragility functions* assigned to given damage state (Coburn and Spence, 2002), whereas economic losses are defined with *vulnerability functions* (Porter, 2002). These functions are commonly given in terms of a structure independent intensity measure (e.g. peak ground acceleration, PGA or spectral acceleration at a particular period). The outputs of vulnerability modelling are estimates of the potential physical damage and direct economic losses (Figure 1.1). Earthquake induced hazards such as liquefaction and landslides are not considered in this study.

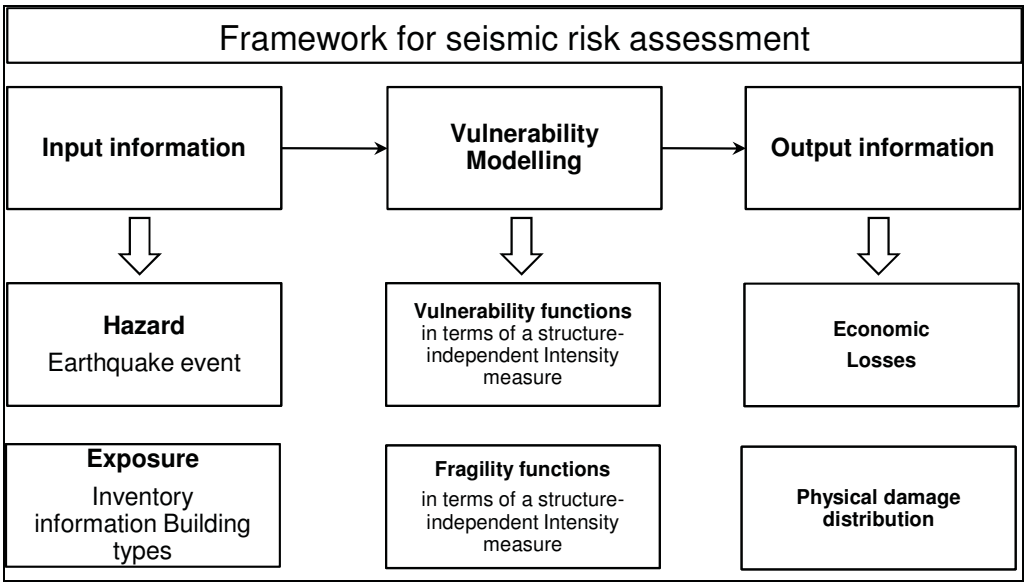

Figure 1.1 Framework for seismic risk assessment.

Vulnerability modelling is usually constrained by limited information and knowledge such that a considerable amount of uncertainties may arise throughout the assessment process (Choun and Elnashai, 2010). The uncertainties are principally of epistemic nature mainly related to the exposure and vulnerability models, whereas both epistemic and aleatory uncertainties are associated with definition of the seismic hazard. The adoption of different input models such as the ground motion models, structural capacity model or repair cost information can potentially have a significant effect on the overall results and conclusions of a risk assessment study (Padgett et al., 2010). Thus, regardless of the methodology employed, one of the most important aspects in development of a seismic vulnerability model is to identify, quantify and incorporate the uncertainties associated with each of the input parameter (Crowley et al., 2005).

In the following sections, seismic vulnerability modelling issues are discussed together with major inherent sources of uncertainties. The emphasis is given to modelling approaches for masonry buildings.

1.2 Fragility and vulnerability functions

It is important to distinguish here between the two following terms related to seismic damageability, fragility functions and vulnerability functions (Porter, 2002). A seismic fragility function defines the probability of some undesirable event or physical damage (e.g., collapse) to take place as a function of an intensity measure, generally structure-independent; e.g. peak ground acceleration, PGA or spectral acceleration at particular period, Sa0.3sec (Figure 1.2a). A seismic vulnerability function defines the economic loss; the damage factor defined as repair to replacement cost ratio; as a function of a structure independent intensity measure (Figure 1.2b). For example, a fragility function can provide the probability that a building will collapse given some level of shaking. Analogous vulnerability functions would provide the damage factor (in terms of repair to replacement cost ratio) for the building given the shaking intensity.

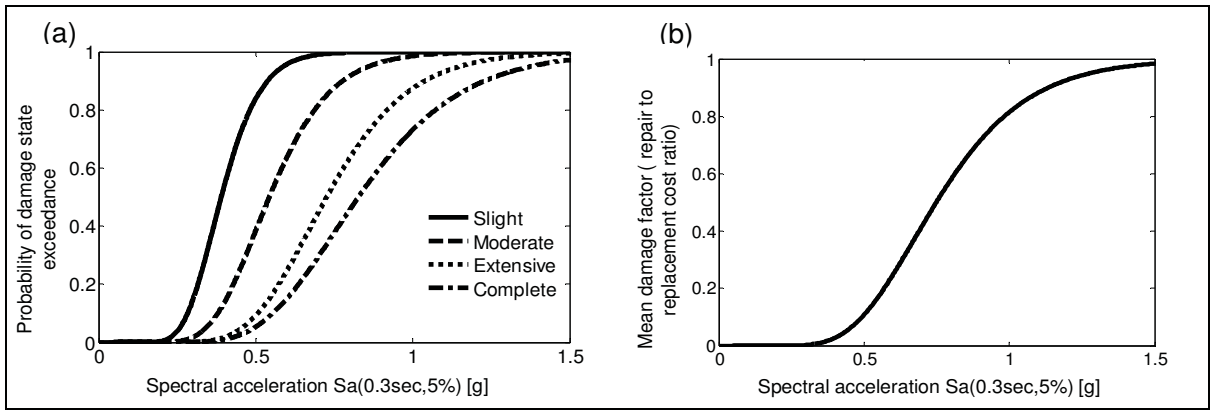

Figure 1.2 Damageability functions: (a) sample fragility functions and (b) vulnerability function.

Besides being defined as functions of the input seismic shaking intensity, the fragility functions can also be conditioned on a structural response parameter (e.g. roof displacement converted to spectral displacement or the inter-storey drift ratio) (Kircher et al. 1997a). In this case they are defined as a displacement fragility function. These fragility functions are an essential component in the seismic vulnerability modelling where displacements are used as a

measure of the extent of seismic induced damage. This type of functions is discussed in more details in the subsequent sections.

Fragility and vulnerability functions can be obtained from empirical, expert opinion, analytical models or any combinations of these models (hybrid approach) (Rossetto and Elnashai, 2005). Whatever the method used to predict the seismic damageability, they all contain uncertainties in the assessment procedures and data used. They include measurement uncertainty related to the observations, inconsistency in the quality of the analysis and database, variability of the ground motion, uncertainty in the judgment of experts, uncertainty due to simplification of models for the strength and stiffness of structural materials and components, uncertainties in seismic demand and capacity of structures due to variations of their geometry and material properties, and uncertainty in the definition of the damage states.

Because of the scarcity of observational damage data in regions of moderate seismicity such as Eastern Canada and the subjectivity of judgmental damage data, recent vulnerability modelling is focused mainly on analytical methods. Analytical methods rely on structural modelling and analytical evaluation of the likelihood of damage by earthquakes of a given intensity, as well as on consideration of uncertainty relative to ground motion and structural parameters. Analytical methods; however, require significant computational effort and generally there are some choices in each component of the methodology. The components of analytical modelling are discussed in detail in the next sections.

1.3 Analytical vulnerability modelling and uncertainty quantification

Analytical approaches for generating fragility and vulnerability functions for a particular building class comprise four general steps: hazard analysis, structural analysis, damage analysis and loss analysis (Porter, 2002) (Figure 1.3). The building class is established in accordance with similarities in the structural system; height and material of construction. A structural analysis is performed on a structural model built for that building class to estimate the structural response to the input ground motion corresponding to various levels of

intensity obtained from the hazard analysis. The results are given in terms of displacements that are considered generally as a good indicator of damage.

The structural displacement response is used as input to a set of displacement fragility functions to determine the probability of being in respective damage states. Finally, the cost of damage is obtained as a sum of the obtained probabilities to determine the total loss. To create a seismic fragility and vulnerability function, the process is repeated for many levels of earthquake intensity. Detailed discussion on these steps is given in the subsequent sections.

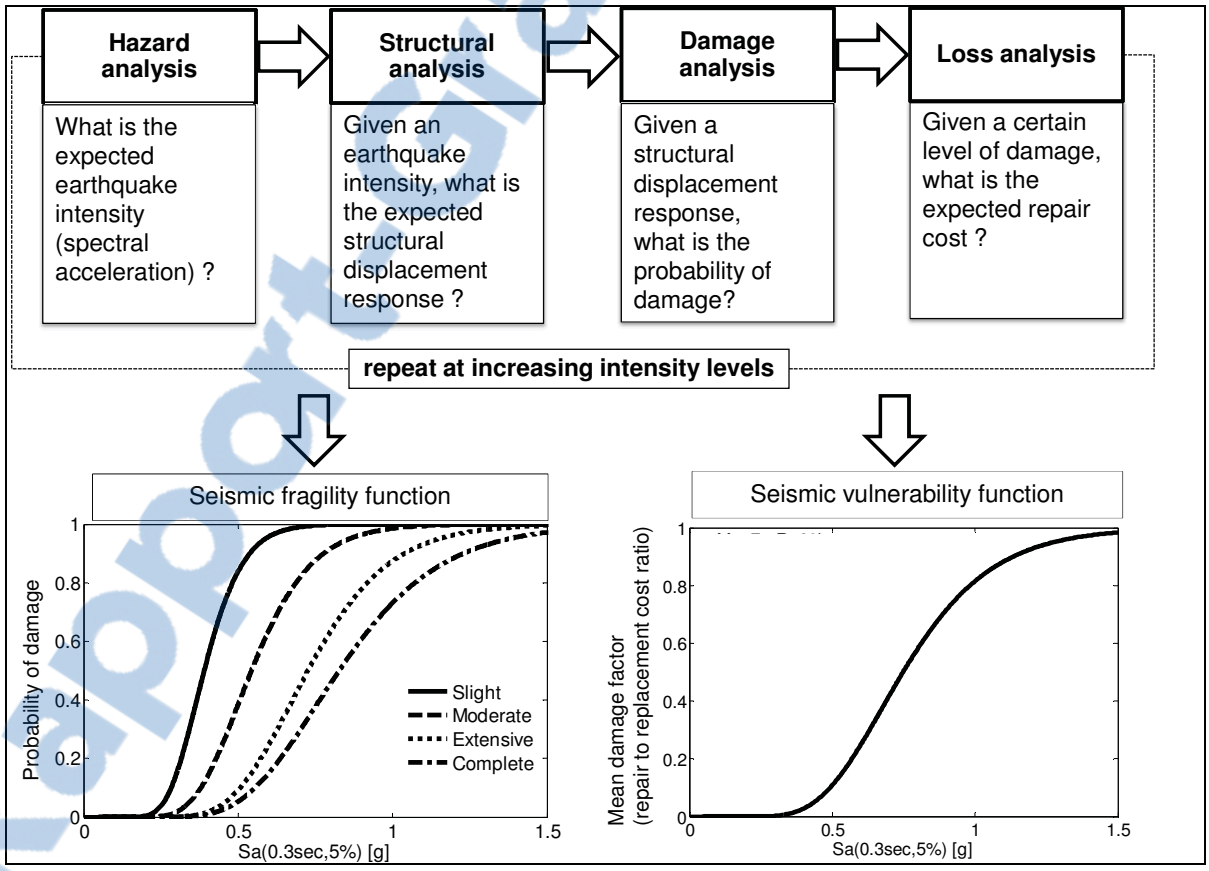

Figure 1.3 Framework for analytical vulnerability modelling.

It should be noted that representing fragility and vulnerability functions in terms of a structure-independent intensity measure provides rapid assessment of damage and losses in the framework of regional scale risk assessment for several classes of buildings with reduced computational time. This is related to the fact that fragility functions can be directly used with the seismic hazard output, typically presented in terms of a structure-independent intensity measure.

There are many different approaches associated to each step of the analytical vulnerability modelling. The ground motion, for example, can be characterized in terms of response spectra or in terms of acceleration time histories. The nonlinear structural analysis can either be static or dynamic; it can be performed including an equivalent single degree of freedom (ESDOF) or a multi-degree of freedom system (MDOF). The damage analysis can either be based on global structural displacement or local inter-storey drift demands. As mentioned in the introductory part, each of the steps involves uncertainty. The major sources of uncertainties in the vulnerability modelling are related: details of the ground motion for a given intensity level, structural properties such as damping, and force-deformation behaviour, damage state definition and repair costs conditioned on damage. A good vulnerability modelling practice should address the important sources of uncertainty.

The input structural parameters to an analytical vulnerability model depend on the selected structural analysis method. For example, if a nonlinear static analysis method is selected, a capacity curve, describing the nonlinear force-deformation characteristics for the considered ESDOF approximation of the building, should be provided along with a set of displacement fragility functions in terms of spectral displacement response (Figure 1.4). This approach is adopted in the vulnerability model of the North American loss estimation tool Hazus (FEMA, 2003) and the European Earthquake Loss Estimation Routine ELER (Erdik et al., 2010). If a nonlinear dynamic analysis is selected, a MDOF model of the structure should be provided along with an inter-storey drift response fragility functions (Porter, 2002) (Figure 1.5).

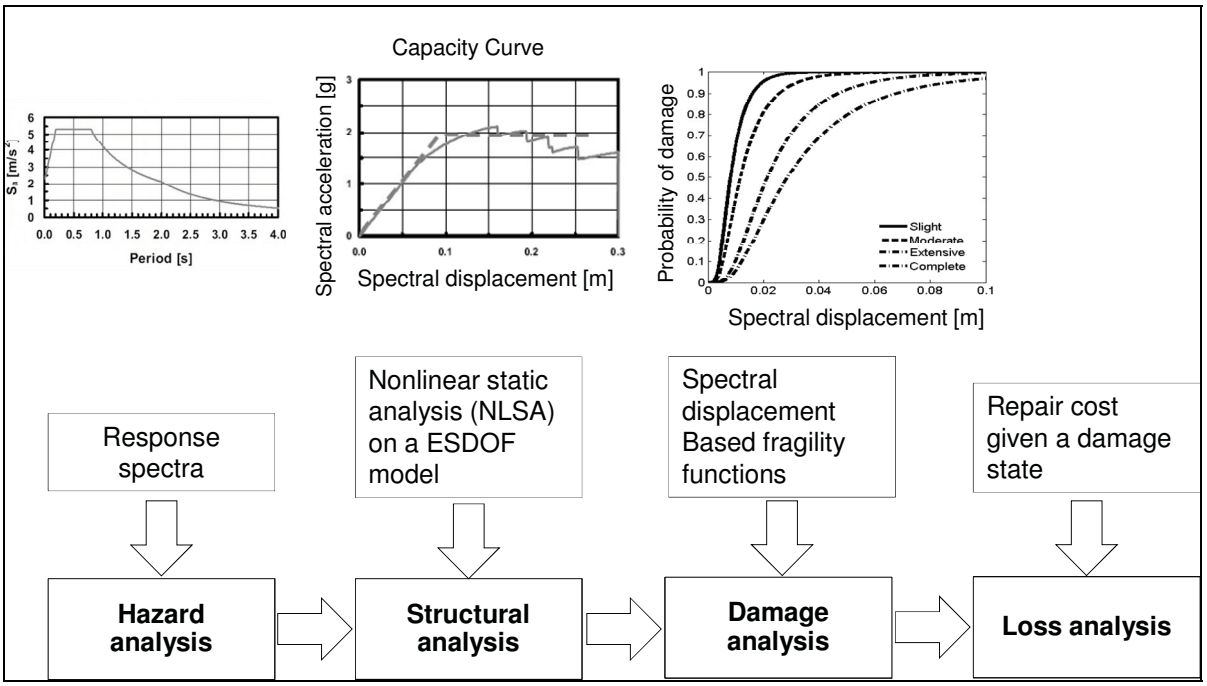

Figure 1.4 Illustration of the required input parameters for nonlinear static structural analysis method.

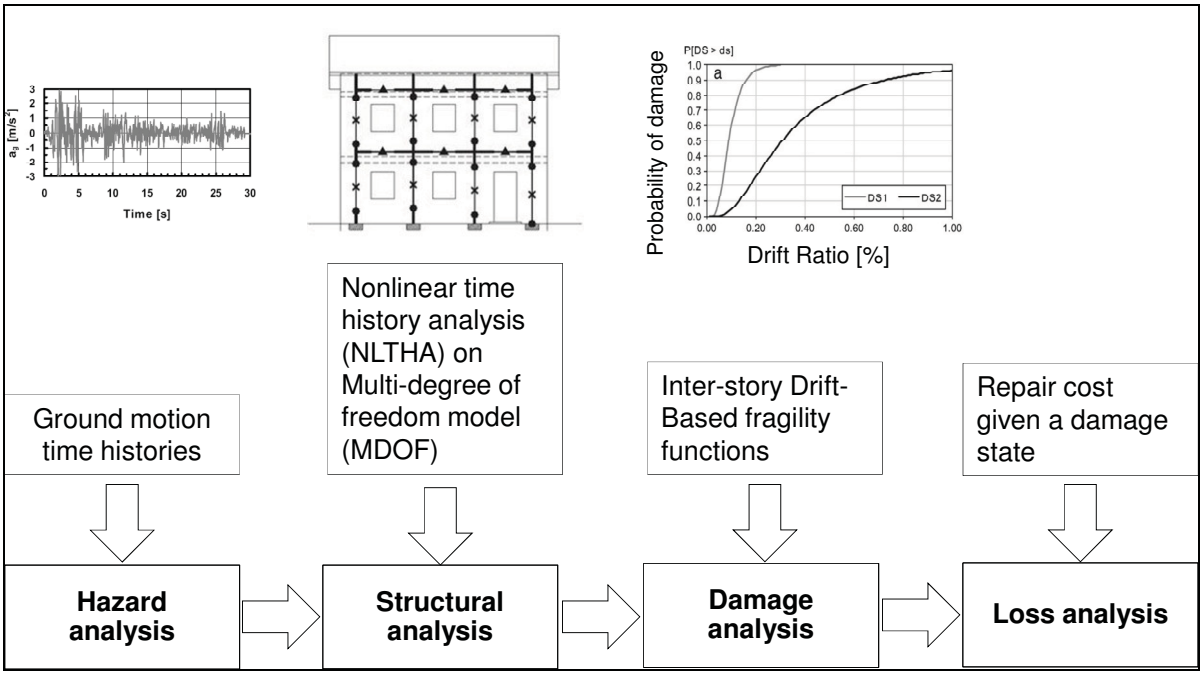

Figure 1.5 Illustration of required input parameters for nonlinear dynamic structural analysis method.

1.4 Structural analysis

The objective of the structural analysis is to obtain the response of the structure for increasing levels of ground motion intensity. The structural analysis stage requires the selection of two inputs: (a) the structural analysis method for seismic demand and (2) the structural model that describe the seismic capacity of the building.

The most commonly used structural seismic demand methods in analytical vulnerability models are: the nonlinear time history dynamic analysis method (NLTHA) applied either on an ESDOF (Akkar et al., 2005; Jeong and Elnashai, 2007) or on a MDOF (Erbrick and Elnashai, 2004; Rota et al., 2010) and the nonlinear static analysis method (NLSA) (Kircher et al., 1997a; Rossetto and Elnashai, 2005; Borzi et al., 2008).

The NLTHA method requires detailed knowledge of the structure and the ground motion. Time-history analyses consist of a step-by-step calculation of the structural response in time domain. All aspects of the ground motion that influence the damage are accounted for through the direct use of acceleration time history records as input. Material nonlinearities of a MDOF system are integrated into the analysis for accurate presentation of the structural properties and increased confidence in the damage evaluations. However, a large number of analyses are required to account for possible uncertainties of the structural capacity under increased levels of seismic demand which makes the method more computationally intensive. In order to reduce the computational effort, ESDOF systems are considered to estimate global displacements only.

To reduce further the computational effort for structural analysis, NLSA methods are used. NLSA methods are often employed for their ability to provide displacement predictions with less computational demand and with reasonable accuracy. The basic concept behind the NLSA is the implicit estimation of the seismic demand to which the structure is exposed using equivalent properties of the structure (e.g. strength, stiffness and deformation capacity). The two basic components of the NLSA are the capacity curve and the input response spectra representing the seismic demand from the hazard analysis.

NLSA requires less computational time and effort than the NLTHA, which offers a considerable advantage in vulnerability modelling of populations of buildings. The most commonly used NLSA methods in vulnerability modelling are the capacity spectrum method (CSM) (Mahaney et al., 1993; ATC 40, 1996) which is the structural analysis method in Hazus (FEMA, 2003) and ELER (Erdik et al., 2010) and the displacement coefficient method (DCM) presented in FEMA356 (FEMA, 2000); FEMA440 (FEMA, 2005) and ASCE-41 (ASCE, 2007).

CSM is based on equivalent linearization approach in which the maximum displacement of a SDOF system can be estimated by the elastic response of a system with increased effective period and damping than the original. The CSM assumes that the equivalent damping of the system is proportional to the area enclosed by the capacity curve (Figure 1.6). The equivalent period is assumed to be the secant period at which the seismic demand, reduced by the additional damping due to the nonlinear response, intersects the capacity curve. Since the equivalent period and damping are both functions of the displacement, the solution to determine the maximum inelastic displacement (i.e., performance point) is iterative. Another version of the CSM is proposed in FEMA440 (FEMA, 2005) in which the equivalent period of the equivalent linear system is obtained from equivalent stiffness that lies between the initial stiffness and the secant stiffness of the inelastic system. The equivalent period and equivalent damping were derived from SDOF systems subjected to a series of earthquake records by finding the optimal pair of equivalent period and equivalent damping that minimizes the error between the response of the equivalent linear system and the actual response of the inelastic system. Another variant of the CSM method is based on the inelastic response spectrum instead of the over damped response spectrum of an equivalent linear system (Chopra and Goel, 1999; Fajfar, 1999). According to this method, the elastic response spectrum is modified using a reduction factor (R_μ) that is a function of the ductility (μ) demand and the period of the elastic system (T), typically defined as R_μ-μ-T relationships.

The DCM is a displacement modification procedure which estimates the total maximum displacement of the system by multiplying the elastic response based on the initial linear properties and damping, by a series of coefficients C_1 and C_2 to generate an estimate of the

inelastic displacement response of the nonlinear system (Figure 1.7). The coefficients are typically derived empirically from series of nonlinear response history analyses on systems with varying periods and strengths. More detailed discussion and evaluation of NLSA methods can be found in (Chopra and Goel, 1999; Powell, 2006; FEMA, 2005; Goel, 2011).

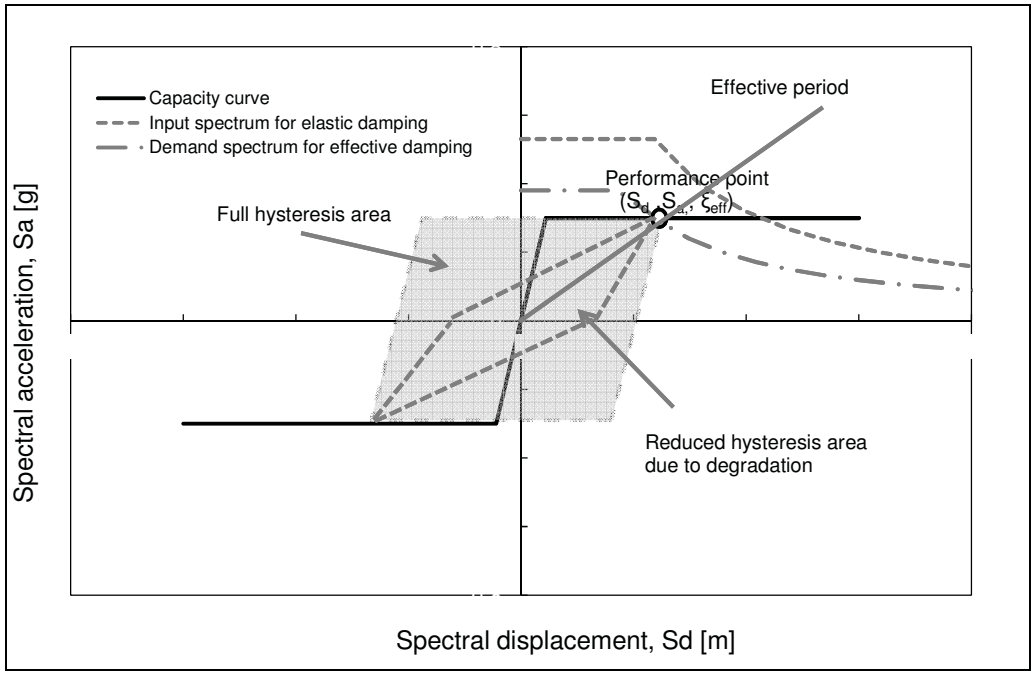

Figure 1.6 Illustration of the capacity spectrum method.

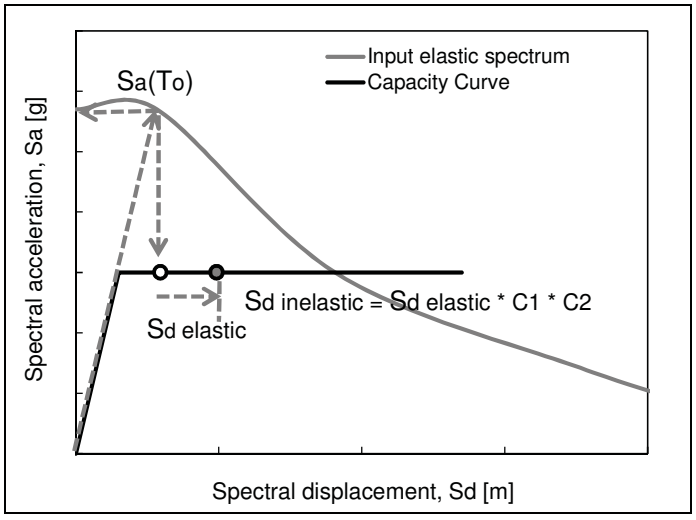

Figure 1.7 Illustration of the displacement coefficient method.

1.5 Structural modelling of seismic capacity for masonry buildings

Several modelling approaches have been proposed for modelling of seismic capacity of masonry buildings within the framework of vulnerability modelling. The objective of the structural modelling is to produce the seismic resistance parameters for the MDOF or the ESDOF such as the strength, stiffness, deformation capacity. These parameters are used as an input to the structural demand analysis according to one of the method presented earlier. The typical output of the structural modelling is the capacity curve that describes the lateral force-deformation resistance of the building. This section starts with a review of the mechanisms of seismic response of masonry buildings followed by the different modelling approaches for the development of capacity curves.

1.5.1 Seismic response mechanisms of masonry buildings

Masonry buildings are composed of vertical walls that resist gravity loads and horizontal elements (diaphragms) that distribute the gravity loads to the walls and transfer the inertial seismic lateral forces to the walls. Typically, masonry buildings exhibit a three dimensional response behaviour under earthquake ground motion effects. The basic mechanisms that a masonry building exhibits under dynamic seismic loads are generally divided into in-plane and out-of-plane mechanisms. The three dimensional response of the building comprises an interaction between those two mechanisms. However, due to the inherent difficulties in the investigation of such complex interaction, the distinction of the two basic mechanisms is commonly drawn to simplify the problem.

The in-plane walls are referred to the walls that are parallel to the dominant direction of ground shaking. Due to their orientation, these walls provide the lateral load resistance of the building and undergo in-plane deformation and stresses. In-plane walls are typically perforated with windows and doors openings. Observation of seismic damage to masonry walls, as well as of laboratory tests, showed that masonry walls subjected to in-plane loading may have typical types of behaviours associated with different failure modes, flexural and shear failures or combination of both (Calderini et al., 2009) (Figure 1.8).

The flexural failure (Figure 1.8a) occurs when the horizontal load produces tensile flexural cracking at the corners and the wall begins to behave as a nearly rigid body rotating about the toe and with progressively increasing cracks oriented towards the more compressed corners (crushing). The diagonal shear failure (Figure 1.8b) is typically characterized by the formation of a diagonal crack, which usually develops at the centre of the wall and then propagates towards the corners. The crack progresses generally through the mortar joints in the case of a regular masonry pattern, but it can also go through the blocks. Another failure mode that may occur is the sliding shear failure (Figure 1.8c), where failure is attained with sliding on a horizontal bed joint plane, usually located at one of the extremities of the wall. However, this failure is only possible for very squat walls. The most commonly observed in-plane failure mechanism from post-earthquake damage surveys is the diagonal cracking shear failure especially in old brick and stone masonry building (Figure 1.9; Tomazevic, 1999; Lutman and Tomazevic; 2002).

The occurrence of different failure modes depends on several parameters: geometry of the wall; boundary conditions; acting axial load; mechanical characteristics of the masonry constituents (compression and shear strength of masonry); masonry geometrical characteristics (block aspect ratio, masonry pattern). It should be noted that it is not easy to distinguish the occurrence of a specific type of mechanism, since two or more failure mechanisms may occur with interactions between them. Flexural failure tends to prevail in slender walls, while diagonal cracking tends to prevail in moderate slender walls over flexure and bed joint sliding for increasing levels of vertical compression. On the other hand, diagonal cracking propagating through blocks tends to prevail over diagonal cracking propagating through mortar joints for increasing levels of vertical compression and for increasing ratios between mortar and block strengths.

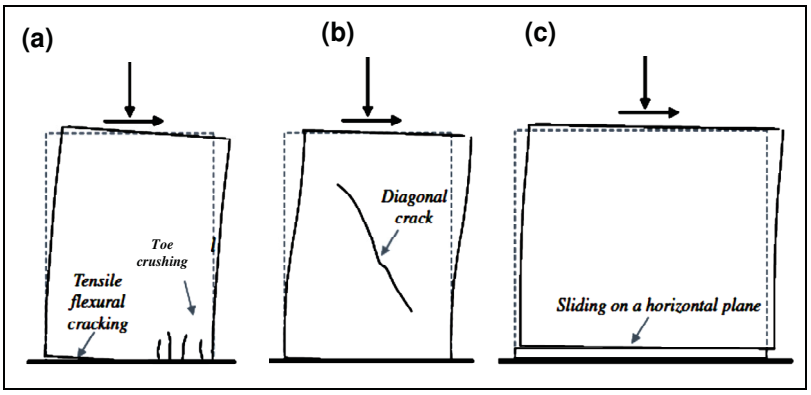

Figure 1.8 In-plane failure mechanisms of masonry walls: (a) flexural failure, (b) diagonal shear failure and (c) sliding shear failure
Taken from Calderini et al. (2009)

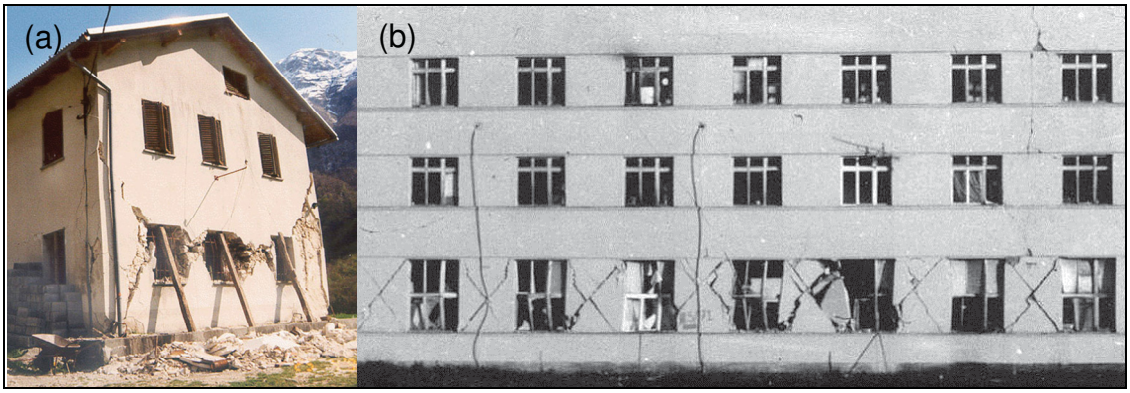

Figure 1.9 Photographs illustrating typical diagonal cracking damage for: (a) a stone masonry buildings and (b) a brick masonry building
Taken from Lutman and Tomazevic (2002)

The force-deformation hysteresis behaviour and the energy dissipation capacity of masonry walls under in-plane cyclic loading are influenced by the failure mechanism. A typical flexural response is shown in Figure 1.10a, where large displacements can be obtained without significant loss in strength, especially when the mean axial load is low compared to the compressive strength of masonry. Limited hysteretic energy dissipation is observed, with negligible strength degradation under load reversals. Figure 1.10b shows typical hysteresis behaviour of walls with diagonal cracking shear mechanism where the response is

characterized by higher energy dissipation compared to rocking mechanisms but by rather rapid strength and stiffness degradation.

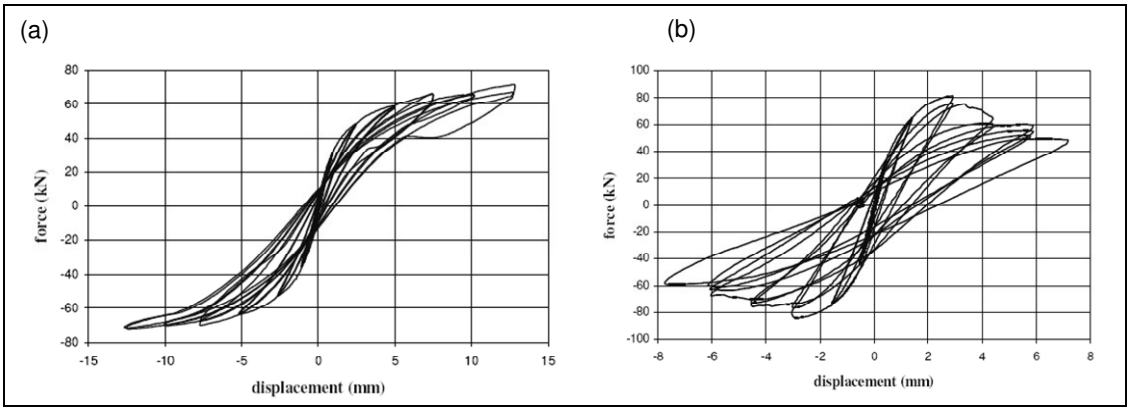

Figure 1.10 Force-deformation hysteresis behaviour of masonry walls: (a) flexural rocking failure mechanism and (b) shear failure mechanism with diagonal cracking
Taken from Magenes and Calvi (1997)

Walls that are perpendicular to the direction of ground shaking are typically vulnerable to the out-of-plane damage. The out-of-plane wall works like a thin plate supported on the edges adjacent to the in-plane walls. The boundary element of the out-of-plane wall is the connections with the floor systems. During an earthquake, the out-of-plane wall vibrates under the seismic force induced by its own mass and the forces transferred from floor and in-plane walls. The vibration and the associated bending deformation may lead to cracking and out-of-plane collapse of the wall.

When not properly connected to floors and in-plane walls, the out-of-plane masonry wall can become unstable and may collapse under out-of-plane vibrations (Bruneau, 1994). However, if the connections between the wall and the floors have sufficient strength, the out-of-plane behaviour is not critical and the seismic response is governed by the in-plane walls (Tomazevic, 1999).

1.5.2 Capacity modelling methods

Analytical methods that are used to predict the seismic capacity of masonry buildings represented by; either a MDOF or an ESDOF system, can be classified into two main categories: simulation-based methods (Rossetto and Elnashai, 2005; Erberik, 2008; Rota et al., 2010) and mechanics-based methods (Oropeza et al., 2010, Lang, 2002, Borzi et al., 2008; Restrepo-Velez, 2003). The simulation based methods uses detailed structural models. The mechanics based methods apply simplified structural mechanics models to develop the strength, stiffness and deformation parameters of the building.

The detailed structural models used in the simulation based methods can be subdivided into: micro-scale models and macro-scale models (Figure 1.11; Calderini et al., 2009). In the micro-scale models, the structure is discretized into finite-elements with inelastic constitutive models at the material level. In the macro-scale models, the structure is discretized into an equivalent frame model with main structural components: masonry piers and spandrels are modelled with force-deformation relationship at the structural member level. The micro-scale models require significantly high computational resources and experience and their use is mainly limited to the prediction of the behaviour of individual structural components (piers or spandrels) and confirmation of the accuracy of the macro-models on the structural level.

The simulation-based methods require detailed knowledge of the inelastic behaviour of the material, large amount of input parameters and consequently longer computational time which would be unsuitable for vulnerability assessment of large number of structures. Therefore, simulation-based methods are commonly limited to vulnerability modelling of a single representative building (Rota et al., 2010).

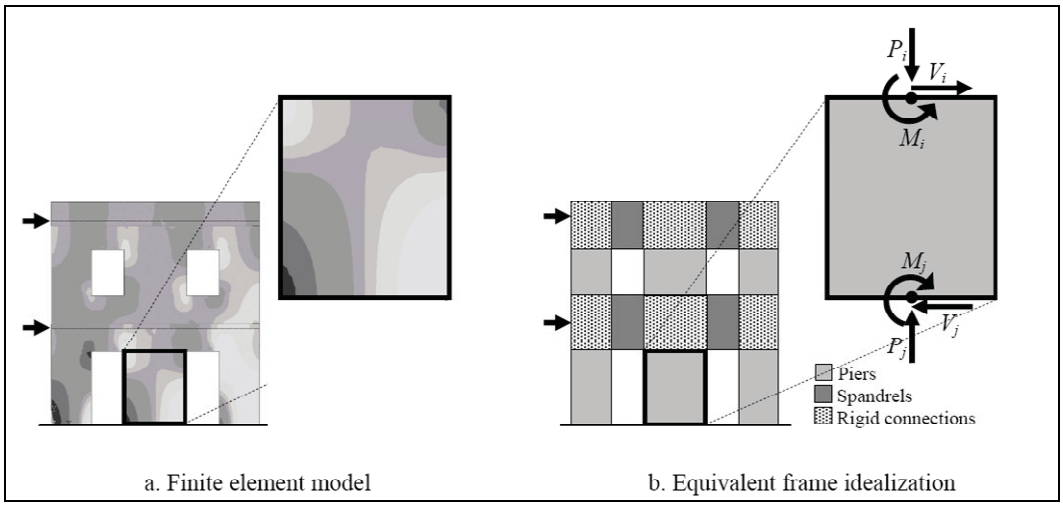

Figure 1.11 Detailed structural models: (a) micro-scale model using finite elements and (b) macro-scale model using the equivalent frame idealization
Taken from Calderini et al. (2009)

The mechanics based methods apply simplified structural mechanics principles to develop the strength, stiffness and deformation parameters of single masonry walls and combine them to produce the capacity curve of the building (Figure 1.12). Tomazevic (1999) and Lang (2002) have shown that the application of simplified mechanical models provided good approximation of the global system capacity when compared with experimental results of shaking table tests conducted on several scaled models of masonry buildings. Such simplification reduces the computation time and more importantly idealizes the system with less number of parameters which is highly desirable when conducting regional scale vulnerability modelling.

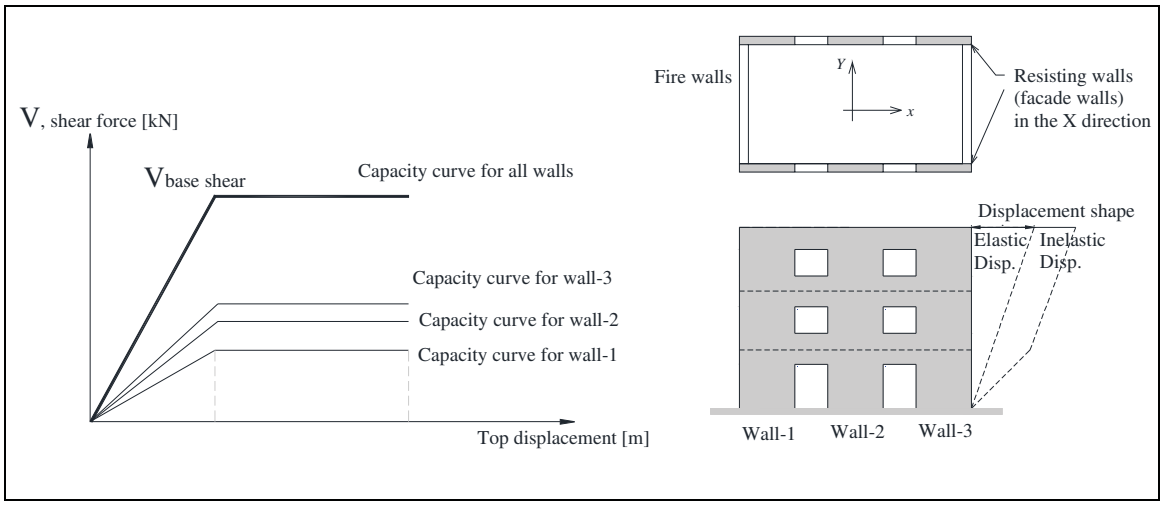

Figure 1.12 Illustration of a capacity curve of a masonry building using mechanics-based models.

The capacity curves developed by either of the methods presented above can be converted to a simplified ESDOF system with global capacity parameters (stiffness, strength and deformation capacity). The ESDOF system is more suitable for seismic demand analysis for population of buildings. This approach has the advantage of reducing the computational effort to practical level and allows conducting large amount of analysis for many structures and the assessment of uncertainties in such models.

The base shear – roof displacement relationships are typically converted to standard capacity curves defined by the spectral acceleration - spectral displacement relationship (Fajfar, 2000). The conversion method from MDOF to ESDOF system is presented as follows:

$$
\begin{aligned}
S_d &= \frac{\Delta}{\Gamma} \\
S_a &= \frac{V}{m^*.\Gamma} \\
m^* &= \sum m_i.\varphi_i \\
\Gamma &= \frac{m^*}{\sum m_i.\varphi^2_i}
\end{aligned}
\qquad (1.1)
$$

Where S_d and S_a are the spectral displacement and spectral acceleration of the ESDOF system, respectively; Δ is the top displacement for the MDOF capacity curve, m^* is the equivalent mass of the ESDOF system, m_i is the concentrated mass of the floors (the mass of the walls is divided between the two levels above and below the i-th floor level, φ_i is the first mode displacement at the i-th floor level normalized such that the first mode displacement at the top story φ =1.0; Γ is modal participation factor that control the transformation from the MDOF to the ESDOF (Figure 1.13a). The above conversion has the advantage to allow a direct comparison with the seismic demand represented with response spectra (Figure 1.13b).

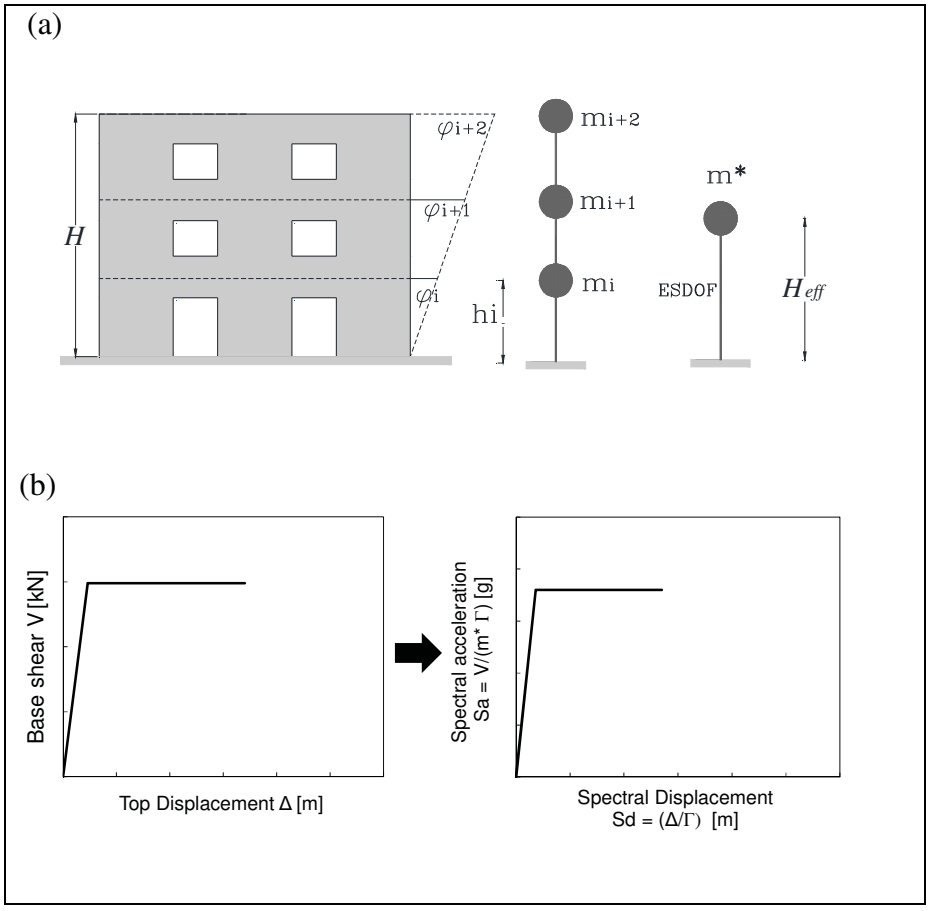

Figure 1.13 Illustration of the conversion of the MDOF system to an ESDOF: (a) the mode shape and mass distribution and (b) the conversion of the capacity curve to the spectral acceleration-displacement domain.

1.6 Damage analysis

Building performance can be measured by mechanical quantities related to the physical condition of the building following an earthquake. In evaluating structural performance, it is of interest that these mechanical quantities do not exceed certain threshold levels defined as damage states. A damage state represent the condition where damage occurred has a direct impact on building use after an earthquake and on the expected losses. For example, a complete damage state corresponds to the demolition of the building.

Well-defined and realistic damage states thresholds are essential for vulnerability modelling. Damage states thresholds are identified using quantitative parameters that correlate best with damage. Inter-story drift ratio and building roof displacement are widely used parameters for damage assessment of structures and are used to develop displacement fragility functions taking into account inherent uncertainties.

Damage state thresholds for masonry buildings are typically identified based on experimental drift ratios of masonry walls tested under cyclic loading (Borzi et al., 2008; Restrepo-Velez, 2003, Ruiz-García and Negrete, 2009; Bosiljkov et al., 2010). Figure 1.14 shows an example for the identification of drift thresholds corresponding to flexural cracking (H_f), shear cracking (H_{dt}), maximum shear strength (H_{max}), and ultimate deformation at 20% loss of strength ($H_{\delta max}$). They are considered as respective damage thresholds for the slight, moderate, extensive, and complete damage states. Based on several test results, the damage state thresholds can be represented in a probabilistic format as a fragility function (Figure 1.15). Typically, the fragility functions are represented by a lognormal probability distribution with a median value and a standard deviation. Lognormal distribution is typically used since it has shown a good fit for structural damage distribution (Wen et al., 2004).

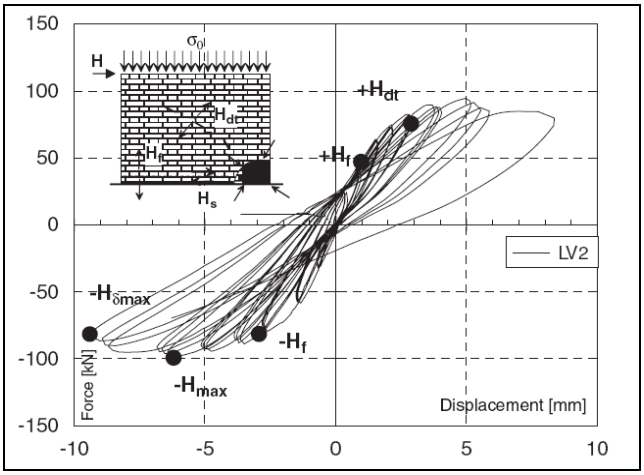

Figure 1.14 Identification of the drift thresholds that corresponds to reaching a specific damage state
Taken from Bosiljkov et al., (2010)

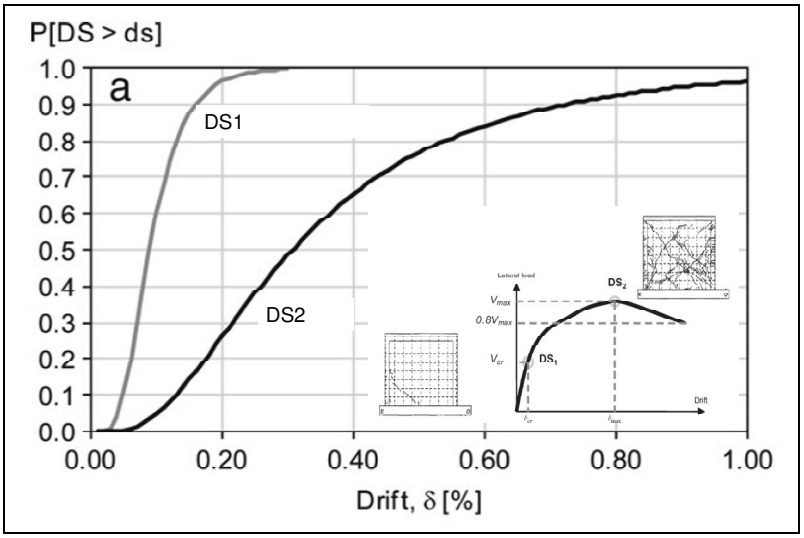

Figure 1.15 Example of a drift-based fragility functions for confined masonry walls
Taken from Ruiz-García and Negrete (2009)

For an ESDOF idealization of the building, the drift-based damage fragility functions can also be converted to spectral displacements fragility functions (Figure 1.16) In this case, they can be convolved directly with the results of the inelastic spectral displacement response from structural analysis (Kircher et al., 1997a, FEMA, 2003, Erdik et al., 2010).

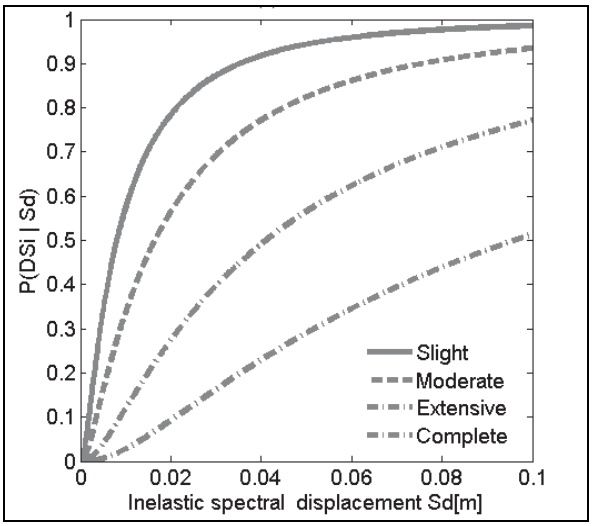

Figure 1.16 Example of a spectral displacement based fragility functions of unreinforced masonry buildings in Hazus.

Another approach to identify damage states of the buildings is based on the developed capacity curves (Lang, 2002; Rota et al., 2010, Frankie, 2010). Figure 1.17 shows an example of an approach proposed by Rota et al. (2010). For the slight and moderate damage states, the global damage threshold are recorded on the capacity curves as displacements at which the first masonry wall reached flexural cracking and the first masonry wall reached the shear cracking, respectively. The extensive damage state is identified at the attainment of maximum base shear capacity of the building whereas the complete damage state refers to displacement corresponding to 20% reduction in base shear. The uncertainty in the damage states thresholds are quantified by conducting several analyses using a range of material properties of the building class.

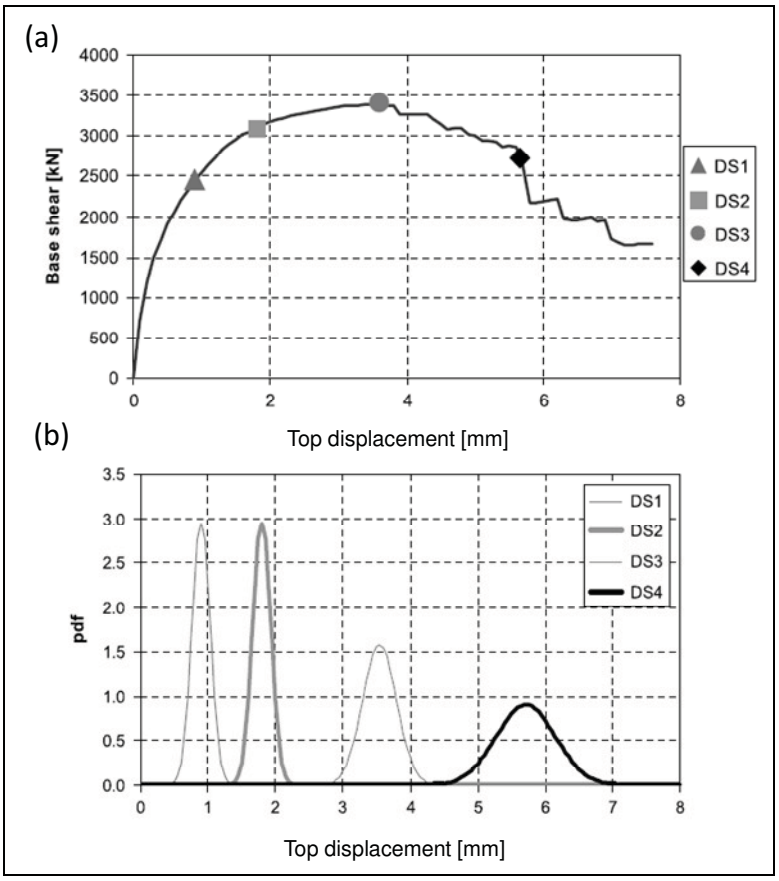

Figure 1.17 Identification of damage states thresholds on capacity curves developed using simulation-based models: (a) the capacity curve and (b) probability distribution of the damage states.
Taken from Rota et al. (2010)

1.7 Loss analysis

The objective of the loss analysis is to relate the expected structural damage to the economic losses due to repair or replacement costs of buildings. This is achieved by applying a so called damage factor (DF) which relates the cost of repair to the cost of replacement cost of the building and which corresponds to reaching of each damage state (i.e. slight, moderate, extensive, complete). The results are summed up to give a mean damage factor (MDF) which when multiplied by the value of the building provides an estimate of economic losses.

Kircher et al. (1997b) proposed DFs calibrated to reflect observed losses following recent earthquake events in California as percentage of total replacement costs: 2% for slight damage, 10% for moderate damage, 50% for extensive damage, and 100% for complete damage. Based on expert opinion and observational and estimated damage cost data available for Turkey, Yucemen (2005) applied different DFs: 5% for slight damage, 30% for moderate damage, 70% for extensive damage and 100% for complete damage. In order to verify these damage factors for Canada, extensive economic data related to damage and repair would need to be gathered, which is beyond the scope of this study.

1.8 Review of existing vulnerability models for stone masonry buildings

In this section, the available vulnerability models and input parameters for stone masonry buildings are reviewed and discussed.

The vulnerability model implemented in the North American regional seismic risk assessment, Hazus (FEMA, 2003) and the earthquake loss estimation routine ELER (Erdik et al., 2010) both apply the NLSA structural analysis method as presented in section 1.3 (Figure 1.4). The required input parameters are the capacity curves and displacement fragility functions for the ESDOF model of building classes along with a response spectral representation of the ground motion input. It has also to be noted that these tools do not explicitly develop fragility and vulnerability functions in terms of a structure-independent intensity measure (e.g. spectral acceleration). For a given earthquake scenario, these tools conduct the structural, damage and loss analyses for each building class in the inventory at each location. Depending on the size of the study area and the density of the built environment, this usually requires significant computational time. However, if the existing buildings are grouped into representative building classes and if sets of fragility and vulnerability functions in terms of a structure-independent intensity measure that directly relates damage and costs to the input ground motion are pre-developed for each building class, the computational time for conducting regional risk assessment is significantly reduced (Porter, 2009).

Hazus reflects the vulnerability information of the construction types in the United States (FEMA, 2003). It considers only one structural class for unreinforced masonry buildings, brick masonry structures with vulnerability information mainly based on expert judgment and observation data (Kircher et al., 1997a). ELER alternatively considers stone masonry buildings with vulnerability information mainly derived from observation damage data collected from Italian earthquakes and expert judgment (Giovinazzi, 2005; Erdik et al, 2010). Figure 1.18 and Figure 1.19 shows the displacement fragility curves and capacity curves computed from the parameters given in Hazus and ELER technical manuals. These figures illustrate the disparities between Hazus and ELER in the definition of the displacement fragility functions and capacity curves, respectively. This justifies the importance of the development of region specific vulnerability input parameters.

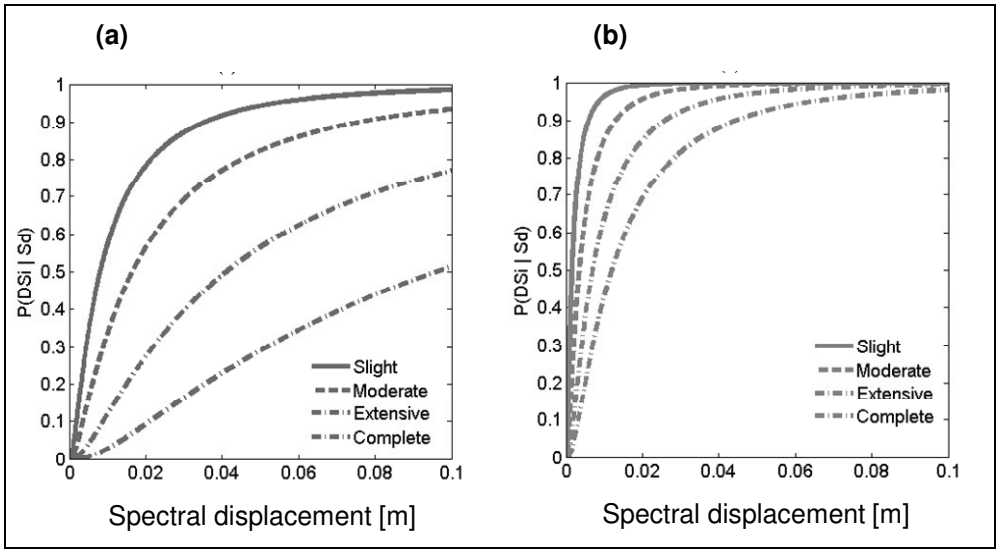

Figure 1.18 Displacement fragility functions for: (a) low-rise brick masonry buildings in Hazus and (b) low-rise stone masonry buildings in ELER.

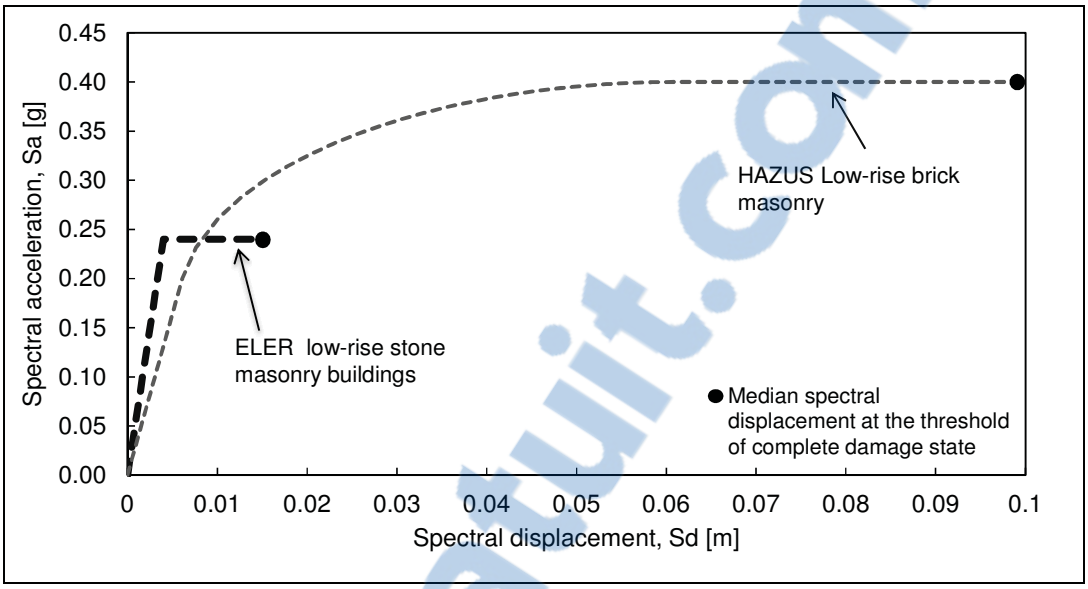

Figure 1.19 Capacity curves for low-rise brick masonry buildings in Hazus and low-rise stone masonry buildings in ELER.

Figure 1.20 presents two sets of analytically developed seismic fragility functions for stone masonry buildings available in the literature in terms of a structure-independent intensity measure (PGA). Figure 1.20a shows a seismic fragility function obtained using the NLTHA structural analysis method combined with a simulation based analytical representative model of a three story masonry building constructed from tuff stones available in Italy (Rota et al. 2010). Figure 1.20b shows a seismic fragility function generated by NLSA structural analysis method combined with a simplified mechanics-based analytical model for two story stone masonry buildings also in Italy (Borzi et al. 2008). Due to the considered structural parameters, these sets of fragility functions are limited in their application to stone masonry classes typically found in Italy. Moreover, the ground motion input used to develop these functions is not necessarily compatible with the seismo-tectonic setting in other regions such as Eastern Canada.

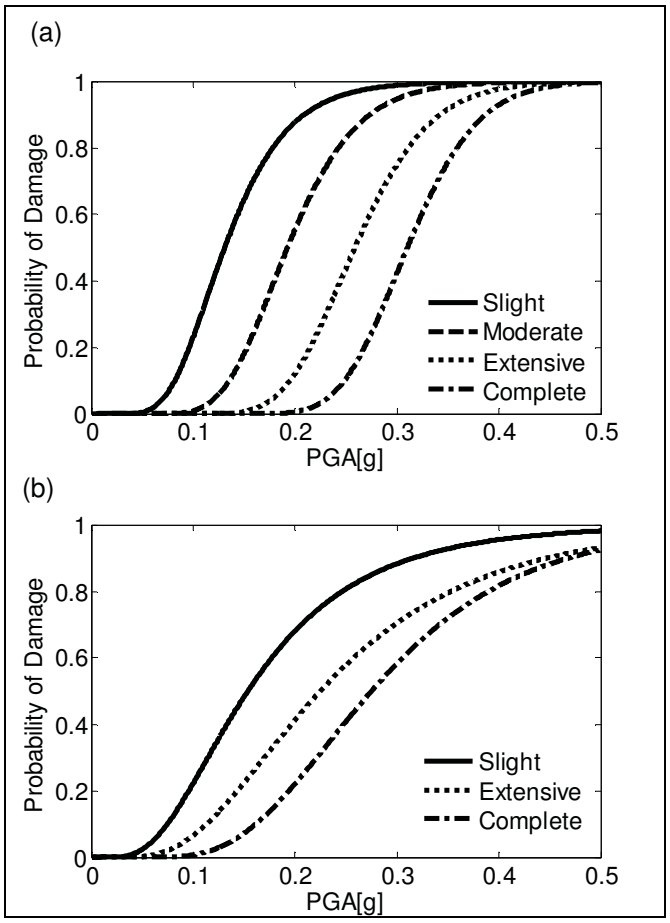

Figure 1.20 Seismic fragility functions for: (1) three story stone masonry buildings (Rota et al. 2010) and (b) two story stone masonry buildings (Borzi et al. 2008).

1.9 Summary

Vulnerability modelling is the key component is regional seismic risk assessment studies of existing buildings. It consists of physical damage and economic loss analyses. The physical damage is generally represented through a set of fragility functions assigned to given damage state whereas economic losses are defined with vulnerability functions. These functions are commonly given in terms of a structure independent intensity measure (e.g. peak ground acceleration or spectral acceleration at a particular period).

Analytical approaches for vulnerability modelling are typically adopted in the regions of moderate seismicity where damage data from past earthquakes are scarce. Despite the high vulnerability of stone masonry buildings, literature review revealed less research is focused on regional seismic vulnerability modelling of these buildings compared to other structural types, e.g. brick masonry and concrete structures.

Analytical approaches for generating fragility and vulnerability functions for a particular building class comprise several steps. The building class is established in accordance with similarities in the structural system; height and material of construction, along with ground motions corresponding to various levels of intensity obtained from the hazard analysis. A structural analysis is performed on a structural model built for that building class to estimate the structural response to the input ground motion. The results are given in terms of displacements that are considered generally as a good indicator of damage. The structural displacement response is used as input to a set of displacement fragility functions to determine the probability of being in respective damage states. Finally, the cost of damage is obtained as a sum of the obtained probabilities to determine the total loss. To create a seismic fragility and vulnerability function, the process is repeated for many levels of earthquake intensity.

Each of the vulnerability modelling steps involves uncertainty. The major sources of uncertainties in the vulnerability modelling are related to: details of the ground motion, structural seismic capacity, damage state definition and repair costs. A good vulnerability modelling practice should address the important sources of uncertainty and investigate their sensitivity to the results.

The review of literature showed that existing vulnerability tools in North America does not consider the stone masonry building classes subjected to Eastern Canada ground motions. Therefore, sets of seismic fragility and vulnerability functions for these buildings need to be developed in order to adequately quantify their seismic risk.

This study will focus on the development of probabilistic assessment tools for seismic vulnerability of stone masonry buildings. These tools will be applied to assess the seismic risk of stone masonry building and other building classes at Old Quebec City. A framework that considers and quantifies different sources of uncertainties will be introduced. In the following chapters, these research issues will be addressed in further details.

CHAPTER 2

DISPLACEMENT BASED FRAGILITY ANALYSIS

2.1 Introduction

The objective of this chapter is to introduce a simplified analytical-based fragility analysis procedure with systematic treatment of uncertainties for development of displacement based fragility functions for typical stone masonry buildings in Old Quebec City. The applied procedure comprises: (1) inventory of the existing buildings, (2) probabilistic displacement-based damage model, (3) probabilistic capacity model, (4) probabilistic seismic demand model. The resulting fragility functions are compared with those implicit in Hazus (FEMA, 2003) and ELER (Erdik et al., 2010) in order to assess differences and the potential disparities in damage estimates. The comparison are conducted in terms of probability of reaching a given damage state.

2.2 Analytical displacement fragility functions

Analytical displacement fragility functions are usually given in the form of lognormal distribution of the probability of being in or exceeding a given damage state for structural response parameter (e.g., spectral inelastic displacement demand). The conditional probability of reaching a particular damage state, DS , given the spectral displacement S_d , is defined by the following equation (Kircher et al., 1997a):

$$P\left[DS \mid S_d\right] = \Phi\left[\frac{1}{\beta_{DS}} \ln\left(\frac{S_d}{\overline{S}_{d,DS}}\right)\right] \tag{2.1}$$

$$\beta_{DS} = \sqrt{CONV(\beta_C, \beta_D)^2 + \beta_T{}^2}$$

where, $\overline{S}_{d,DS}$ is median value of the spectral displacement at which the building reaches the threshold of damage state *DS*, β_{DS} is standard deviation of the natural logarithm of spectral displacement for damage state *DS*, and Φ is standard normal cumulative distribution function. Three major sources contribute to the total variability of any given damage state: the variability in the capacity model β_C, the variability in the demand model β_D, and the variability in the threshold of a damage state from the damage model β_T. The convolution (CONV) is evaluated by conducting seismic demand analyses on capacity curves and obtaining the probability of being or exceeding different damage states. The details of these procedures are explained in the following sections.

2.3 Inventory

An inventory has been carried out to characterize the typical stone masonry buildings present in Old Québec City (Vieux Québec). Besides a street survey, the inventory consisted of review of architectural reports, dissertations and historic documents. The inventory methodology and the sources of information can be found in (Nollet et al., 2012). The inventory of buildings in the Old section of Québec City identified 168 buildings of stone masonry buildings that represent 14% of 1220 buildings in the study area (Figure 2.1).

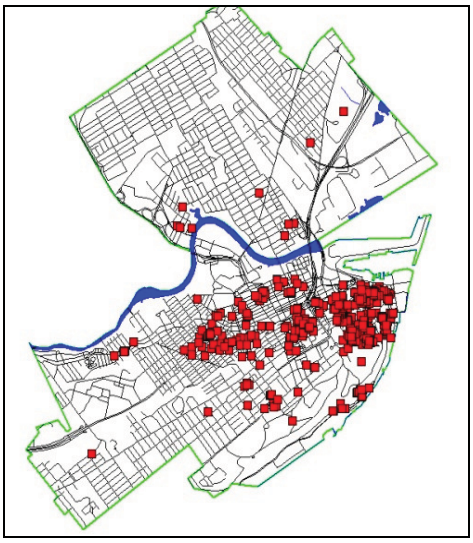

Figure 2.1 Location of stone masonry buildings at Old Quebec City.

Figure 2.2 shows an illustration of the three main topologies of stone masonry buildings used as structural prototypes for this study. These buildings were constructed during the 18th and mid-19th century. The massive façade walls are relatively thick, ranging from 0.4 to 0.6 m, and have regular window and door openings on front and rear sides of the building. The typical story height ranges from 2.7 to 3.3 m. Lateral fire walls are of the same thickness as the façade walls. The massive façade and lateral fire walls provide the vertical and lateral resistance. The stone walls were built of limestone blocks bonded with lime mortar. The openings are bridged with wooden lintels. The typical floor is made of wood joists resting on the façade walls with steel anchors. During the elaboration of this study, no specific information regarding the mechanical properties of stone masonry at Old Québec City could be found in the literature and experimental results were not yet available. This adds a layer of uncertainty in the proposed procedure. In order to demonstrate the procedure for fragility analysis, Typology-1 is the most frequent typology in the study area and is retained as representative of low-rise stone masonry buildings.

Figure 2.2 The three main typologies of stone masonry buildings at Old Québec City.

2.4 Displacement based damage model

The relatively good statistical correlation observed between the earthquake induced displacement and the extent of structural damage contributed to the development of modern performance-based seismic assessment methods. These methods consist of the evaluation of the structure-specific deformation capacity and earthquake-induced displacement demand (Ruiz-García and Negrete, 2009).

Building structural seismic performance is assessed using mechanical quantities, such as inter-story drift, related to the physical condition of the building following an earthquake. For evaluation of the structural performance, it is of interest that these mechanical quantities do not exceed given threshold values defined as damage states (e.g. slight, moderate, extensive and complete). These damage states represent the undesirable condition that has direct consequence on building use during and after an earthquake and on the expected economic and social losses. Well-defined and realistic damage states are extremely important due to their direct impact on the fragility function parameters.

Simplified displacement-based procedures were proposed for assessment of the structural performance of masonry structures (Calvi, 1999; Restrepo-Vélez, 2003). In these procedures, damage of masonry structures is related to the capacity of in-plane loaded walls to sustain the top of the wall horizontal displacement (drift). Note that masonry walls can be subjected to out-of-plane failure mode orthogonal to the earthquake direction, depending mainly on the quality of floor to wall connection. In this case, walls can fail locally especially at top stories where dynamic amplification is higher. However, for walls that are properly anchored to floors, the out-of-plane behavior should not be critical and the building damage is governed by the in-plane behavior. This assumption is valid for most of the existing stone masonry buildings in the Old Québec City, which were provided with steel anchors for improvements in the floor to wall connections.

The procedure for assessment of the structural performance proposed by Restrepo-Vélez (2003) is adopted in this study. For the MDOF masonry structure, a linear shape is assumed for the elastic behavior, whereas a soft first story deformed shape is assumed for the inelastic

behavior (Figure 2.3a). The later is the most common failure mechanism of masonry structures under earthquake loading (Tomaževic, 1999). The procedure assumes modeling of the masonry structure as an ESDOF with effective global parameters. The displacement threshold relative to a given structural damage state at the effective height of the ESDOF, equivalent to the spectral displacement ($S_{d,DSi}$) in Equation 2.2, is obtained based on the assumed deformed shape of the structure.

Drift thresholds for masonry walls are generally identified from laboratory experiments on masonry wall elements. Drift threshold on the ESDOF of each damage state, $S_{d,DSi}$, is defined as follows:

$$S_{d,DSi} = \theta_{DS1} k_1 H + (\theta_{DSi} - \theta_{DS1}) k_2 h_s \tag{2.2}$$

where, H is total height of the building, h_s is height of the first story, θ_{DS1} is drift threshold for the first story walls at the elastic limit, θ_{DSi} is the drift threshold for the first story walls at higher damage states in the non-linear domain, k_1 is the effective height coefficient of the building at which the displacement of the MDOF system equals the spectral displacement for an ESDOF system, and k_2 is the effective height of the first story walls with openings that deform in the inelastic range. The respective values for the studied two story buildings are k_1 = 0.7 and k_2 = 0.95 (Restrepo-Vélez 2003).

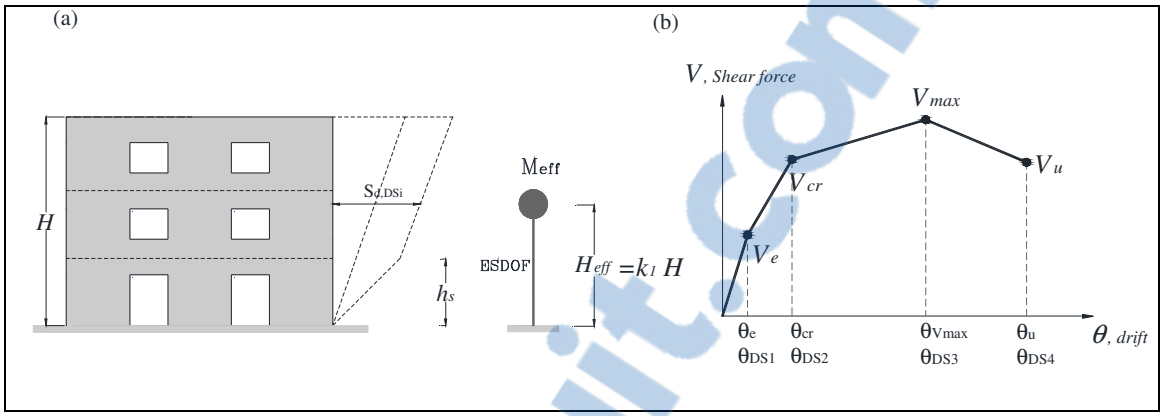

Figure 2.3 Simplified model for computation of damage states: (a) MDOF deformed shape and conversion to ESDOF, and (b) identification of drift thresholds for masonry walls.

The damage state drift thresholds are identified on the drift-shear force envelope curve for the stone masonry walls shown in Figure 2.3b (Bosiljkov et al. 2010; Tomaževic and Weiss, 2010). The in-plane response of stone masonry walls is strongly nonlinear. With increase of the lateral force, the displacement due to cracking increases and walls experience both strength and stiffness degradation. The thresholds on the horizontal axis correspond to flexural cracking (θ_{DS1}), shear cracking (θ_{DS2}), maximum shear strength (θ_{DS3}), and ultimate deformation at 20% loss of strength (θ_{DS4}). They are considered as respective damage thresholds for the slight, moderate, extensive, and complete damage states.

For this study, damage states drift thresholds values were derived from representative literature experimental data (Tomaževič and Lutman, 2007; Tomaževic and Weiss, 2010; Vasconcelos, 2005; Elmenshawi et al., 2010; Magenes et al., 2010, Rota et al., 2010). The drift thresholds were obtained according to the above mentioned criteria for stone masonry walls tested under cyclic loading (Table 2.1).

Table 2.1 Drift ratios for damage state thresholds for stone masonry walls.

Sample number	θ_{DS1} [%]	θ_{DS2} [%]	θ_{DS3} [%]	θ_{DS4} [%]
1	0.06	0.10	0.28	0.45
2	0.07	0.13	0.34	0.46
3	0.07	0.20	0.36	0.48
4	0.08	0.20	0.40	0.51
5	0.08	0.26	0.41	0.61
6	0.08	0.28	0.41	0.67
7	0.09	0.30	0.58	0.86
8	0.09	0.30	0.60	1.00
9	0.09	0.30	0.70	1.00
10	0.10	0.41	0.80	1.20
11	0.10	0.41	1.15	1.83
12	0.10	0.47	1.19	1.92
13	0.11	0.50	1.19	2.01
14	0.12	0.57	1.38	2.14
15	0.12	0.66	1.42	2.33
16	0.13	0.85	1.65	2.33

The empirical cumulative distribution function (CDF) for each damage state was obtained by sorting the drift data in ascending order, and plotting them against a probability equal to *i/(n+1)*, where *i* is position of the drift ratio and *n* is the size of the sample (Ruiz-García and Negrete, 2009). A lognormal CDF was then fitted with the advantage of being fully defined by only two statistical parameters: the central tendency (median) and dispersion (lognormal standard deviation) (Figure 2.4). These values were then implemented in Equation 2.2 to simulate the displacement of the ESDOF system. The story height was assumed to have a fixed value equal to the median height observed from the inventory (h_s=3.0 m). The resulting displacement threshold data were then represented with lognormal distributions which actually represent the displacement fragility functions for the ESDOF system (Table 2.2).

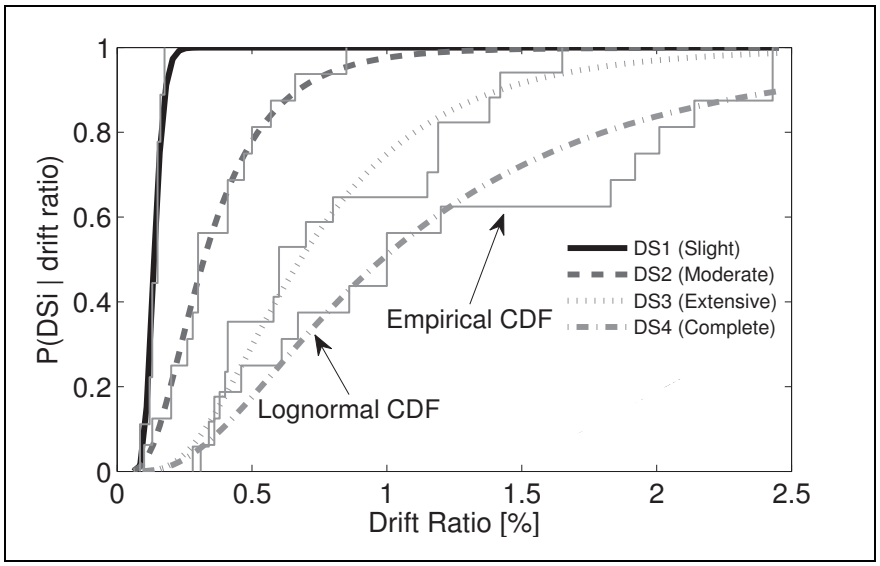

Figure 2.4: Drift threshold variability for low-rise stone masonry buildings.

Table 2.2 Median and dispersion of the displacement based damage states for two story stone masonry building and respective values implicit in Hazus and ELER

	Quebec Stone low-rise (two-story)		**ELER stone low-rise**		**Hazus pre-code URM low-rise**	
Damage state	Median S_d [m]	Dispersion β_T	Median S_d [m]	Dispersion β_T	Median S_d [m]	Dispersion β_T
DS1 [Slight]	0.005	0.20	0.002	0.4	0.008	0.4
DS2 [Moderate]	0.012	0.38	0.004	0.4	0.016	0.4
DS3 [Extensive]	0.021	0.40	0.007	0.4	0.041	0.4
DS4 [Complete]	0.028	0.50	0.011	0.4	0.096	0.4

Figure 2.5 illustrates the developed fragility functions for the considered low-rise stone masonry building compared to respective fragility functions implicit in Hazus (pre-code low-rise unreinforced masonry buildings) and ELER (simple stone low-rise buildings). The difference in the respective fragility functions comes from the information used in their developments. For Hazus and ELER, the median and standard deviation for different damage

states are based on empirical data and expert opinion. The respective dispersion is assumed constant for all damage states, $\beta_{T,DSi} = 0.4$. On the other hand, the developed fragility curves in this study are based on observed experimental behaviour of stone walls where dispersion comes from the variability of specimen-to-specimen testing data. The dispersion is the lowest for slight damage state, $\beta_{T,DS1} = 0.2$, and is highest for complete damage state, $\beta_{T,DS4} = 0.5$. This increase in dispersion results from the rapid degradation of stone walls with increasing displacement demand and imprecisions in recording the respective displacement accurately. Moreover, the large variety in specimen-to-specimen mechanical properties and stone block arrangement of the tested walls contribute to increasing the dispersion in the identification of higher damage state thresholds.

Limitations exist regarding the direct comparison of fragility functions between different models because of the different assumptions, information and tools used in the development process. Hence, the objective of the comparison given in Figure 2.5 is rather to show the importance for the development of fragility functions that reflect the specific characteristics of the considered structures.

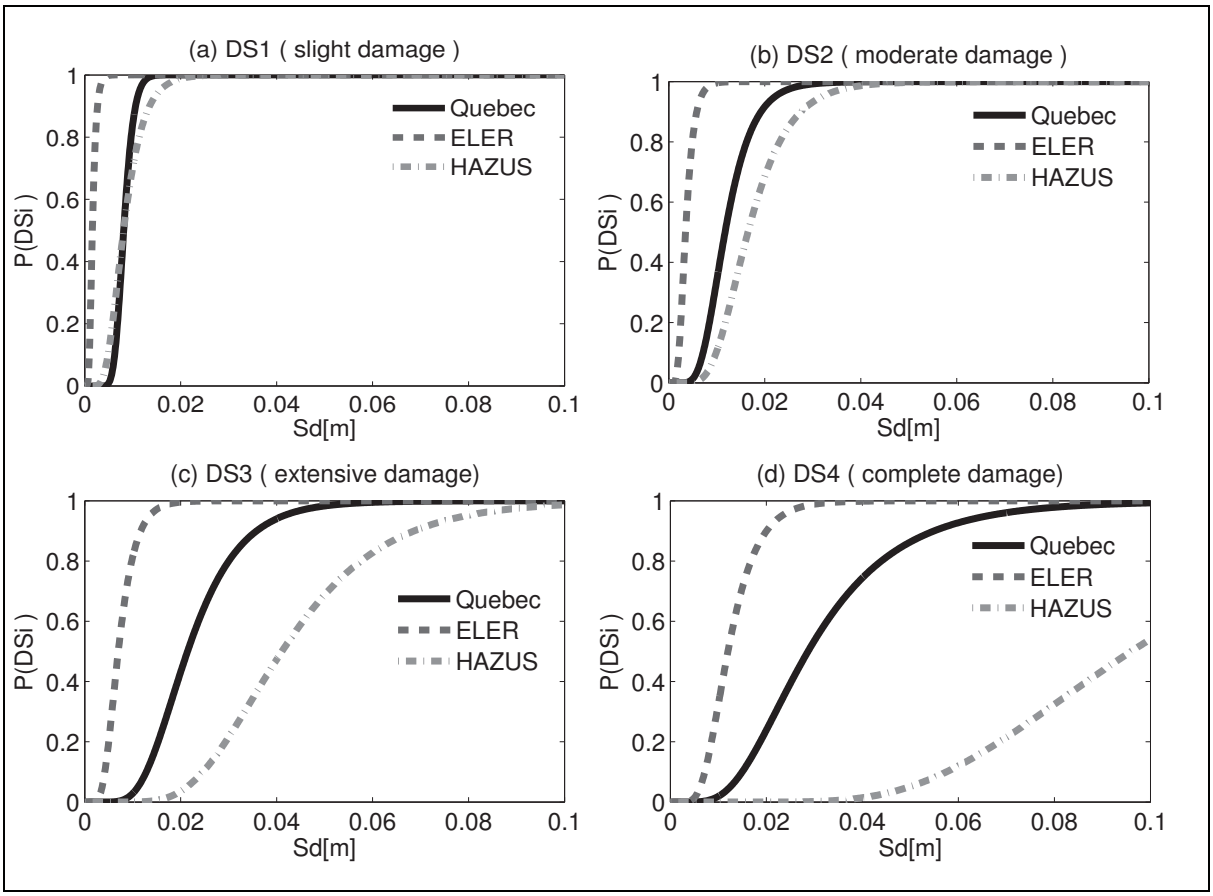

Figure 2.5 Comparison of displacement-based threshold fragility curves for two story stone masonry building developed in this study with those implicit in Hazus pre-code unreinforced masonry and ELER simple stone for (a) slight, (b) moderate, (c) extensive and (d) complete damage state.

2.5 Capacity model

Based on the literature review presented in the previous chapter, mechanics-based models for developing capacity curves are particularly suitable for regional scale vulnerability studies. Tomazevic (1999) and Lang (2002) have shown that the application of simplified mechanical models provided good approximation of the global system capacity when compared with experimental results on several scaled models of masonry buildings. Such simplification reduces the computation time and more importantly idealizes the system with less number of parameters which is highly desirable when conducting regional scale vulnerability modelling.

In order to develop a representative capacity model for the considered building typology, a simplified mechanical model is used to develop the base shear - roof displacement relationships similar to the one proposed by (Lang, 2002). The elastic deformation of the building is approximated by a linear function up to the point where the shear capacity of the wall is attained. The inelastic deformation is assumed as perfectly plastic and concentrated at the first story only, which is the typical damage observed in masonry buildings (Tomazevic, 1999). The effective stiffness of the elastic part is determined using the secant stiffness at the capacity, $V_{y,}$ and is selected such that the area under the bilinear curve is equivalent to the area under the experimental curve applying the energy equivalence criterion (Magenes and Calvi, 1997). The base shear strength of the building in a given direction is assumed equal to the sum of the shear strengths of the first story walls in that direction (Figure 2.6).

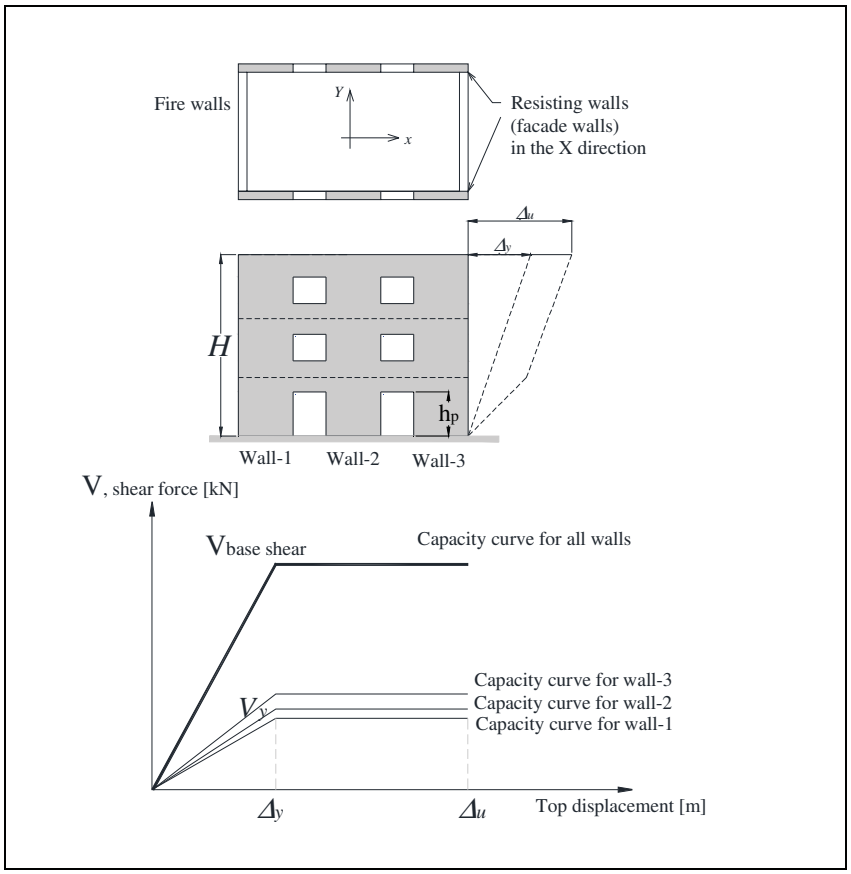

Figure 2.6 Simplified mechanical model for capacity curve evaluation of stone masonry buildings.

Two mechanical criteria are considered to evaluate the shear strength of the first story walls based on the expected failure mechanism given by Equation 2.3: the shear strength corresponding to reaching of the flexural rocking failure criterion, V_r (Magenes and Calvi, 1997), and the shear strength at the attainment of diagonal tension cracking failure criterion, V_{dt} (Turnsek and Cacovic, 1971). These two criteria provided good approximation of the shear strength of stone masonry walls when compared with experimental results (Mazzon, 2010; Tomazevic, 1999; Magenes et al., 2010; Vasconcelos, 2005). Typically, the observed damage is mixed flexure and shear failure mechanisms.

$$V_r = \left(\frac{L^2.t.\sigma_0}{h_p}\right).\left(1-\frac{\sigma_0}{0.85 f_m}\right)$$
$$V_{dt} = \left(\frac{L.t.f_{dt}}{b}\right).\sqrt{\left(1+\frac{\sigma_0}{f_{dt}}\right)} \qquad (2.3)$$

where, L is the wall length; t is the wall thickness; h_p is the height of pier element between openings; σ_0 is the average axial stress; f_m is the compressive strength of masonry; f_{dt} is the diagonal tension strength of masonry; and b is a factor depending on the aspect ratio (height/length= h_p / L), b=1.0 for $h_p / L \le 1.0$, b=1.5 for $h_p / L \ge 1.5$, or b= h_p / L for $1 < h_p / L < 1.5$. The governing failure mechanism depends on the axial stress, aspect ratio, compression and diagonal tension strength of masonry.

Using the assumption of constant elastic drift over the building height equals to the drift of the first story θ_y, the elastic top displacement of the wall Δ_y with total height H, can be written as follows:

$$\Delta_y = \theta_y.H \qquad (2.4)$$

This assumes that the drift of the first story is equal to the drift of the pier. In reality the displacement over one storey is not uniform. The piers as the most slender part of a wall and will deform the most, where the joint regions are rather stiff and will deform less. Nevertheless, Lang (2002) showed that this assumption provided reasonable approximation of the elastic deformation when compared with experimental results. The elastic drift of the first story is evaluated as follows:

$$\left\{ \begin{array}{c} \theta_y = \dfrac{\Delta_{y,pier}}{h_p} \\ \Delta_{y,pier} = \dfrac{V_y}{K_{e,pier}} \\ K_{e,pier} = \dfrac{1}{\left(\dfrac{h_p^{\,3}}{12EI_{eff}} + \dfrac{\upsilon h_p}{GA_{eff}}\right)} \end{array} \right\} \theta_y = V_y\left(\frac{h_p^{\,2}}{12EI_{eff}} + \frac{\upsilon}{GA_{eff}}\right) \qquad (2.5)$$

Where H is the total height of the building , $K_{e,pier}$ is the elastic stiffness of the pier for fixed-fixed boundary conditions , υ is the shear coefficient which equals 1.2 for rectangular cross-sections, EI_{eff} and GA_{eff} are the effective flexural stiffness and shear stiffness, respectively. Lang (2002) showed that the effective stiffness of the linear elastic part of the bilinear can be approximated equals 0.5 of the uncracked stiffness ($0.5EI$ and $0.5GA$) when compared with experimental results. The median ultimate deformation capacity at the top of the wall Δ_u is estimated using the median drift threshold of the complete damage state from the damage model.

The base shear – roof displacement relationships are then converted to standard capacity curves defined by the spectral acceleration - spectral displacement relationship. The conversion method from MDOF to ESDOF system presented by Fajfar (2000) is used for that purpose (equation 1.1; section 1.5.2; chapter 1).

The stone masonry buildings in Old Quebec City were mainly built of local limestone blocks bonded with lime mortar. As mentioned earlier, no specific information on material mechanical properties is currently available. These properties are therefore obtained from the literature data (Mazzon, 2010; Tomazevic, 1999, Magenes et al., 2010) and may introduce significant variability in the developed capacity curves. The mechanical properties that are required to evaluate the seismic resistance of stone masonry walls are: the compressive strength (f_m), the elastic modulus (E_m), the diagonal tension strength (f_{dt}) and the shear modulus (G). In order to take into account the uncertainties in the material properties on the capacity curves, a series of analyses is conducted varying material properties of stone masonry structural elements according to values reported in the literature and given in Table 2.3. The empirical correlations between the mechanical properties suggested by Tomazevic (1999) are used as follows: the elastic modulus is taken as 1100 times the compression strength, the diagonal tension strength is defined as 6% of the compression strength, and the shear modulus is taken as 25% of the elastic modulus. The specific weight of stone masonry was assumed 22 kN/m^3.

Table 2.3 Variability in stone masonry material properties.

Case	**Compression strength, f_m[MPa]**	**Diagonal tension strength, f_{dt} [MPa]**	**Elastic Modulus E_m[MPa]**	**Shear Modulus, G_m[MPa]**
i	5.0	0.3	5500	1375
ii	3.0	0.18	3300	825
iii	2.0	0.12	2200	550
iv	1.0	0.06	1100	275
v	1.0	0.03	1100	275

The procedure is used to develop capacity curves for the two stories Typology-1 with geometrical properties shown in Figure 2.7. An Example of the transformation of the capacity curve of the MDOF to the ESDOF is illustrated in Figure 2.8 for a modal participation factor $\Gamma = 1.26$ and effective mass $m^* = 132$ tons.

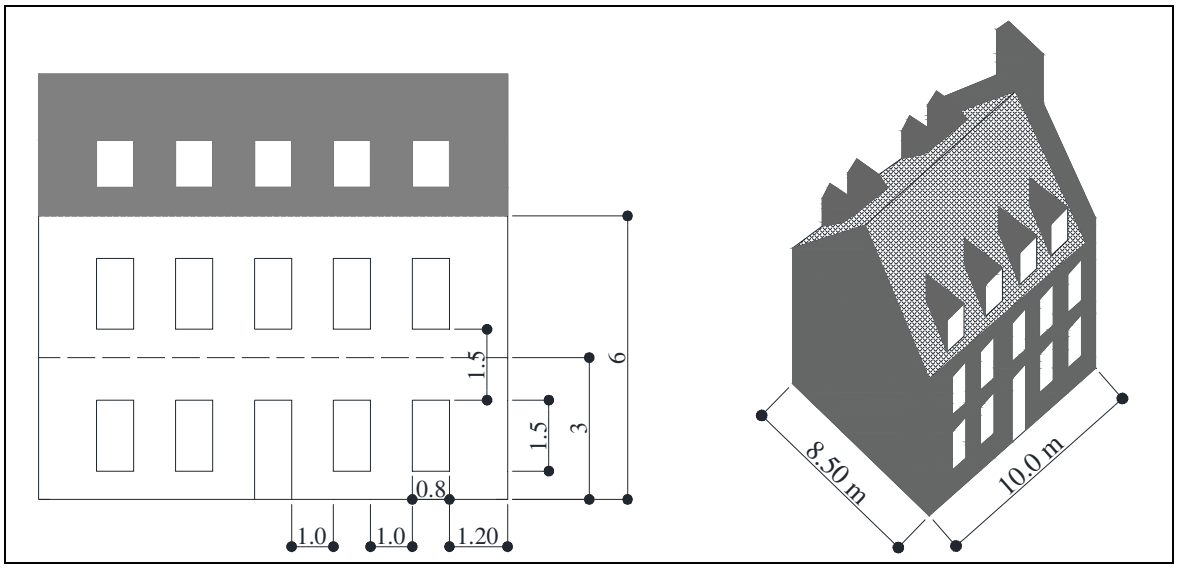

Figure 2.7 Geometrical parameters of the façade walls of typology-1 two story stone masonry buildings (dimensions are in [m]).

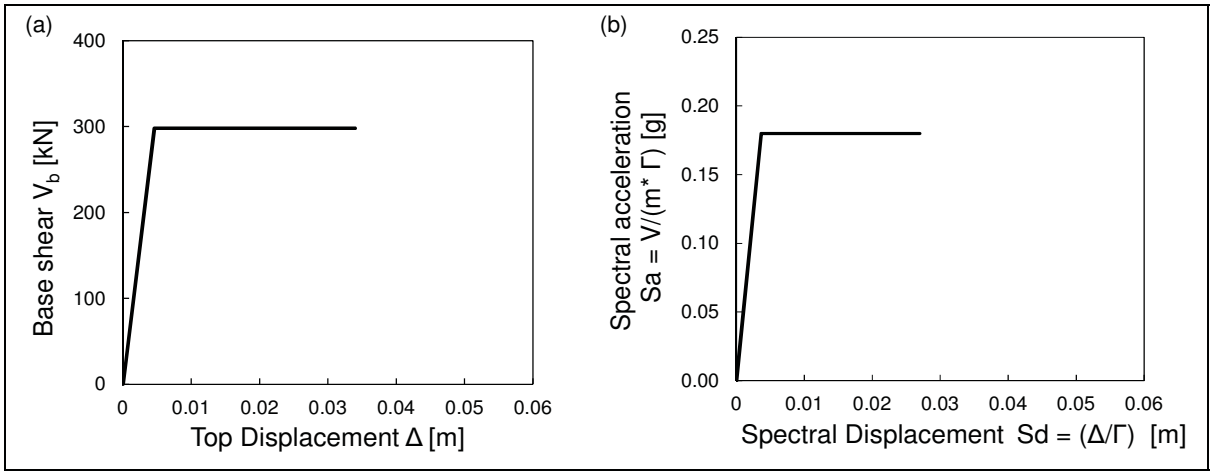

Figure 2.8 The capacity curve for typology-1 (case v) in terms of: (a) base shear-top displacement of the MDOF and (b) spectral acceleration-displacement of the ESDOF.

The capacity curves for all cases in terms of spectral displacement and acceleration are shown in Figure 2.9. It can be observed that the effects of the uncertainty in the diagonal tension strength have significant influence on the lateral strength of the building. The capacity curves (i), (ii) and (iii) are representative for higher diagonal tension strength

structural elements, whereas capacity curves (iv) and (v) are typical for structural elements with lower diagonal tension strength. That uncertainty in the diagonal tension strength can eventually change the governing response mechanism and consequently the overall strength of the building. For comparative purposes, the figure also shows the simulated median capacity curve that is retained for damage analysis and respective Hazus and ELER curves. The large deformation capacity of the Hazus capacity curve can be explained by the estimated relatively high displacement thresholds (Figure 2.5).

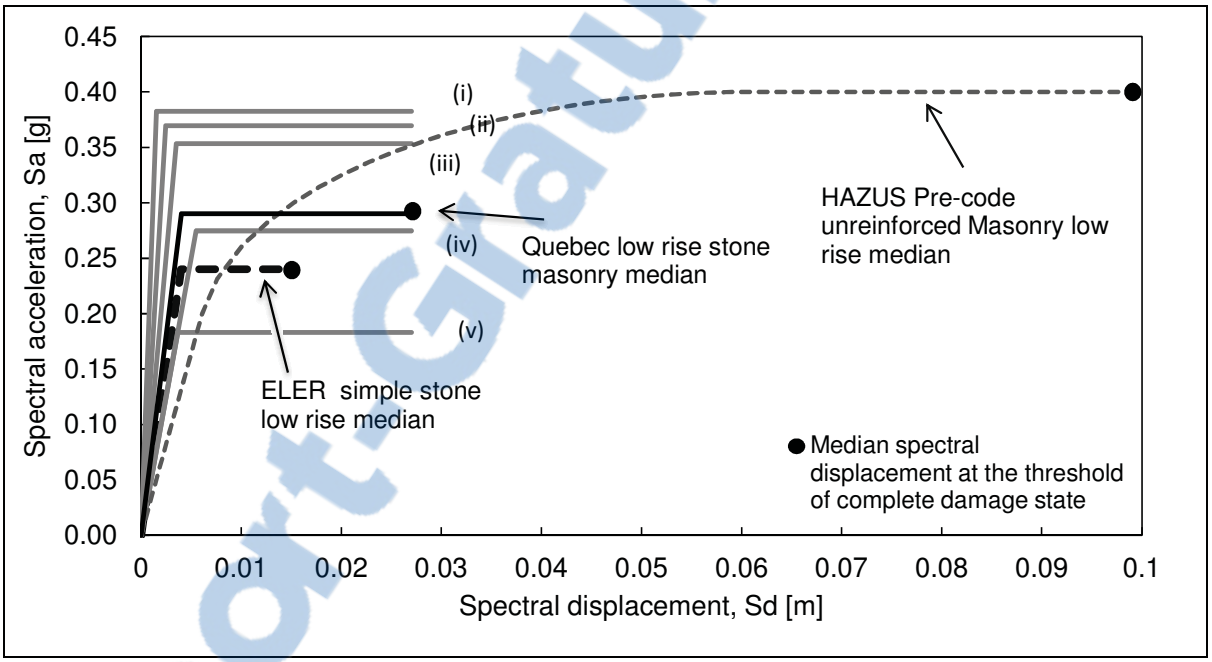

Figure 2.9 Capacity curves for stone masonry typology with varying material properties and comparison with respective median capacity curves implicit in Hazus and ELER.

Table 2.4 gives the simulated median and corresponding dispersion of the capacity parameters, the fundamental period of vibration $T_y = 2\pi\sqrt{S_{dy}/S_{ay}}$ and the yield acceleration of the plateau of the capacity curve (S_{ay}), and respective values implicit in Hazus and ELER. As for the damage state thresholds, Hazus and ELER median and dispersion of capacity parameters, are based on expert opinion and empirical data. The dispersion in the capacity parameters developed in the present study comes from the variability in experimentally obtained mechanical properties of stone walls. The advantage of the applied mechanical

model is the flexibility for investigation and quantification of uncertainties. The applied mechanical model can also be applied to explore the potential effects of retrofitting on the increase of the seismic capacity of the building in a simplified manner. Analyses were also conducted to develop the capacity parameters for one and three stories stone masonry building typologies (Appendix-I).

Table 2.4 Median and dispersion of capacity parameters of stone masonry buildings and respective values implicit in Hazus and ELER

	Quebec stone, low-rise	**ELER stone, low-rise**	**Hazus pre-code URM , low-rise**
Median fundamental period of vibration T_y [sec]	0.18	0.19	0.35
Dispersion fundamental period of vibration (β) T_y [sec]	0.34	-	-
Median yield acceleration S_{ay} [g]	0.30	0.24	0.20
Dispersion yield acceleration (β) S_{ay} [g]	0.26	0.30	0.30

2.6 Seismic demand model

In this section, the contribution of the variability in the seismic demand on the fragility of stone masonry buildings is discussed. The seismic behavior of structures is characterized by the amount of damage, indicating that inelastic deformation occurred during the earthquake. As the linear analysis cannot predict such behavior in an explicit manner, nonlinear analysis is generally applied using nonlinear static or dynamic time history analyses. While the later is time consuming and requires detailed selection and scaling of the ground motion records prior to conducting the dynamic response analysis, the nonlinear static analysis represents a simple and reasonably accurate alternative. It is particularly effective for low-rise buildings dominated by the first mode response (FEMA, 2005). Ruiz-Garcia and Miranda (2007) proposed an attractive nonlinear static procedure which includes the uncertainty in the seismic demand. It applies statistical analysis of the displacement demand predicted from the

dynamic response of nonlinear SDOF systems subjected to a series of ground motions to obtain a simplified expression for median and dispersion of displacement demand. The procedure used for assessing the combined variability in capacity and seismic demand, $CONV(\beta_C, \beta_D)$ in Equation 2.1 consists of the following steps:

1) The capacity parameters, median and standard deviation values of the fundamental period and yield acceleration (T_y, S_{ay}), are obtained based on the probability distribution presented in (Table 2.4).
2) The spectral displacement response (S_d) is evaluated for each sampled pair of capacity parameters at different levels of seismic demand using the displacement coefficient method (FEMA, 2005). This widely used nonlinear static procedure essentially modifies the elastic response of the ESDOF system with 5% damping by multiplication with a series of coefficients to generate an estimate of the inelastic displacement demand, S_d , as follows,

$$
\begin{aligned}
S_d &= C_1.C_2.S_a(T_y).\frac{T_y^2}{4.\pi^2}.g \\
C_1 &= 1+\frac{R-1}{a.T_y^2} \\
C_2 &= 1+\frac{1}{800}\left[\frac{R-1}{T_y}\right]^2 \\
R &= \frac{S_a\left(T_y\right)}{S_{ay}}
\end{aligned}
\tag{2.6}
$$

where, C_1 is modification parameter which relates the expected maximum displacement of an inelastic ESDOF system with elastic-plastic hysteresis properties to the displacement calculated from the elastic spectral response; C_2 accounts for the effects of pinched hysteresis shape, stiffness degradation, and strength deterioration on the maximum displacement response; $S_a(T_y)$ is the spectral acceleration at the fundamental period of the system, T_y; a is a constant referring to the site class (a=130 for site class B,

rock, typical for Old Québec City) (NBCC, 2010); S_{ay} is the yield acceleration of the system and R is the strength ratio of the system.

3) The seismic demand is represented with a response spectrum which can be scaled to different peak ground accelerations (PGA). The uniform hazard spectrum for Québec City with 2% probability of exceedance in 50 years is used in this study (Adams and Halchuk, 2003). Figure 2.10 shows an illustration of the above procedure.

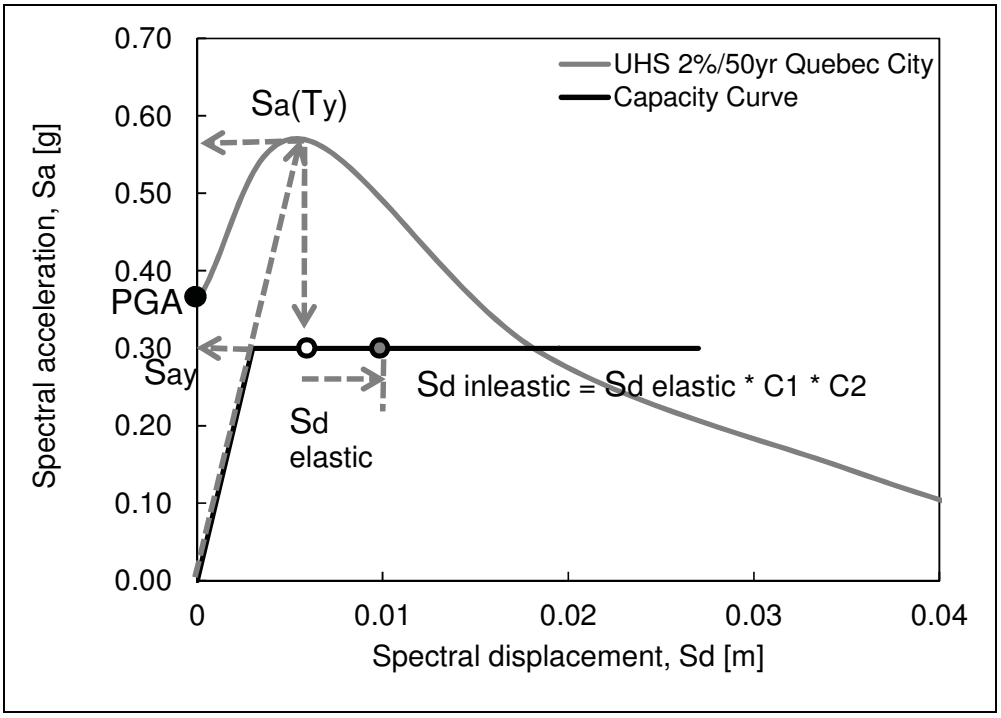

Figure 2.10 Illustration of the procedure to calculate the inelastic spectral displacement demand using the DCM.

4) The closed form nonlinear solution (Ruiz-Garcia and Miranda, 2007) is used to assess the variability in seismic demand for each T_y and S_{ay} pair at each level of PGA. It estimates the variability of the coefficient C_1 as follows,

$$\beta_{C_1} = \left[\frac{1}{A_1} + \frac{1}{A_2.(T+0.1)}\right].\alpha$$
$$\alpha = A_3.\left[1-\exp(-A_4(R-1))\right] \quad (2.7)$$

where, A_1 = 5.876, A_2 = 11.749, A_3 = 1.957, and A_4 = 0.739. The above procedure allows obtaining the lognormal distribution parameters for the inelastic displacement demand, i.e., lognormal median $\lambda_{Sd}(PGA_j) = \ln(S_d)$ from Equation 2.6 and lognormal standard deviation $\beta_{Sd}(PGA_j)$ from Equation 2.7. Figure 2.11 shows an illustration of the probability distribution of the inelastic displacement demand at a given PGA. Table 2.5 shows example calculations for the displacement demand.

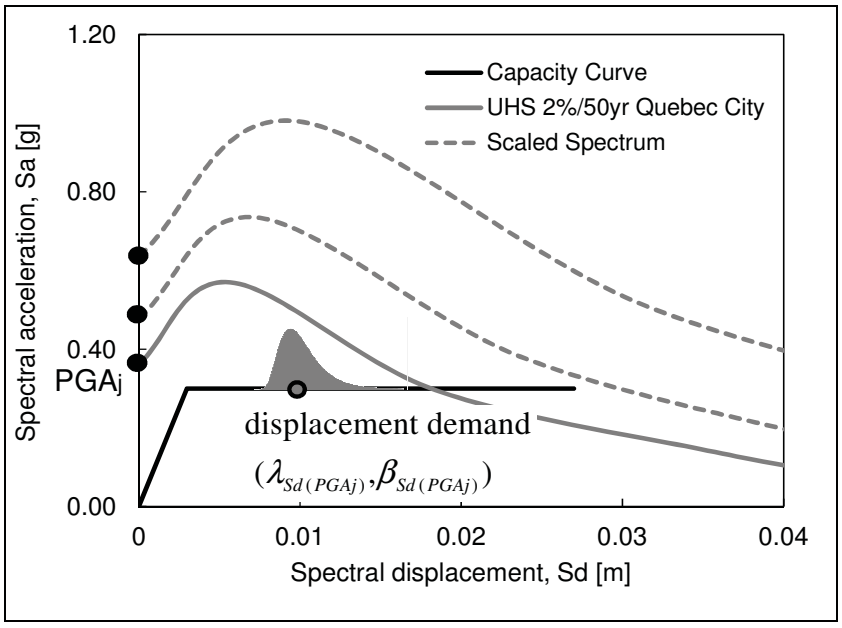

Figure 2.11 Illustration of the variability in displacement demand at a given level of PGA.

Table 2.5 Example evaluation of the displacement demand using the DCM.

$PGA_j[g]$	**0.21**	**0.36**	**0.51**	**0.66**	**0.81**
$\bar{S}_d[m]$	0.004	0.009	0.014	0.020	0.031
$\lambda_{Sd}(PGA_j) = \ln(\bar{S}_d)$	-5.413	-4.657	-4.238	-3.908	-3.478
$\beta_{Sd}(PGA_j)$	0.547	0.576	0.610	0.622	0.620

5) The process is repeated by gradually increasing the PGA value (Figure 2.12a). The probability, P_{ij}, of exceeding a certain damage state DS_i at a specific level of PGA is calculated as follows:

$$P_{ij}(S_d > S_{d(DSi)} \mid PGA_j) = 1 - \Phi\left[\frac{\ln(S_{d(DSi)}) - \lambda_{Sd(PGAj)}}{\beta_{Sd(PGAj)}}\right] \tag{2.8}$$

The displacement threshold is taken equal to the median spectral displacement of $S_{d(DSi)}$ for different damage states from the damage model (Figure 2.4b). At each PGA level, there are four evaluated probability values, P_{ij} (Figure 2.12b).

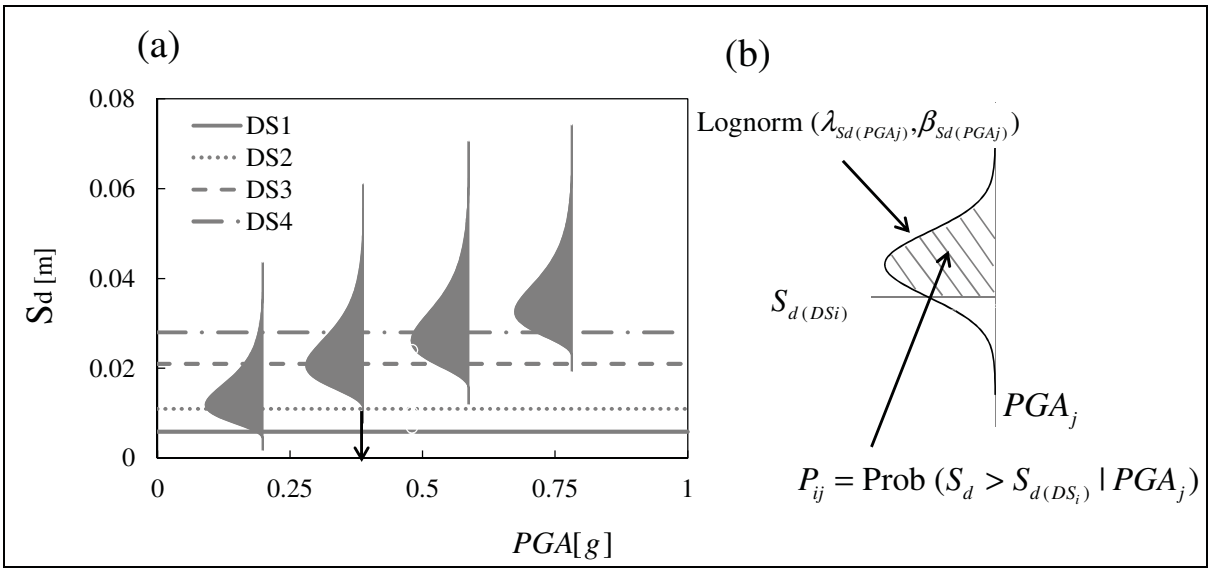

Figure 2.12 Seismic demand model: (a) lognormal distribution of the inelastic displacement demand for various levels of PGA (black arrow indicates PGA with 2%/50 years for Quebec city for soil-class B), and (b) evaluation of the probability of exceedance a specific damage state.

Table 2.6 Example evaluation of the probability of exeedance of each damage state.

Median displacement thresholds of each damage state (Table 2.2)					
$S_{d(DS1)}[m]$	0.005	$\ln(S_{d(DS1)})$	-5.116		
$S_{d(DS2)}[m]$	0.012	$\ln(S_{d(DS2)})$	-4.423		
$S_{d(DS2)}[m]$	0.021	$\ln(S_{d(DS3)})$	-3.863		
$S_{d(DS4)}[m]$	0.028	$\ln(S_{d(DS4)})$	-3.576		
Probability of exeedance of each damage state at different levels of PGA $P_{ij}(S_d > S_{d(DSi)} \mid PGA_j) = 1 - \Phi\left[\frac{\ln(S_{d(DSi)}) - \lambda_{Sd(PGAj)}}{\beta_{Sd(PGAj)}}\right]$					
$PGA_j[g]$	0.21	0.36	0.51	0.66	0.81
$P_{DS1,PGAj}$	0.168	0.706	0.926	0.985	0.998
$P_{DS2,PGAj}$	0.013	0.259	0.628	0.858	0.959
$P_{DS3,PGAj}$	0.000	0.045	0.253	0.540	0.777
$P_{DS4,PGAj}$	0.000	0.014	0.126	0.355	0.614

6) The probability data points shown in Table 2.6 is then fitted with a lognormal probability distribution in terms of spectral displacement through mapping between the PGA level and the corresponding median displacement demand $\bar{S}_d$ as shown in Figure 2.13.

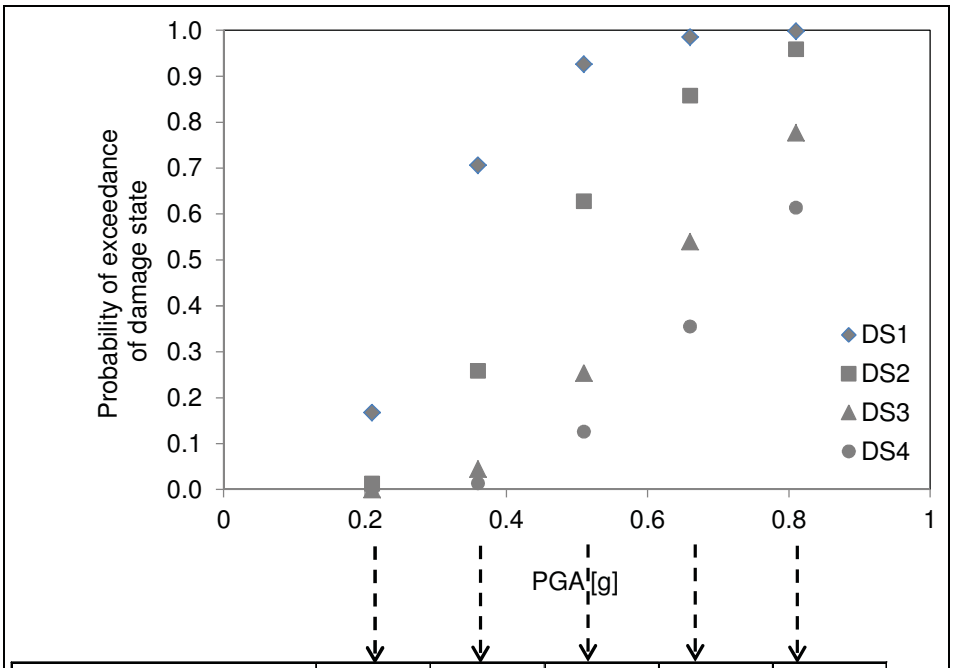

$PGA_j[g]$	0.21	0.36	0.51	0.66	0.81
$\bar{S}_d[m]$	0.004	0.009	0.014	0.020	0.031
$\lambda_{Sd}(PGA_j) = \ln(\bar{S}_d)$	-5.413	-4.657	-4.238	-3.908	-3.478

Figure 2.13 Mapping between the probabilities points in terms of PGA to spectral displacement.

The fitting is conducted using the definition of the standard normal variable $Z(DSi) = \Phi^{-1}(P_{DSi})$ for a lognormal function is linearly proportional to $\ln(\bar{S}_d)$ (Figure 2.14a). The slope of the linear relation is the lognormal standard deviation $\bar{\beta}_{DSi}$ which represents the combined variability of capacity and demand $CONV(\beta_C, \beta_D)$ (Figure 2.14b).

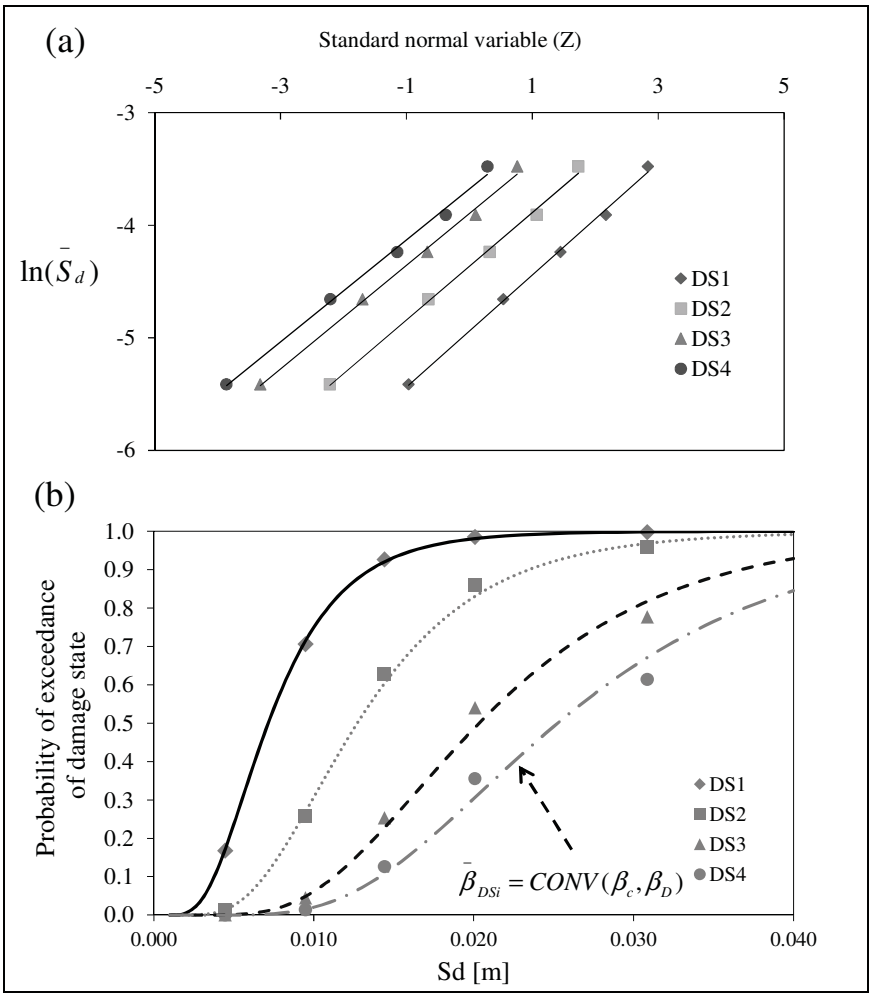

Figure 2.14 Fitting of the probability distribution of combined uncertainty of capacity and demand parameters for different damage state (a) the standard normal variable domain and (b) the cumulative lognormal functions.

The final displacement based fragility function lognormal distributed are given in (Table 2.7) along with the respective values implicit in Hazus and ELER. The $\bar{\beta}_{DSi} = CONV(\beta_C, \beta_D)$ value combined with the lognormal standard deviations of the damage state thresholds, β_T, obtained from the damage model (Table 2.2) yields the total lognormal standard deviation for each damage state $\beta_{DS} = \sqrt{CONV(\beta_C, \beta_D)^2 + \beta_T{}^2}$).

Table 2.7 Fragility curves parameters for stone masonry buildings and respective values implicit in Hazus and ELER.

	Quebec Stone, low-rise		**ELER stone, low-rise**		**Hazus pre-code URM, low-rise**	
Damage state	Median S_d [m]	Total dispersion β_{DS}	Median S_d [m]	Total dispersion β_{DS}	Median S_d [m]	Total dispersion β_{DS}
DS1 [Slight]	0.005	0.53	0.002	1.02	0.008	0.99
DS2 [Moderate]	0.012	0.61	0.004	1.02	0.016	1.05
DS3 [Extensive]	0.021	0.62	0.007	1.02	0.041	1.10
DS4 [Complete]	0.028	0.67	0.012	1.02	0.096	1.10

2.7 Fragility based damage assessment

The resulting displacement based fragility functions with combined variability in capacity, seismic demand and damage state threshold, were used to determine the damage state probabilities for low-rise stone masonry buildings in Old Québec City for seismic input motion with 2% probability of exceedance in 50 years (Adams and Halchuk, 2003).

The displacement coefficient method (Equation 2.8), was used to evaluate the spectral displacement demand as an input to the displacement based fragility curves. The median period $T_y = 0.18\text{sec}$ and yield acceleration $S_{ay} = 0.3g$ of the low-rise stone masonry buildings were obtained from the capacity model and the corresponding 2%/50 years spectral acceleration for 5% damping $S_a(T_y)$ = 0.58g. The estimated spectral displacement was S_d = 0.01m. For the given spectral displacement demand, discrete damage state probabilities are evaluated as the difference of the cumulative probabilities of reaching or exceeding successive damage states (Figure 2.15a).

The computed final damage state probabilities are compared to the respective damage probabilities obtained applying displacement fragility curves defined in Hazus and ELER (Figure 2.15b)**.** Damage estimates generated by this study indicate that slight to moderate damage will be the most probable damage experienced by the considered stone masonry buildings. As expected, Hazus shows highest probability of no to slight damage due to the higher deformation capacity assumed for brick masonry, whereas the highest probabilities of extensive and complete damage are predicted with ELER due to the assumed lower deformation capacity.

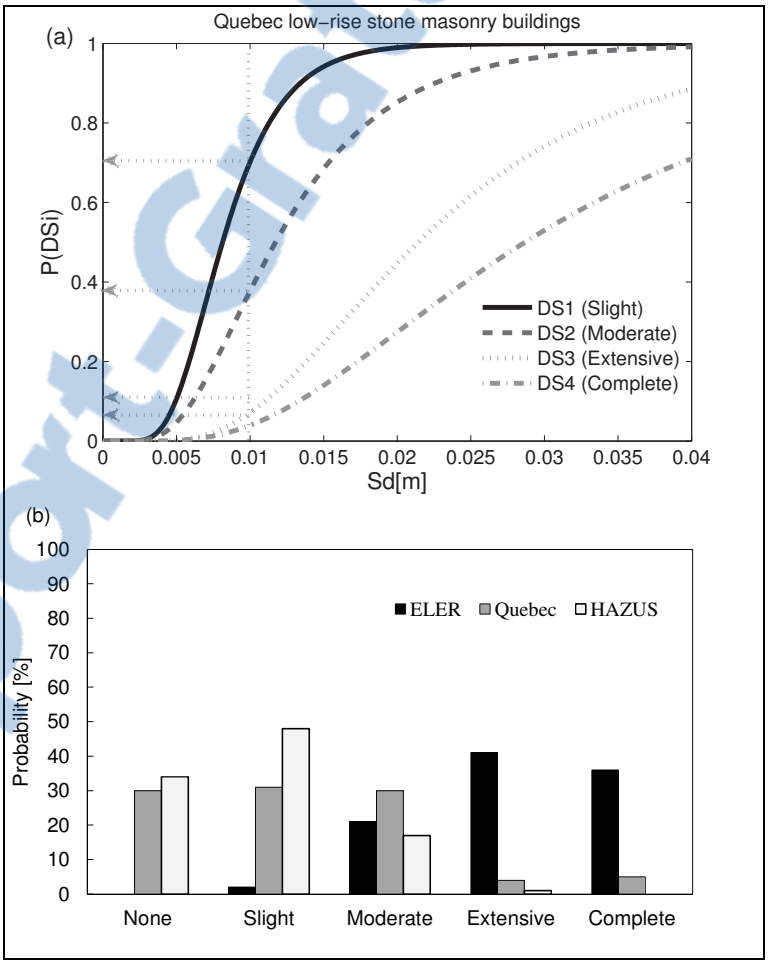

Figure 2.15 Fragility based damage assessment for a spectral displacement corresponding to uniform hazard spectrum with probability of 2%/50 years: (a) fragility curves for low-rise two-story stone masonry buildings in Old Québec City and (b) respective damage state probabilities compared with those obtained with fragility curves implicit in Hazus and ELER.

2.8 Summary and conclusions

A robust procedure for analytical displacement based fragility analysis of stone masonry buildings was presented. Old Québec City was selected as a study area representative for historical urban centers in Eastern Canada. The first step consisted of inventory of the existing stone masonry buildings and characterization of representative typology. Respective building capacity model was developed using a simplified mechanical model with linear elastic and perfectly plastic domains. Displacement based procedure was then used to develop damage state fragility functions, based on drift thresholds of stone masonry walls, assigned based on literature data. A simplified probabilistic seismic demand analysis was proposed to capture the combined uncertainty in capacity and demand on the fragility curves. The generated fragility curves were determined for low-rise stone masonry buildings as functions of spectral displacement. The results of damage assessment for a 2%/50 years uniform hazard seismic scenario indicate that slight to moderate damage will be the most probable damage experienced by these stone masonry buildings.

A comparison of the developed fragility functions was made with those implicit in the seismic risk assessment tools Hazus and ELER. Significant differences have been observed. These differences were replicated in comparatively significant disparities among the probability estimates for different damages states. Hazus showed highest probability of occurring no to slight damage due to the assumed higher deformation capacity, whereas the highest probabilities of extensive and complete damage were predicted with ELER due to the assumed lower deformation capacity. This comparative example showed the importance of the development of specific fragility functions that reflect the generic construction characteristics for the considered study area and emphasized the need of critical use of existing risk assessment tools and the obtained results. It can be expected that using drift thresholds and mechanical characterization obtained from laboratory testing of stone masonry walls representative of those existing in Old Québec City would help to reduce the uncertainties in the damage prediction.

The proposed methodology for fragility analysis can easily be applied to other building types provided that damage state drift thresholds and material properties are available. It has several advantages, first of all in the use of simplified mechanical models for capacity curves generation which proved particularly effective for carrying out analyses of uncertainties with significantly reduced computational time, and then in the use of experimental displacement based damage criteria instead of relying on expert opinion. On the other hand, it does not consider the possible out-of-plane failure mechanisms that might occur in case where poor connection between floor and wall exists. This issue should be considered in future research. In addition, the increased uncertainties in the identification of the complete damage state from experimental data due to the rapid degradation of the stone walls after reaching peak strength should also be taken into consideration.

CHAPTER 3

SEISMIC HAZARD COMPATIBLE VULNERABILITY MODELLING

3.1 Introduction

This chapter presents the results of an effective vulnerability analysis procedure for stone masonry buildings in terms of seismic hazard compatible fragility and vulnerability functions for sets of earthquake scenarios. This vulnerability analysis is based on the work developed in the previous chapter work on stone masonry buildings that developed the two main inputs for the vulnerability analysis: (1) capacity curves that characterize the nonlinear behaviour of the existing stone masonry buildings and (2) displacement based fragility functions that represent the probability of exceedance of specified damage state under various levels of structural displacement response (e.g., slight, moderate, extensive, complete). These two inputs are convolved with response spectra to estimate the structural damage to buildings for a series of earthquake magnitude-distance combinations. The obtained results for typical stone masonry in the old historic centre of Québec City are given.

3.2 Vulnerability modelling procedure

The vulnerability analysis is the essential component of any risk assessment study and describes the relationship between the intensity of the seismic motion and the probability of occurrence of building damage. The vulnerability analysis conducted in this study is shown in Figure 3.1. For a given building type, earthquake magnitude, distance and soil class, the procedures consists of:

1) seismic hazard definition in terms of response spectra defined by structure-independent intensity measures IM (e.g. spectral acceleration at a particular period);
2) structural analysis on the capacity curves developed in Chapter 2, to estimate the seismic demand;
3) damage analysis using the displacement based fragility functions developed in Chapter 2, for the estimated the damage states and,

4) Loss analysis in terms of the mean damage factor (MDF). The MDF is the sum of the probabilities of being in each damage state obtained from the fragility functions, multiplied by a damage factor (DF) that reflects the expected repair to replacement cost ratio for a building experiencing a specific damage state.

To establish the fragility and vulnerability functions in terms of structure-independent IMs, the procedure is repeated for increasing intensity levels. The above procedure revealed to be powerful for conducting rapid vulnerability assessment and the analysis of uncertainties. It is additionally suitable as the structure-independent IM is typically available from the results of seismic hazard analysis (Adams and Halchuk, 2003).

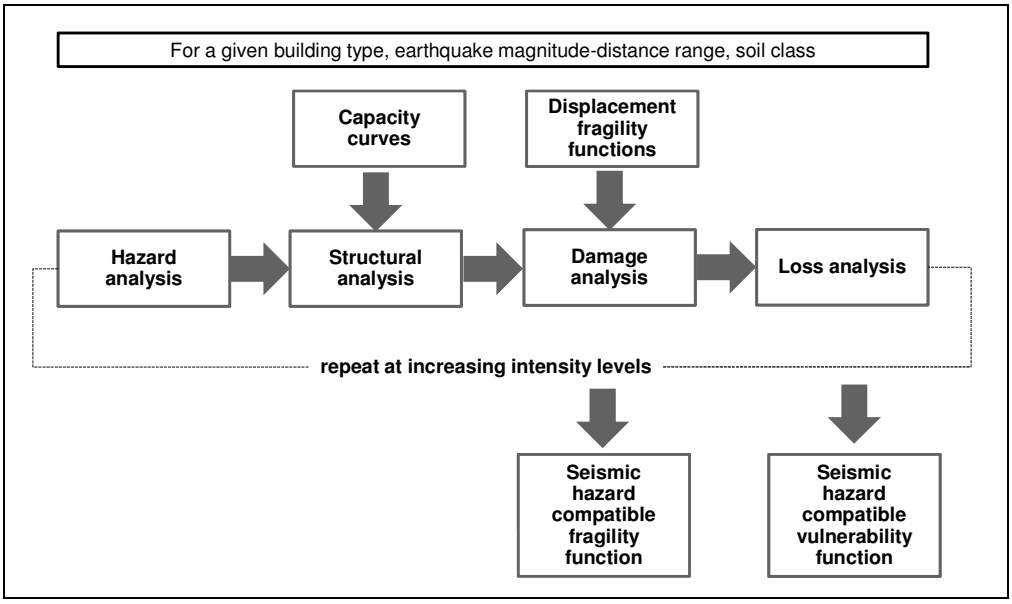

Figure 3.1 Vulnerability modelling procedure.

The structural analysis is conducted in the spectral acceleration (S_a) vs. spectral displacement (S_d) format. The structural response is evaluated using the capacity spectrum method (CSM; Mahaney et al., 1993; ATC 40, 1996). In order to avoid computationally costly iterations to find the structural displacement response (i.e. the performance point) in the CSM procedure, the procedure is amended according to the procedure proposed by (Porter, 2009). The outline

of the procedure is presented herein and more details of the computations can be found in the Appendix-II.

In the CSM, the performance point is typically obtained based on the assumption that the nonlinear response of the system can be modelled as a linear ESDOF with effective period and effective damping. The effective damping of the system is proportional to the area enclosed by the capacity curve to represent the hysteresis energy dissipation. The effective period is assumed to be the secant period at which the seismic ground motion demand, reduced for the equivalent damping, intersects the capacity curve.

The first step of the analysis is to determine the performance point on the spectral acceleration S_a - spectral displacement S_d capacity curve for the considered earthquake magnitude-distance scenario. The corresponding effective damping (ξ_{eff}) is calculated from Equation 3.1. The parameters are shown in Figure 3.2.

$$\xi_{eff} = \xi_e + k\left(\frac{Area}{2\pi S_d S_{ay}}\right)$$
$$Area = 4S_{ay}\left(S_d - S_{dy}\right) \tag{3.1}$$

where ξ_e is the elastic damping ratio of the building, k is the degradation factor that approximately account for the possible strength and stiffness degradation under cyclic loading.

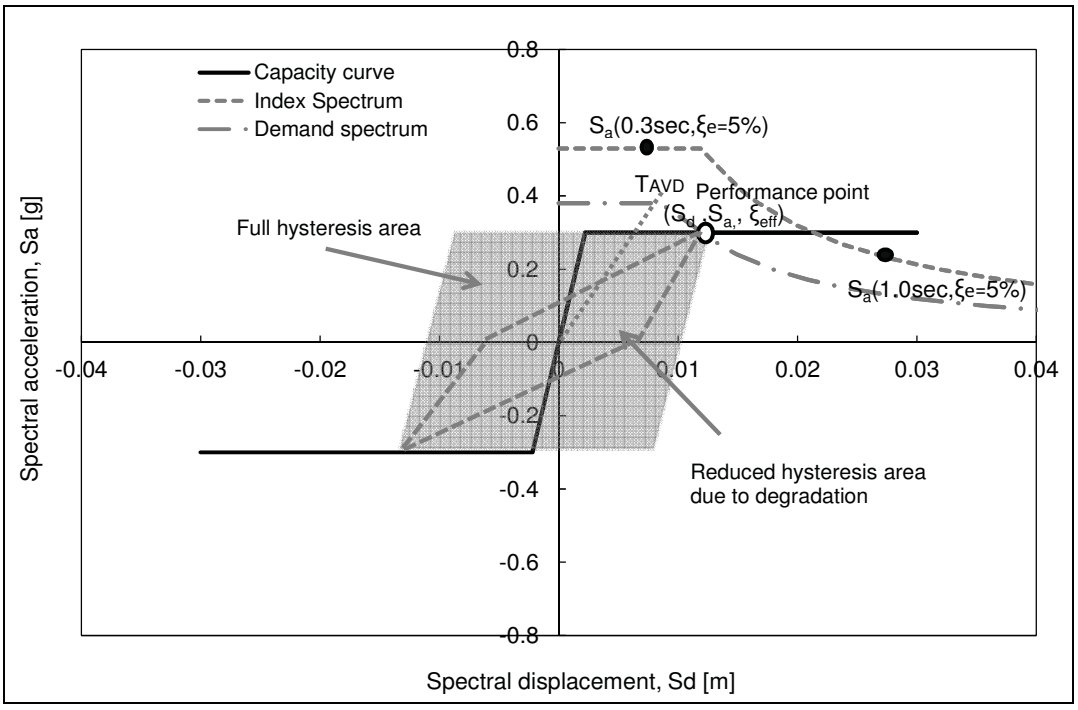

Figure 3.2 Illustration of the evaluation of the performance point in the CSM.

The performance point (S_d,S_a, ξ_{eff}, T) lies on an idealized, site-soil adjusted response spectrum with the same effective damping ratio and called the demand spectrum. Considering the effect of damping, the demand spectrum is then related to a 5% damped site-soil adjusted response spectrum referred to as the index spectrum. The index spectrum has a constant acceleration portion parameterized via its spectral acceleration at 0.3sec denoted by (Sa0.3 sec, 5%), and a constant velocity portion parameterized via (Sa1.0 sec, 5%). These are the structure-independent IMs. The associated values of the structure-independent IMs of the site-soil response spectrum are obtained using the spectral reduction factor (ATC-40, 1996) relationship as shown in Equation 3.2.

$$
\begin{aligned}
&S_a = S_a(0.3\sec, 5\%)/R_A \qquad 0 < T < T_{AVD} \\
&S_a = S_a(1.0\sec, 5\%)/R_V T \qquad T_{AVD} \le T \\
&R_A = 2.12/(3.21 - 0.68\ln\xi_{eff}) \\
&R_V = 1.65/(2.31 - 0.41\ln\xi_{eff}) \\
&T_{AVD} = \frac{S_a(1.0\sec, 5\%)R_A}{S_a(0.3\sec, 5\%)R_V}
\end{aligned}
\tag{3.2}
$$

Where R_A and R_V are the spectral reduction factor for the constant acceleration and velocity regions, respectively. The T_{AVD} denotes the period at the intersection of the constant acceleration and velocity regions.

The second step is to work forward from the performance point into a set of displacement based fragility functions, previously developed in Chapter 2, to determine the probability of damage state as follows:

$$
\begin{aligned}
P\left[DS = ds \mid S_d = x\right] &= 1 - \Phi\left(\frac{\ln\left[x/\lambda_1\right]}{\beta_1}\right) && ds=0 \\
&= \Phi\left(\frac{\ln\left[x/\lambda_{ds}\right]}{\beta_{ds}}\right) - \Phi\left(\frac{\ln\left[x/\lambda_{ds+1}\right]}{\beta_{ds+1}}\right) && 1 \le ds \le 3 \\
&= \Phi\left(\frac{\ln\left[x/\lambda_4\right]}{\beta_4}\right) && ds=4
\end{aligned}
\tag{3.3}
$$

Where $P\left[DS = ds \mid S_d = x\right]$ denotes the probability of structural damage state ds given that S_d takes on some particular value x, and Φ denotes the cumulative standard normal distribution. The parameters λ_{ds} , β_{ds} denote, respectively, the median and logarithmic standard deviation values of the fragility function to resist damage state *ds* from 0 as no damage, 1 as slight damage, 2 as moderate damage, 3 as extensive damage and 4 as complete damage. The obtained probabilities are recorded conditioned to the computed IM in the previous step (Figure 3.3).

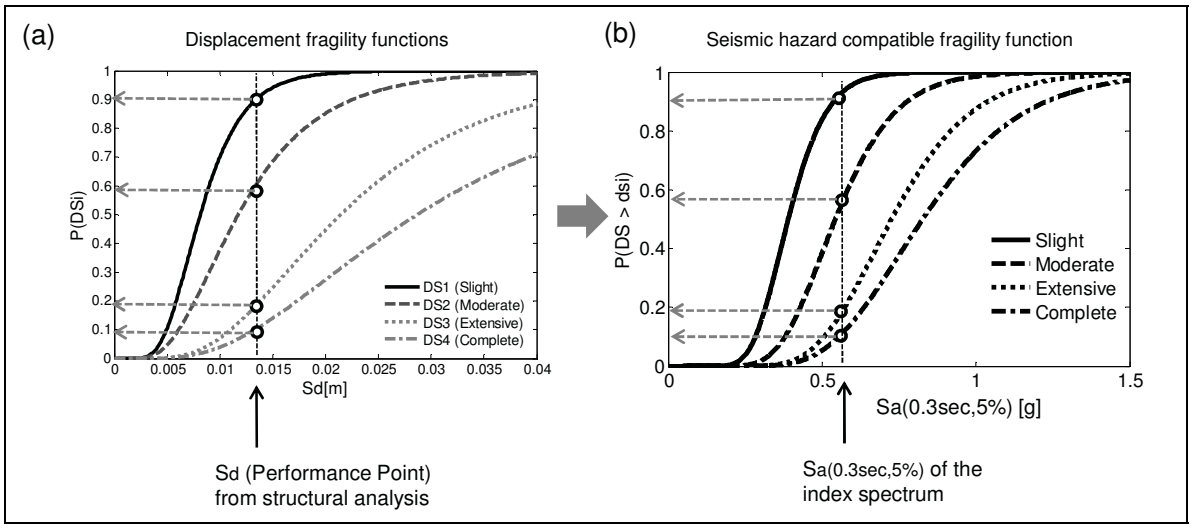

Figure 3.3 Illustration of the mapping of damage state probabilities from: (a) the spectral displacement response, to (b) to the structure-independent IM fragility function.

Finally, the integration of the loss conditioned on the probability of being in each damage state was conducted to determine the MDF at the computed IM (Figure 3.4). The DF, central value in a range of damage factors, used to predict the MDF were calibrated based on post-earthquake damage data (Kircher et al., 1997b) as : 2% of the building structural system replacement cost for slight structural damage, 10% for moderate damage, 50% for extensive damage, and 100% for complete damage as follows:

$$MDF = \sum_{dsi=1}^{4} P[DS = ds_i \mid S_a(0.3\text{sec},5\%)].DF_{dsi} \qquad (3.4)$$

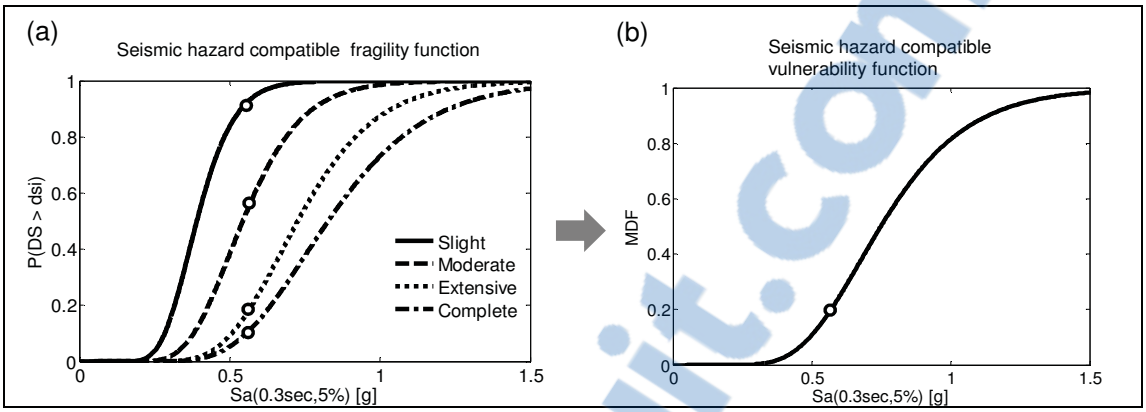

Figure 3.4 Illustration of the mapping from: (a) the seismic fragility function to (b) the vulnerability function.

To establish the fragility and vulnerability functions in terms of structure-independent IMs, the procedure is repeated for increasing intensity levels. The computed probabilistic damage states and mean damage factor are recorded for respective structure-independent IM. The data are then fitted to provide suitable hazard compatible seismic fragility and vulnerability functions as a lognormal cumulative probability functions (Figure 3.4).

The vulnerability modelling approach developed in this study was inspired by the procedure employed in Hazus (FEMA, 2003) which applies the CSM for structural analysis and capacity and displacement fragility curves for damage analysis. However, Hazus procedure does not offer seismic fragility functions in a tabular or graphical form plotted against a structure-independent intensity measure. Moreover, Hazus vulnerability procedure involves iteration to estimate structural response with the help of the capacity spectrum method. It is thus difficult to relate back the predicted damage to a structure-independent intensity measure. In order to overcome these difficulties, the proposed methodology provides a non-iterative solution to the CSM starting with a given value for the structural response S_d, calculating the respective S_a for the performance point on the capacity curve, calculating the effective damping, and going back to the associated values of Sa0.3 sec and Sa1.0 sec for 5% of the site-soil-adjusted idealized demand (input) response spectrum. Then, the method uses the performance point to compute the probability of a given damage state and relates the two end products: damage vs. structure-independent intensity measure, Sa0.3 sec and 5%

damping in this case. The Hazus vulnerability procedure, on the other hand, starts from the demand spectrum given Sa0.3 sec and Sa1.0 sec for 5% damping, calculating forward the performance point with S_d and S_a for respective effective damping, which requires iterative procedure, and then estimates the probability of the damage states. The computational demands of the iteration can be significant for a large portfolio or a probabilistic risk assessment, whereas having predefined fragility functions in terms of a structure-independent IM greatly reduces the computational demands.

3.3 Scenario based vulnerability assessment

The procedure described above is applied to obtain sets of fragility and vulnerability functions for typical stone masonry buildings in Old Quebec City. The earthquake scenarios are generated based on two moment magnitudes, M6 and M7, and ranges of hypocentral rupture distances (R) varying from 10 to 30 and from 20 to 60 km, respectively. The idealized elastic response spectra is built using the Sa(0.3sec) and Sa(1.0sec) for 5% damping computed with ground motion prediction equation (GMPE) for reference site-class C developed by Atkinson and Boore (2006) for Eastern North America - AB06 (Figure 3.5). Details of the AB06 GMPE can be found in Appendix-III.

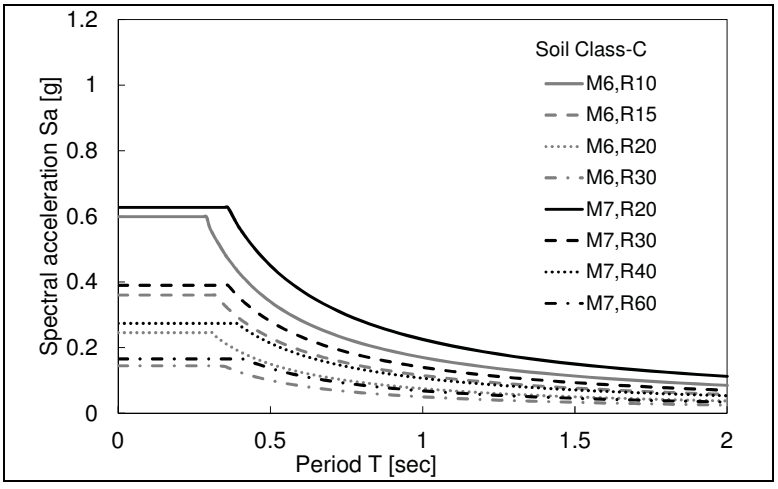

Figure 3.5 Idealized response spectra for scenario earthquakes using Sa0.3 sec and Sa1.0 sec values from AB06 GMPE. M is moment magnitude and R is hypocentral distance in km.

The structure-independent IM (Sa0.3 sec, with 5% damping) is selected to represent the demand on short period systems such as stone masonry buildings. In order to take into account the possible strength and stiffness degradation under seismic loading for masonry buildings, a degradation factor *k* of 0.2 was fixed in the calculation of effective damping at the performance point as typically recommended for unreinforced masonry buildings (FEMA, 2003). The developed fragility functions are shown in Figure 3.6 and the corresponding vulnerability functions are shown in Figure 3.7. It can be observed from Figs. 3.6 and 3.7 that the shape of the developed fragility and vulnerability functions are more sensitive to earthquake magnitude than to hypocentral distances when expressed as functions of Sa0.3sec.

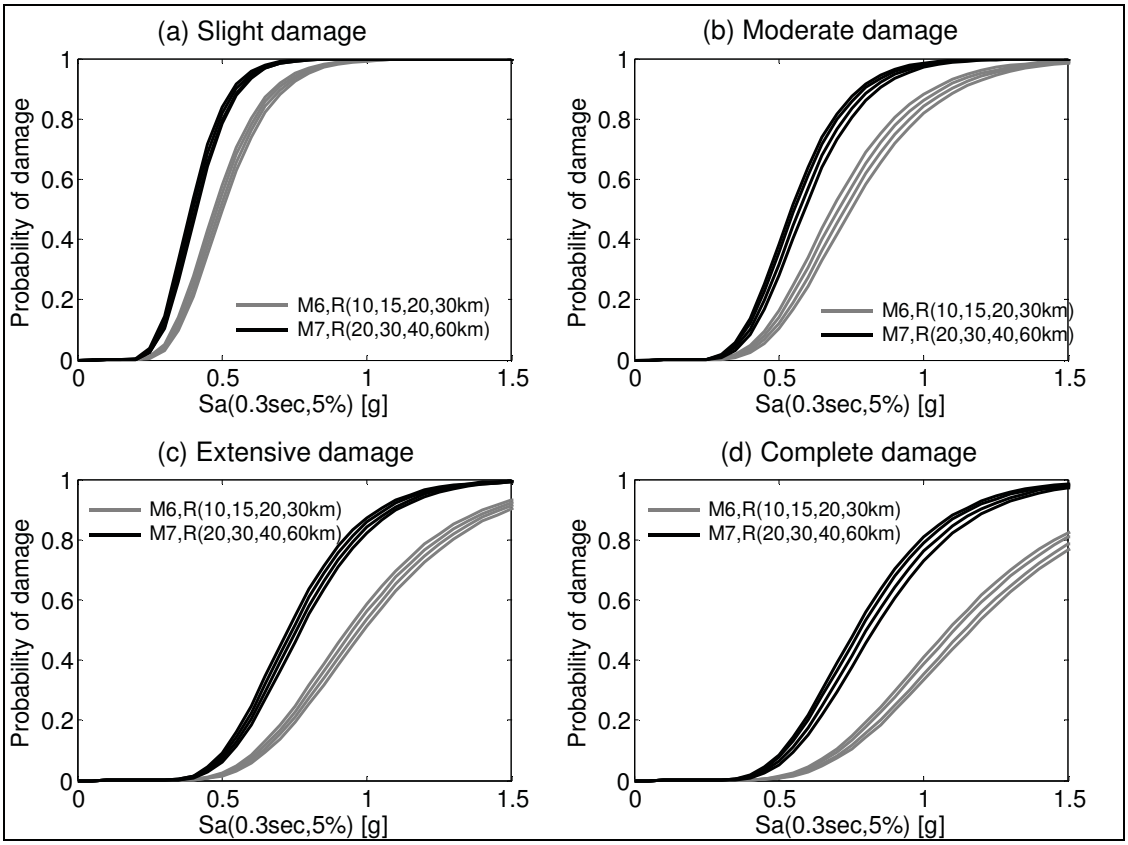

Figure 3.6 Seismic fragility functions for: (a) slight, (b) moderate, (c) extensive and (d) complete damage.

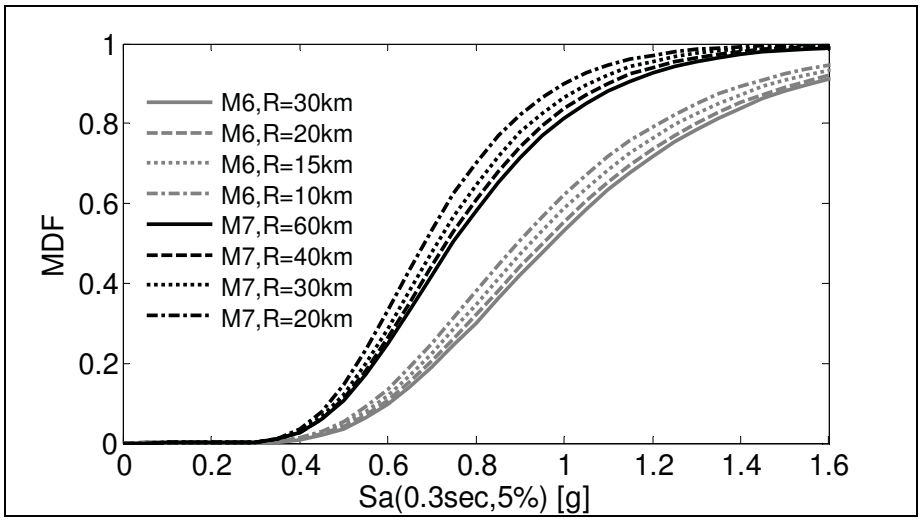

Figure 3.7 Vulnerability functions for different earthquake scenarios given as function of the IM Sa0.3 sec and 5% damping.

The sensitivity of the shape of the fragility and vulnerability functions to earthquake magnitude can be explained by several factors: (1) the magnitude has more influence on the response spectrum shape and consequently on the shape of the idealized spectrum determined by Sa0.3sec and Sa1.0sec; (2) in the structural analysis stage, the response in terms of spectral displacement demand, i.e., the performance point, typically falls on the constant velocity portion of the idealized spectrum, the range between 0.3s and 1.0s which is more influenced by magnitude than by hypocentral distance as shown in Figure 3.8; (3) for nearly similar IM values of Sa0.3sec, e.g. M7R20(Sa0.3sec=0.62g) and M6R10(Sa0.3sec=0.59g), the respective M7R20 spectrum induces more displacement demand than M6R10 spectrum; and (4) the predicted displacement demand is combined to the lognormal fragility functions to predict damage which additionally increases the differences in the predicted damage as shown in Figure 3.9.

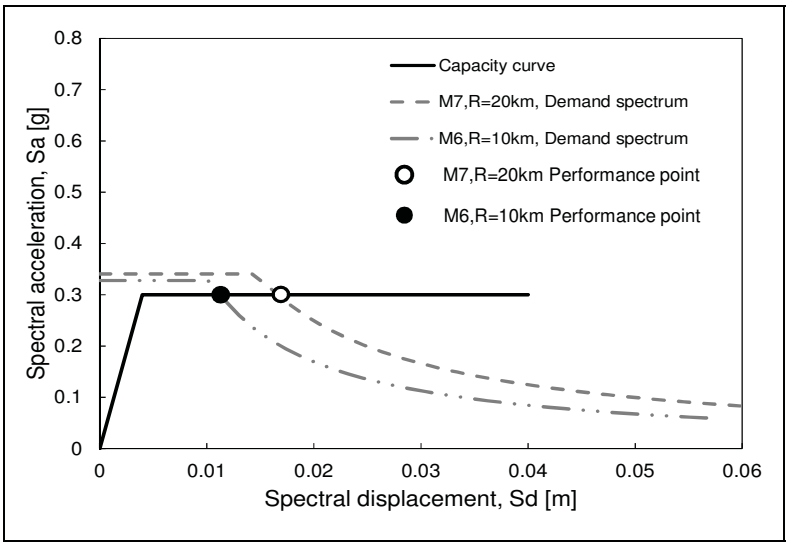

Figure 3.8 Illustration of the earthquake magnitude influence on the performance point and the demand spectra.

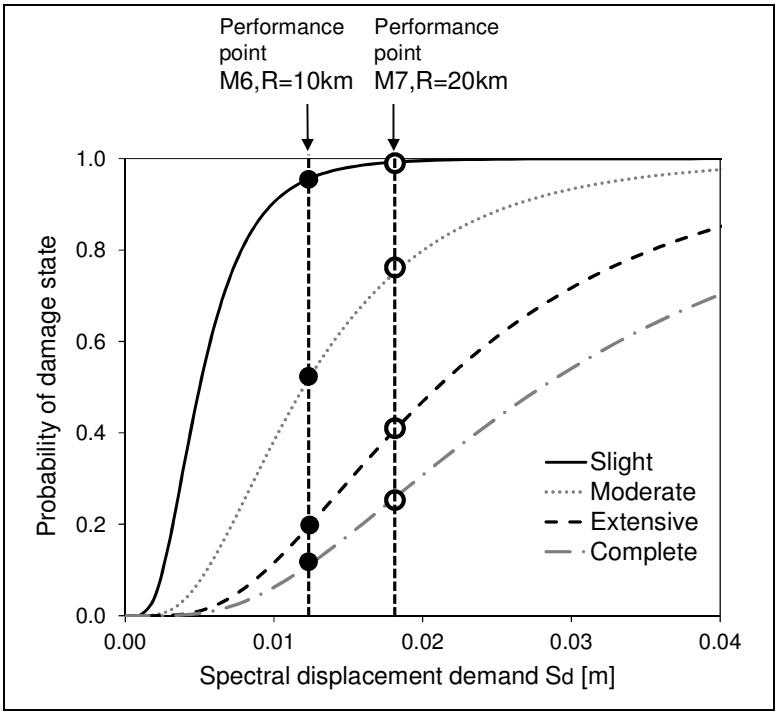

Figure 3.9 Illustration of the earthquake magnitude influence on the predicted displacement and the corresponding damage.

The developed functions are used to predict the damage distribution for IM of Sa0.3sec from the response spectra for respective shaking scenarios. The damage distributions are shown in Figure 3.10 and Table 3.1 . As expected, the most damaging scenario is M7R20, which generates average MDF of 28% and 18% of red-tagged buildings according to the ATC-20 safety tag color (ATC, 1996), i.e., complete damage state. It can also be noted that the proportion of buildings in the complete damage state (18%) is higher than that in the extensive damage state (11%). This can be explained by the relatively small gap between the extensive and complete damage states of the developed displacement fragility functions. This is typical for buildings with low deformation capacity such as stone masonry buildings. The extensive damage state typically reflects a system which has reached its peak strength, after which only a slight increase in displacement demand results in rapid collapse.

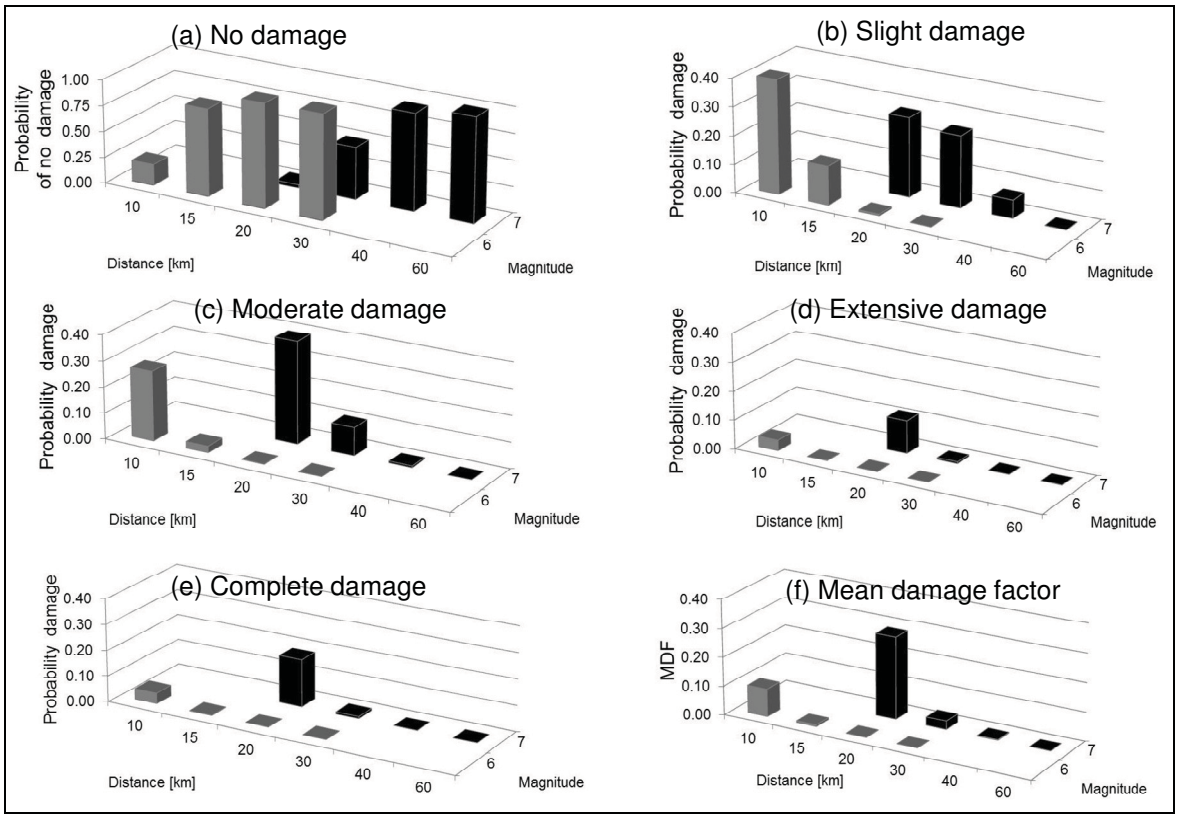

Figure 3.10 Seismic damage de-aggregation for stone masonry buildings (a) none, (b) slight, (c) moderate, (d) extensive, (e) complete damage and (f) mean damage factor

Table 3.1 Probability of damage distribution for different M and R for stone masonry buildings.

	Probability of no damage					
	Distance (R) [km]					
Magnitude (M)	10	15	20	30	40	60
6	0.20	0.84	0.99	1.00		
7			0.03	0.50	0.93	1.00
	Probability of slight damage					
	Distance (R) [km]					
Magnitude (M)	10	15	20	30	40	60
6	0.45	0.14	0.01	0.00		
7			0.28	0.25	0.06	0.00
	Probability of moderate damage					
	Distance (R) [km]					
Magnitude (M)	10	15	20	30	40	60
6	0.27	0.02	0.00	0.00		
7			0.39	0.11	0.01	0.00
	Probability of Extensive damage					
	Distance (R) [km]					
Magnitude (M)	10	15	20	30	40	60
6	0.04	0.00	0.00	0.00		
7			0.11	0.01	0.00	0.00
	Probability of Complete damage					
	Distance (R) [km]					
Magnitude (M)	10	15	20	30	40	60
6	0.07	0.00	0.00	0.00		
7			0.18	0.01	0.00	0.00
	Mean damage factor (MDF)					
	Distance (R) [km]					
Magnitude (M)	10	15	20	30	40	60
6	0.11	0.01	0.00	0.00		
7			0.28	0.03	0.00	0.00

3.4 Summary and conclusions

A robust analytical procedure for the development of seismic hazard compatible fragility and vulnerability functions of stone masonry buildings is presented. The vulnerability analysis procedure is a subsequent step of the development of the two main inputs for the vulnerability analysis: (1) capacity curves that characterize the nonlinear behaviour of the existing stone masonry buildings and (2) displacement based fragility functions that represent the probability of exceedance of specified damage state under various levels of structural response. These two inputs are convolved with response spectra to estimate the structural damage to buildings for a series of earthquake magnitude-distance combinations. The results are sets of seismic hazard compatible vulnerability functions that can be directly used with seismic hazard analysis output that is typically presented in terms of structure-independent intensity measure (IM). Therefore, the procedure revealed to be powerful for conducting rapid vulnerability assessment of building classes. Moreover, the procedure leads to the reduction of the computational time of vulnerability assessment when a sensitivity analysis is to be conducted. A scenario-based vulnerability assessment of stone masonry building was also conducted as an example to demonstrate the capacities of the procedure. As expected, the most damaging scenario was M7R20, which generates average MDF of 28% and 18% of red-tagged buildings, i.e., complete damage. The presented vulnerability assessment procedure will be used to develop vulnerability functions for other buildings types present in Old Québec City with proper specific capacity and displacement based fragility functions (Chapter 5).

CHAPTER 4

SENSITIVITY ANALYSIS ON VULNERABILITY MODELLING

4.1 Introduction

Vulnerability modeling is usually constrained by limited information and knowledge and uncertainties arise throughout the assessment process. One of the most important aspects in development of a seismic vulnerability model is to identify, quantify and incorporate the uncertainties associated with each of the input parameter (Crowley et al., 2005).

The objective of this chapter is to investigate the uncertainties in analytical vulnerability modelling of stone masonry buildings. The conducted sensitivity analyses will contribute to the identification of critical parameters with significant impact on the damage estimates.

The following parameters were considered in the sensitivity analyses: (1) structural parameters: yield acceleration S_{ay} of the capacity curve, elastic damping ratio ξe, and degradation factor k ; (2) damage parameters: displacement fragility functions defined by median λ and standard deviation β ; and (3) loss parameters: repair cost ratio DF. A base case scenario was run first with default parameters used for the development of the vulnerability function for the low-rise stone masonry building. For each parameter, a set of increments was considered next in the range of ±25% and ±50% and with respect to the base case scenario. The vulnerability functions were then developed by varying the values of the considered parameter and leaving the remaining parameters unchanged, i.e., with values equal to those of the base case scenario. The respective sensitivity was determined by measuring the deviation from the base-case scenario. The absolute value of the difference from the base-case scenario MDF (swing) is retained as a measure of the sensitivity (Porter et al., 2002), where parameters that have larger swing have more impact on the final MDF results and are considered critical for the analytical vulnerability modeling. In addition, three levels of structure-independent IMs were considered, IM (Sa0.3 sec) = 0.4g, 0.5g and 0.6g, to study the impact of the seismic intensity on the sensitivity to each of the considered parameters.

4.2 Variation in structural parameters

The investigate structural parameters are: (1) the yield acceleration of the capacity curves S_{ay}, (2) the elastic damping ratio ξ_e and (3) the structural degradation factor k.

Capacity curve reflects the lateral resistance envelope for an ESDOF representation of a building under seismic loading. The simplified mechanical model presented in chapter 2 is used for the development of ideal elasto-plastic capacity curves, which considers variable material properties (e.g., compressive strength, shear strength). The median capacity curve with S_{ay}=0.3g is selected for the base-case scenario, and the yield spectral acceleration is varied in the predefined increments of ±25% and ±50%.

The CSM adopted for the structural analysis assumes a simple ESDOF system with equivalent effective damping, defined as a sum of the elastic damping and the hysteretic damping (ATC, 1996). The elastic viscous damping considers the energy dissipated by the structure in the elastic range. This dissipation can be attributed to various mechanisms such as interaction between structural and non-structural elements, small cracking effects during elastic loading. The base-case scenario elastic damping is fixed to 10% (FEMA, 2003; Benedetti et al., 1998).

The hysteretic damping reflects the energy dissipated under cyclic earthquake loading, i.e., area enclosed by the hysteresis loop under the capacity curve, and is dependent on the response amplitude (ATC, 1996). This considers potential degradation of the structural energy-absorption capacity during the cyclic earthquake loading defined by a degradation factor, k, which is a function of the strong motion duration and the structural system. The assumed degradation factor for the base-case scenario is k=0.2 (FEMA, 2003). Table 4.1 shows the investigated variations in the structural parameters.

Table 4.1 Variation in structural parameters for sensitivity analysis.

Structural parameter	**Range of variation**				
	-50%	**-25%**	**Base-case scenario**	**25%**	**50%**
Yield acceleration of the capacity curve S_{ay} [g]	0.15	0.225	0.3	0.375	0.45
Elastic damping ratio ξ_e [%]	5	7.5	10	12.5	15
Degradation factor k [-]	0.1	0.15	0.2	0.25	0.3

4.3 Variation in damage parameters

Displacement based fragility functions represents the probability of being in or exceeding a specific damage state for a given a displacement response. It is typically presented in a form of lognormal cumulative distribution function with a median (λ, threshold displacement of a damage state), and a lognormal standard deviation (β) that includes the uncertainties of being in a damage state. In order to investigate these parameters, the sensitivity analysis was conducted for two conditions: (1) varying λ for all damage states while keeping the same β as for the base-case scenario, and (2) varying β for all damage states while λ remained the same as for base-case scenario. Table 4.2 shows the investigated variations in the damage parameters and Figure 4.1 shows an example for a complete damage state with incremental λ (a) and with incremental β (b).

Table 4.2 Variations in the damage states medians and standard deviations.

Damage states median S_d[m]	**Range of variation**				
	-50%	**-25%**	**Base-case scenario**	**25%**	**50%**
DS1 [Slight]	0.003	0.005	0.006	0.008	0.009
DS2 [Moderate]	0.006	0.009	0.012	0.015	0.018
DS3 [Extensive]	0.011	0.016	0.021	0.026	0.032
DS4 [Complete]	0.014	0.021	0.028	0.035	0.042
Damage states standard deviation β	Range of variation				
	-50%	-25%	Base-case scenario	25%	50%
DS1 [Slight]	0.27	0.40	0.53	0.66	0.80
DS2 [Moderate]	0.31	0.46	0.61	0.76	0.92
DS3 [Extensive]	0.31	0.47	0.62	0.78	0.93
DS4 [Complete]	0.34	0.50	0.67	0.84	1.01

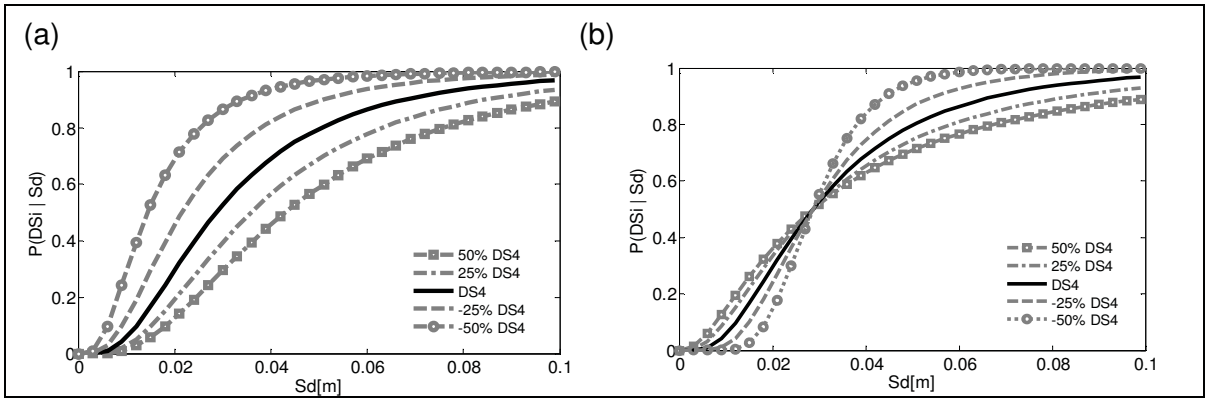

Figure 4.1 Displacement fragility curves for complete damage state:
(a) incremental median and (b) incremental standard deviation.

4.4 Variation in loss parameters

The damage factor (DF) defines the expected repair to replacement cost ratios for each damage state. The base-case scenario DFs are those recommended by Kircher et al. (1997b). These factors were calibrated according to the observed damage states during past destructive

earthquakes in California to better reflect observed earthquake losses. The investigated ±25% and ±50% values for DFs are also listed in Table 4.3. Note that the damage factor corresponding to complete damage state cannot be higher than one.

Table 4.3 Damage factors corresponding to different damage states.

Damage state	**Damage factor (DF)**				
	-50%	**-25%**	**Base-case scenario**	**25%**	**50%**
Slight	0.01	0.015	0.02	0.025	0.03
Moderate	0.05	0.075	0.10	0.125	0.15
Extensive	0.25	0.375	0.50	0.625	0.75
Complete	0.50	0.75	1.00	1.00	1.00

4.5 Sensitivity analysis results

Table 4.4 and Figure 4.2 illustrate the sensitivity of the resulting MDF to the studied input parameters indicated with the deviation from the base case scenario input parameters for ±25% and ±50% ranges. The computation was conducted for three different levels of ground motion intensity, (i.e., for structure independent IM) as (Sa0.3sec) = 0.4g, 0.5g, and 0.6g. As expected, whatever the value assigned to the varying parameters, the intensity of the ground shaking controls the magnitude range of the MDF. Among the considered parameters, MDF is most sensitive to the variations in structural parameters (shear and flexural strength of the masonry that define the yield acceleration of the capacity curve) and damage parameters (median and standard deviation of the displacement fragility curves). The MDF is moderately sensitive to the values of the elastic damping, degradation parameter and the DF. The dependency of the variation of the swings on the IM can be better understood using the resulting vulnerability functions in the following sections.

Table 4.4 Sensitivity of the MDF to input parameters at different shaking intensities (IM).

IM (Sa0.3sec)	**0.4g**		**0.5g**		**0.6g**	
MDF (base scenario) at the respective IM	0.03		0.11		0.25	
Parameters	Swing (±25%)	Swing (±50%)	Swing (±25%)	Swing (±50%)	Swing (±25%)	Swing (±50%)
Capacity curves (S_{ay})	0.05	0.16	0.14	0.36	0.23	0.51
Fragility curves median (λ)	0.06	0.15	0.16	0.33	0.25	0.49
Fragility curves Std. dev.(β)	0.05	0.09	0.10	0.18	0.10	0.18
Degradation factor (k)	0.02	0.04	0.06	0.12	0.10	0.21
Elastic damping (ξe)	0.02	0.04	0.06	0.12	0.10	0.20
Damage factors (DFs)	0.01	0.02	0.02	0.06	0.09	0.18

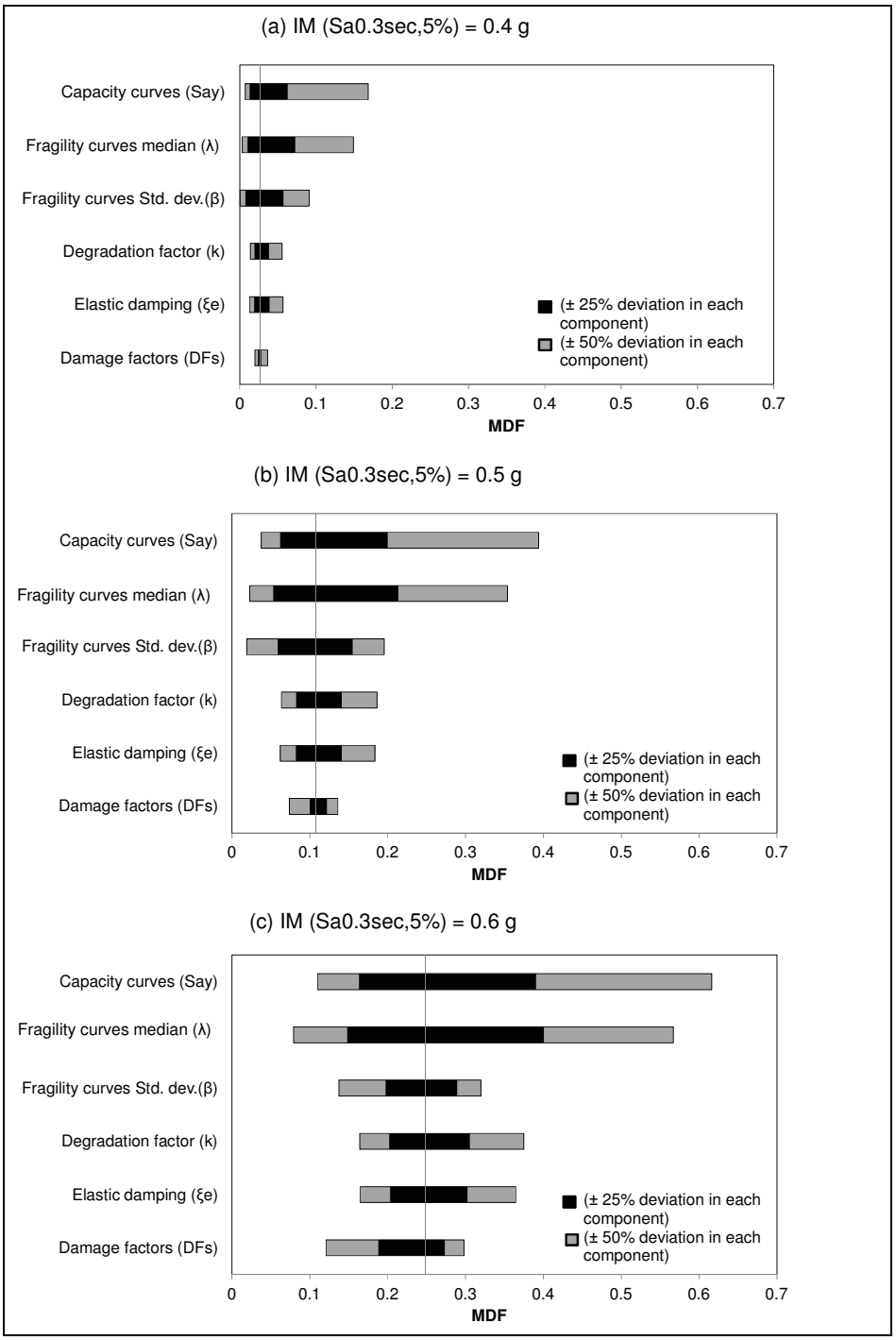

Figure 4.2 Tornado diagrams showing the effect of variation of the input parameters on the MDF results for (a) IM=0.4g, (b) IM=0.5g and (c) IM=0.6g.

4.6 Discussion of the sensitivity analysis results

4.6.1 Structural parameters

The sensitivity of the MDF to the variation in the yield acceleration of the capacity curve, elastic damping and degradation parameter is illustrated in the vulnerability functions shown in Figure 4.3a, b and c at increasing levels of seismic intensity. The sensitivity of MDF to the variation of the structural parameters is mainly due to the difference in the predicted displacement response, i.e., performance point, using CSM. The variation of the yield acceleration has larger effect on the displacement response (performance point) than the elastic damping and the degradation parameter. The displacement response at the performance point is input to the displacement fragility functions, which give the probability of the damage states for that displacement. Due to the log-normal definition of the fragility functions, a slight increase in displacement demand leads to an amplified response in the damage probabilities and consequently in the MDF. This illustrates the complex interaction of the capacity and the displacement fragility functions for damage prediction.

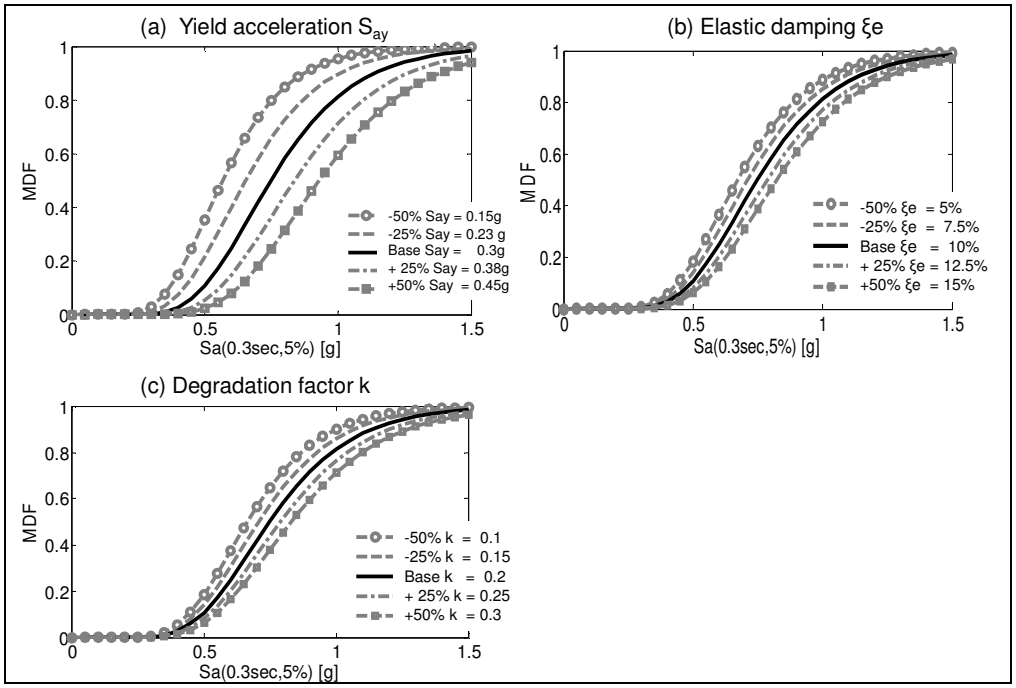

Figure 4.3 Vulnerability functions for variation in input parameters: (a) yield acceleration, (b) elastic damping (c) degradation factor.

4.6.2 Damage parameters

The predicted MDF shows a relatively higher sensitivity to the variation of the median of the displacement fragility functions (λ) compared to the variation in the standard deviation (β) as illustrated in Figure 4.4a and b. Likewise, the MDF sensitivity to both parameters is a function of the IM. The high sensitivity to the variation in the median of the displacement fragility functions can be attributed to the lognormal shape of the displacement fragility functions. This can be illustrated in Figure 4.5 for the prediction of MDFs at different levels of IM. The MDF is inversely proportional with λ (Figure 4.5a) and proportional to the variation of β (Figure 4.5b). The straight line trends show higher sensitivity to the median threshold values of the damage states and lower sensitivity to the standard deviation. At a specific displacement demand, the probability of being in a specific damage state is nonlinearly decreasing with increasing the median, which consequently affects the MDF in a similar manner. The sensitivity to β decreases at IMs that induces displacement demand near the median displacement threshold λ (e.g. the slope of the trend line for Sa0.3sec =0.6g), whereas it increases at IMs that induces displacement demands away from the median λ (e.g. the slope of the trend line for Sa0.3sec =0.5g). This was also reflected in the shape of the vulnerability function, where the sensitivity to β is dependent on the IM that induce a displacement demand near or far from the median thresholds as reflected in the displacement fragility functions (Figure 4.1b).

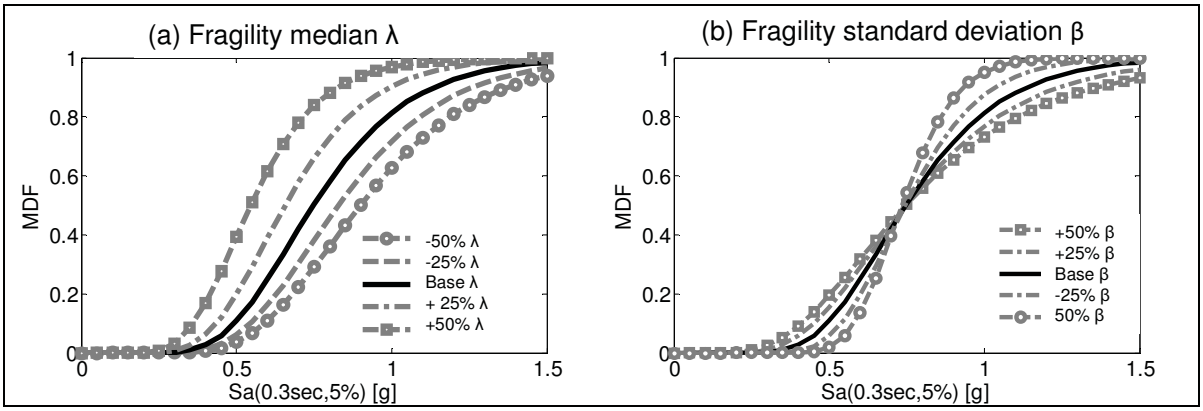

Figure 4.4 Vulnerability functions for variations in input parameters: (a) displacement fragility median and (b) displacement fragility standard deviation.

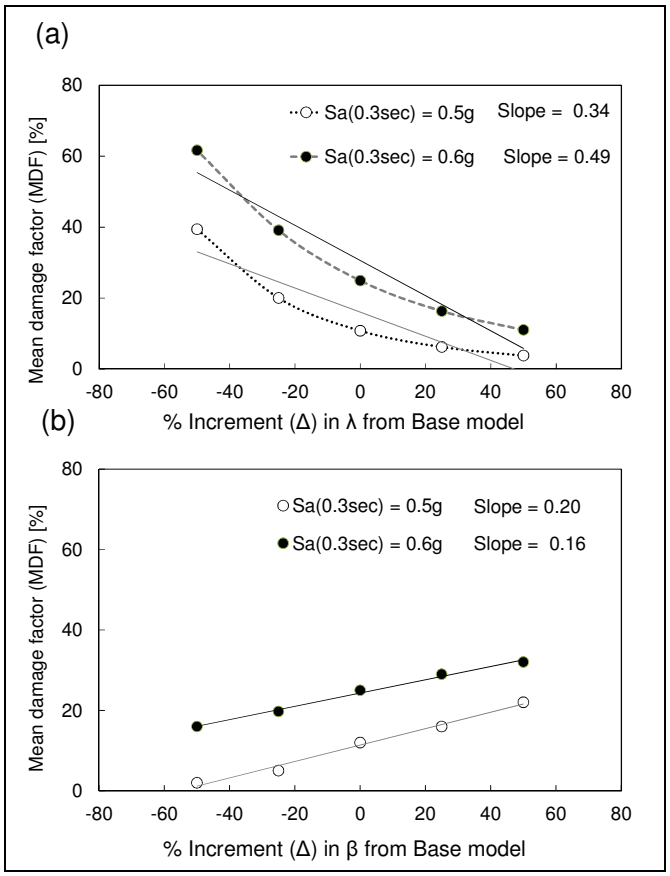

Figure 4.5 Illustration of the sensitivity of the MDF to (a) incremental median and (b) incremental standard deviation of the displacement fragility functions.

4.6.3 Loss parameters

The sensitivity of the MDF to variation in the DFs is also dependent on the IM as illustrated by the slopes of trend lines (Figure 4.6). This is due to the increased probability of complete damage state, which when multiplied by the corresponding DF produces higher MDF. The influence of lower DF values (-50%, -25%) is more pronounced especially at IM higher than 0.4g as indicated in the vulnerability functions shown in Figure 4.7. Note that in the case of increased DFs (+25%, +50%), the complete damage state DF remained the same as the one for the base-case scenario. This results in respective vulnerability functions very close to that of the base-case scenario (Figure 4.7).

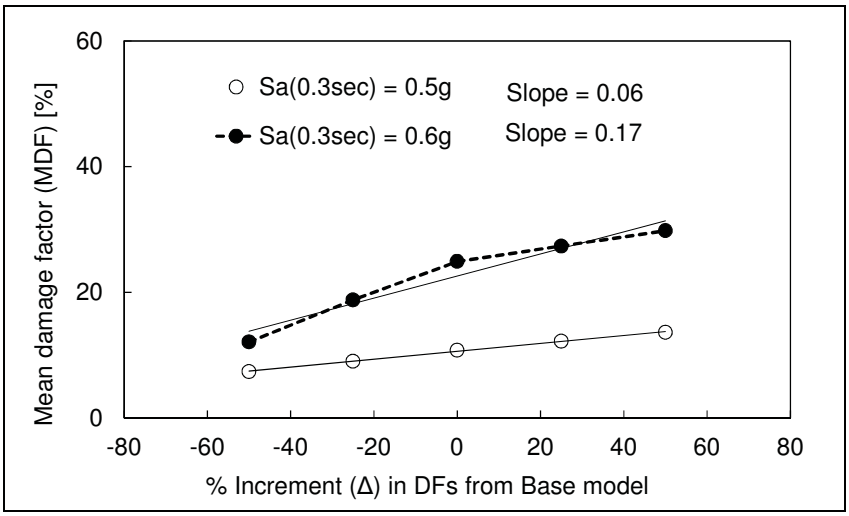

Figure 4.6 Illustration of the sensitivity of the MDF to the uncertainty in the DFs.

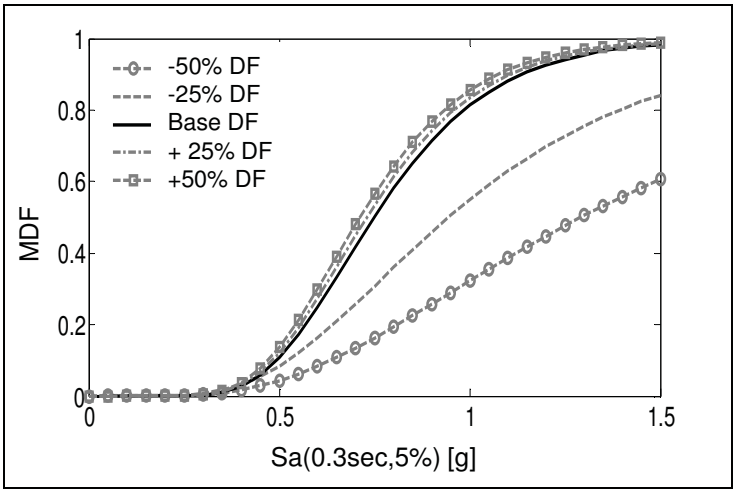

Figure 4.7 Vulnerability functions for variations in input parameters in damage factors.

4.7 Summary and conclusions

One of the most important aspects in development of a seismic vulnerability model is to identify, quantify and incorporate the uncertainties associated with each of the input parameter. Uncertainties in analytical vulnerability modelling of stone masonry buildings were conducted to investigate the sensitivity of the resulting vulnerability functions to the variation of the input parameters.

Three sets of parameters were considered in the analyses: structural parameters (capacity curves yield acceleration, elastic damping, degradation factors), damage parameters (displacement fragility functions median and standard deviation), and loss parameters (repair cost ratio). For each parameter, a set of increments was considered: ±25% and ±50% against the base case scenario. The respective vulnerability functions were developed by varying one parameter at a time while keeping all the others as for the base case scenario. The sensitivity was determined by measuring the deviation from the base-case scenario using tornado diagrams for different levels of seismic intensity. The results showed that MDF was most sensitive to the variation in the medians of the displacement fragility functions and the yield acceleration of the capacity curve. The magnitude of the MDF sensitivity to the variation in the standard deviation of the displacement fragility functions and the DFs corresponding to each damage state depended largely on the ground motion intensity levels. The MDF was moderately sensitive to the elastic damping and the degradation parameter. The observed MDF sensitivity could be reduced with additional knowledge, particularly related to the median threshold values for damage states of the stone masonry buildings and the mechanical properties that affect the capacity curve (i.e. the shear and flexural strength of masonry)

CHAPTER 5

SEISMIC RISK ASSESSMENT OF EXISTING BUILDINGS IN OLD QUÉBEC CITY

5.1 Introduction

This chapter presents the results of an analytical seismic risk assessment study of the Old Québec City, Canada. The framework of seismic risk assessment consists of three components: hazard, inventory, and vulnerability of the inventory given the seismic hazard. The vulnerability modeling consists of the development of analytical seismic fragility and vulnerability functions using the procedure presented in chapter 3. The analytical functions are conditioned to a structure-independent hazard intensity measure (IM), e.g. spectral acceleration at a particular period. The study include an inventory analysis of some 1220 existing buildings, mainly pre-code unreinforced brick and stone masonry. The distribution of the potential damage is evaluated for a scenario M6.2R15 event which corresponds to a probability of exceedance of 2% in 50 years (Adams and Halchuk, 2003). The resulting distribution of damage for the selected seismic scenario is presented.

5.2 Seismic risk assessment input models

The analytical seismic risk assessment framework for existing buildings requires three input models: (1) buildings inventory model of existing buildings types and classification of buildings according to construction material, height and design level, (2) seismic hazard model using a ground-motion prediction equation compatible to the seismo-tectonic settings at the study region to estimate shaking intensity in terms of a structure-independent IM, (3) vulnerability model represented as seismic hazard compatible fragility functions in terms of structure-independent intensity measure (IM) which in this study is Sa(0.3sec). The output is the estimated damage magnitude and distribution. Figure 5.1 shows the flow chart for seismic risk assessment methodology.

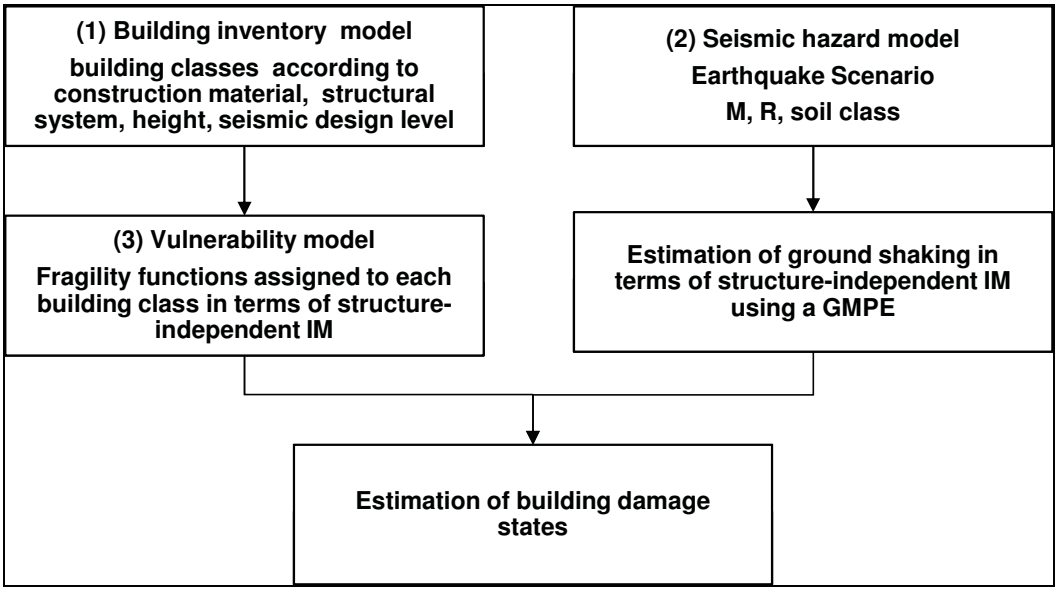

Figure 5.1 Flow chart for seismic risk assessment of building classes.

5.2.1 Inventory

The building inventory was compiled by a combination of data from the municipal database of the city of Québec and from the field survey of 1220 buildings (Nollet et al. 2012). The inventoried buildings were classified according to: (1) construction material, e.g. wood, steel, concrete, stone masonry; (2) structural system, e.g. frame or wall structure; (3) seismic design code level, e.g. pre-code for building not seismically designed and mid-code for buildings designed according to moderate seismic provisions; (4) height, e.g. low-rise with 1 to 3 stories, mid-rise with 4 to 7 stories. This classification scheme is the same as that employed by the Hazus methodology (FEMA, 2003). The typologies used in this study are described in Table 5.1.

Examination of the inventory given in Table 5.1 reveals that the dominant building types are the pre-code unreinforced brick masonry (62%) and stone masonry buildings (14%) as shown in Figure 5.2. Moreover, 70% of the existing buildings were built before the introduction of seismic provisions in building codes (before 1950), while 91% were built before 1970 considered as a reference year in terms of seismic code requirements.

Table 5.1 Distribution of building classes within the study area with buildings types and heights were selected according to the Hazus methodology (FEMA, 2003).

Building type	**Height**	**Number of buildings**	**Code level**	
			Pre-code (before 1970)	**Mid-code (after 1970)**
W1L (wood light frame)	Low-rise	131	86	45
S1L (Steel Moment Frame)	Low-rise	32	20	12
S1M (Steel Moment Frame)	Mid-rise	12	12	-
S2L (Steel braced frames)	Low-rise	30	14	16
S2M (Steel braced frames)	Mid-rise	24	24	-
S5L (Steel frames with URM infill)	Low-rise	33	33	-
C1L (Concrete moment frame)	Mid-rise	25	0	25
URMBL (Unreinforced Brick masonry)	Low-rise	469	469	-
URMBM (Unreinforced Brick masonry)	Mid-rise	296	296	-
URMSL (Unreinforced stone masonry)	Low-rise	168	168	-
Total number		1220	1122	98

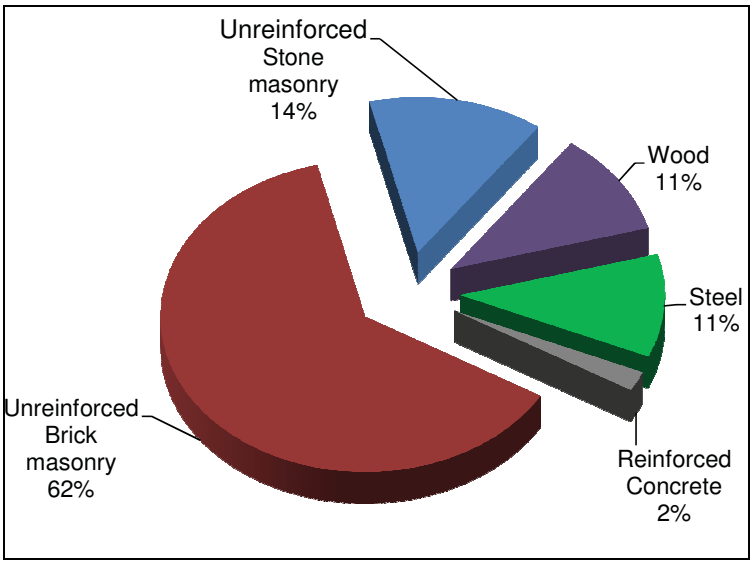

Figure 5.2 Distribution of buildings according to construction material.

5.2.2 Seismic hazard

The seismic hazard is defined with scenario of M6.2 at a distance 15km (M6.2R15) selected to match the National Building Code of Canada probability level of 2%/50 years (NBCC, 2010). Atkinson and Boore (2006)-AB06 ground motion prediction equation was used to develop the response spectra for the selected scenario. The ground motion parameters retained for the vulnerability modeling are the spectral accelerations at 0.3sec and 1.0sec that characterize the response spectral input in the vulnerability model. For site class B (rock), the predominant soil type in Old Québec City Sa(0.3sec)=0.38g and Sa(1.0sec)=0.07g (Figure 5.3).

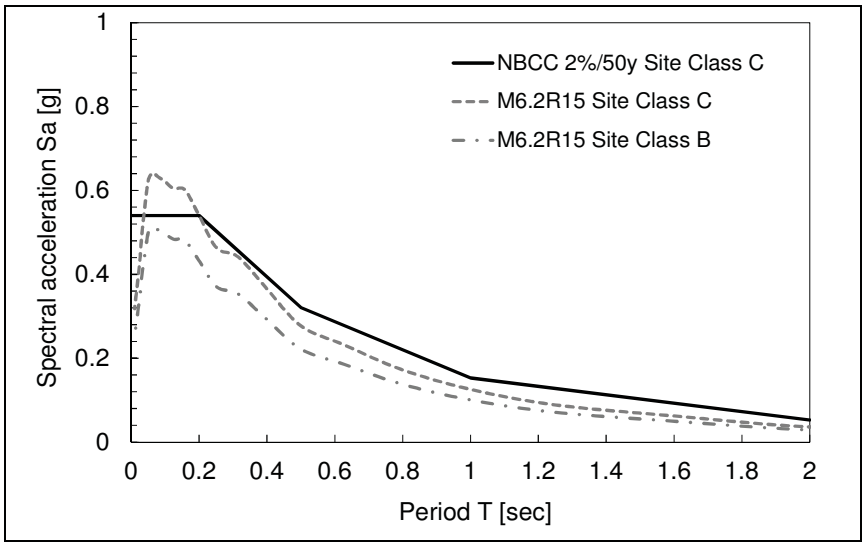

Figure 5.3 Response spectra for the selected M6.2R15 scenario on site class C (very dense soil and soft rock) and B (rock), and the NBCC 2%/50 years uniform hazard spectrum for Quebec City for site-class C.

5.2.3 Vulnerability

Due to similar construction practices in Canada and in United States, capacity curves and displacement based fragility functions available in the Hazus technical manual (FEMA, 2003) are used for the vulnerability modeling for the building types listed in Table 5.1 using the methodology presented in Chapter 3. For stone masonry buildings, which are not explicitly considered by Hazus, capacity curves and fragility functions are those generated in Chapter 2. Figure 5.4 shows an example of the fragility functions for low-rise stone and brick masonry buildings in terms of Sa0.3sec as the a representative IM for short period building systems. These fragility functions indicate that the stone masonry buildings are more vulnerable than brick masonry buildings, showing higher damage potential with increasing IM. This difference is attributed to the input capacity curves and displacement based fragility curves) for the respective building classes. The developed fragility functions in terms of structure-independent IM in this study for all buildings types in the considered inventory are presented in Appendix-III.

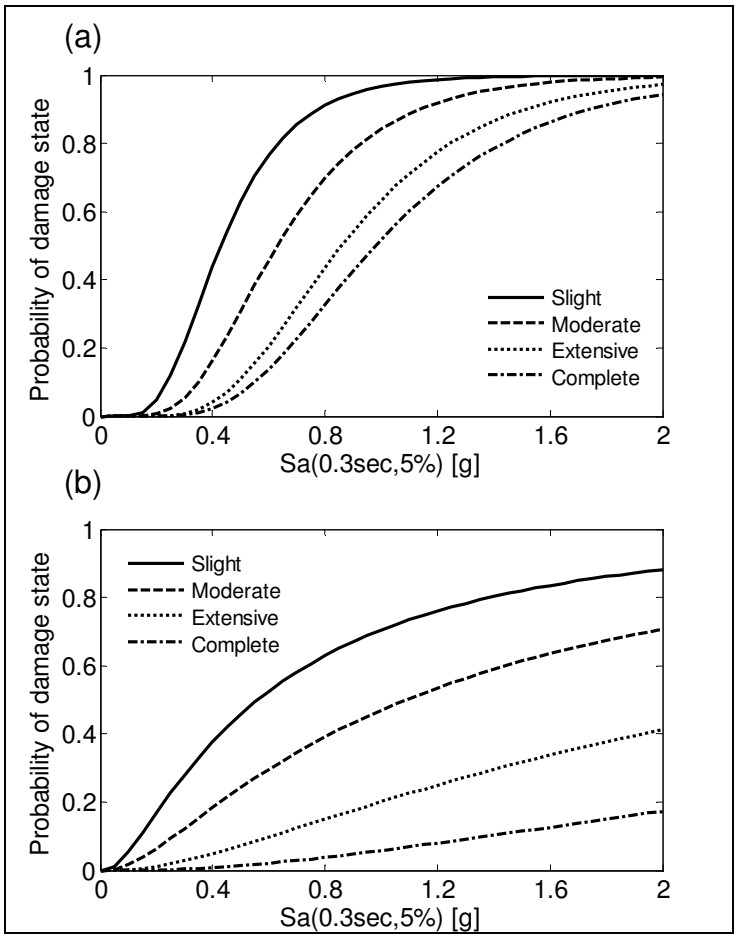

Figure 5.4 Fragility functions for (a) low-rise stone masonry buildings, and (b) low-rise brick masonry buildings.

5.3 Results

The potential damage for the considered M6.2R15 scenario is given in Figure 5.5. The total number of buildings that will be subject to certain degree of damage is 369, or 30% of the buildings. A summary of the proportion of buildings by construction material type and damage states is shown Figure 5.6. Predictably, most of the expected damage will occur in the pre-code stone and brick masonry buildings. Approximately 39% of the stone masonry buildings (65 buildings out of 168) and 33% of the brick masonry buildings (252 buildings out of 765) will suffer certain damage.

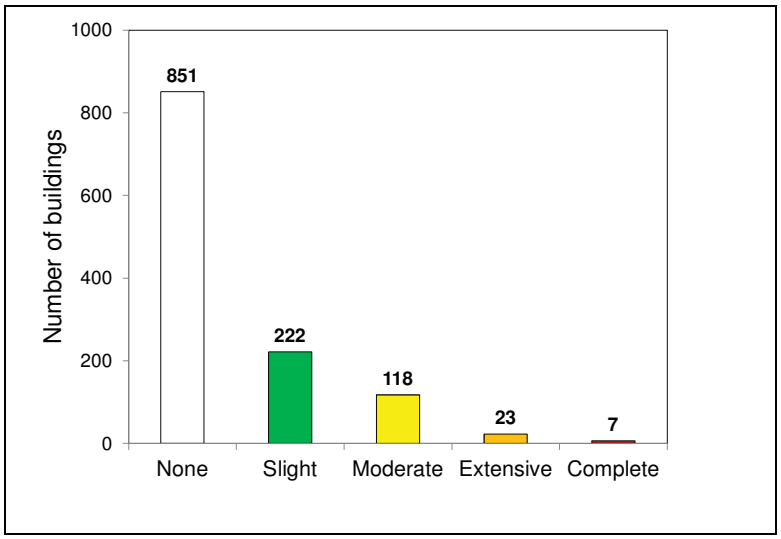

Figure 5.5 Total number of buildings in each damage state for a scenario event M6.2R15.

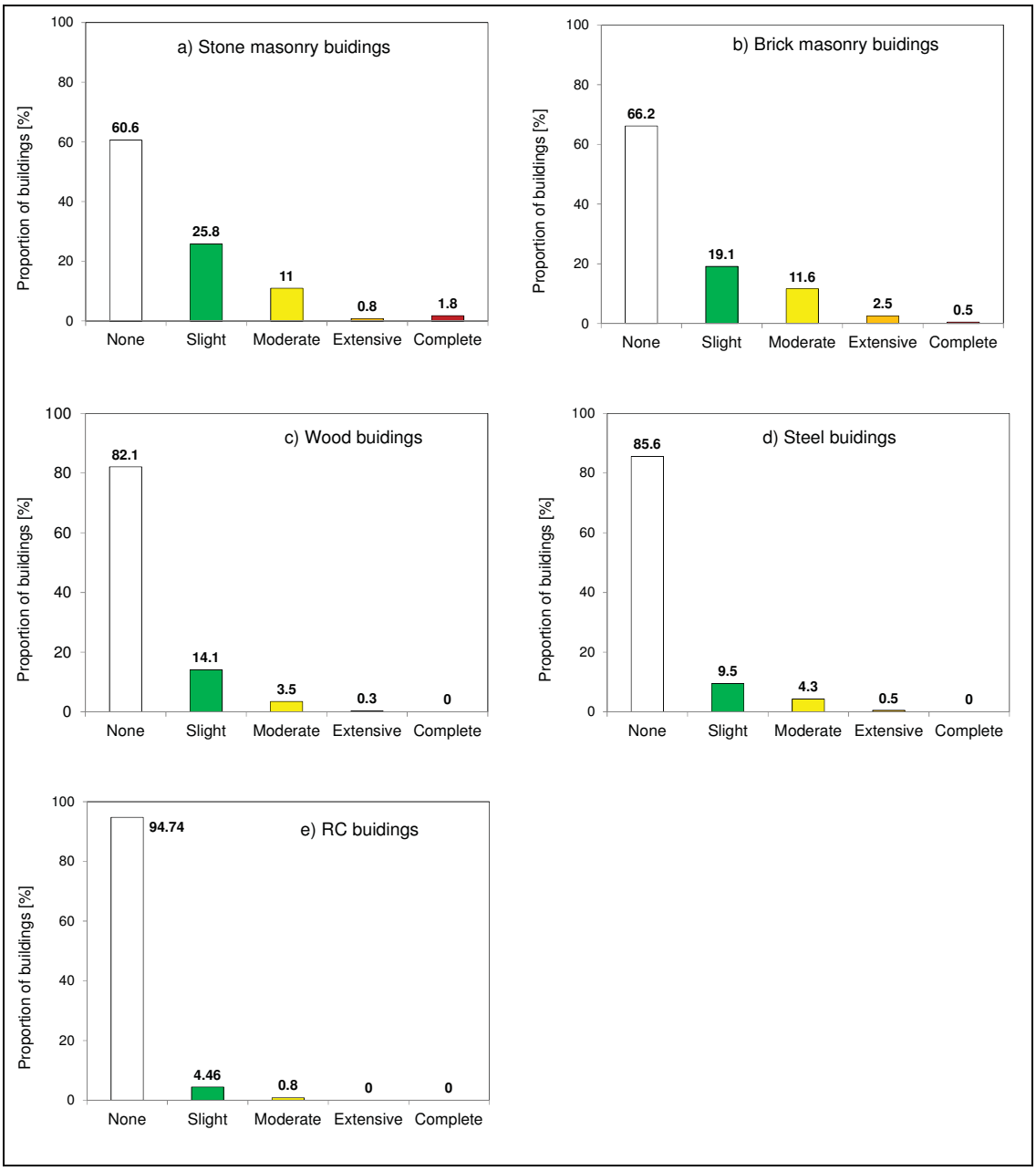

Figure 5.6 Proportion of buildings by construction material type in each damage state for a scenario event M6.2R15: (a) stone masonry buildings; (b) brick masonry buildings; (c) wood frame buildings; (d) steel frame buildings and (e) RC frame buildings.

5.4 Comparison with HAZUS

The results of the damage assessment scenario were compared with the damage estimates obtained applying the Hazus software. The same ground motion parameters, Sa0.3s=0.38g and Sa1.0s=0.07g, where used. The comparison of probability of structural damage was conducted for the four building classes: pre-code unreinforced masonry low-rise buildings (URML_Precode), pre-code steel braced frame buildings (S2L_Precode), pre-code light wood frame buildings (W1L_Precode) and pre-code steel moment frame buildings (S1L_Precode). The results expressed in percentage damage are given in Table 5.2 which indicates that almost identical results are obtained by both methods. This comparison confirms the validity of the developed procedure. The Hazus methodology has been subjected to extensive testing against occurred damages during past earthquakes to ensure accurate risk assessments. More details on the comparison are presented in Appendix-V.

Table 5.2 Comparison of probability of damage using the developed methodology with HAZUS software.

	URMBL_Precode		**S2L_Precode**		**W1L_Precode**		**S1L_Precode**	
Probability [%]	Fragility functions	HAZUS software	Fragility functions	HAZUS software	Fragility functions	HAZUS software	Fragility functions	HAZUS software
None	64	66	86	87	79	79	89	84
Slight	19	18	9	9	16	16	8	13
Moderate	13	12	5	4	5	5	3	3
Extensive	4	3	0	0	0	0	0	0
Complete	1	1	0	0	0	0	0	0

5.5 Summary and conclusions

A seismic risk assessment scenario of existing buildings inventory in Old Québec City was conducted. Many of the buildings were built before the introduction of seismic provisions, hence the need to predict their seismic performance. The assessment was performed for a scenario event of magnitude 6.2 at distance 15km with a probability of exceedance of 2% in 50 years. The inventory consisted of 1220 buildings classified according to their material type (e.g. concrete, wood, stone masonry), height (e.g. low, medium), and design level (e.g. pre-code, recent code). The modeling procedure consisted of generation of a set of analytical fragility functions in terms of a structure-independent intensity measure and respective to the encountered building types. The study showed that most of the expected damage will be concentrated in the old brick and stone masonry buildings, with 33% and 39% of damaged buildings in the respective classes. The damage results are almost identical with those obtained by applying the Hazus software for the same input parameters.

.

SUMMARY, CONCLUSIONS AND RECOMMENDATIONS

Summary

Earthquakes represent a major natural hazard that regularly impact the built environment in seismic prone areas worldwide and cause considerable social and economic losses. Recent earthquakes, e.g., 2009 L'Aquila earthquake in Italy and 2010 Christchurch earthquake in New Zealand, showed that most of the damage and economic losses were related to old vulnerable masonry buildings. The high losses incurred due to destructive earthquakes promoted the need for assessment of the performance of existing buildings under potential future earthquake events. This requires improved seismic vulnerability and risk assessment tools needed to assist informed decision making with the objective to minimize potential risks and to develop emergency response and recovery strategies.

In Eastern Canada, most of the existing buildings were built before the introduction of the seismic provisions in building codes. In particular, pre-code masonry buildings types are predominant in dense urban centers such as Québec City and Montreal in the Province of Québec. The potential economic and social losses due to strong earthquake events can thus be extensive. On the other hand, although masonry buildings represent major and most vulnerable part of the existing building stock, less research was devoted to study the seismic vulnerability of this type of buildings compared to other structural types, e.g. reinforced concrete and steel buildings.

Many historic buildings in the old urban centers in Eastern Canada such as Old Québec City are made of stone masonry and represent un-measurable architectural and cultural heritage. These buildings were built to resist gravity loads only and generally offer poor resistance to lateral seismic loads. The high seismic risk related to stone masonry buildings is even more aggravated due to their location in densely populated urban centers in a way that the consequences of failure of these structures tend to be severe with regards to human casualties, heritage damage and economic losses. Seismic vulnerability assessment of stone

masonry buildings is therefore the first necessary step in developing seismic retrofitting and pre-disaster mitigation plans for the older urban centers.

Typical seismic risk assessment studies on regional scale consist of three major components: hazard, exposure, and vulnerability of the exposure with respect to the seismic hazard. Seismic hazard defines the intensity of the expected earthquake motion at a particular location over a given time period; exposure identifies the built environment (buildings and infrastructures) in the area affected by the earthquake; and vulnerability refers to the exposure susceptibility to earthquake impacts defined by the expected degree of damage and loss that would result under different levels of seismic loading. The key component is the vulnerability modelling. The vulnerability is typically presented with sets of fragility functions describing the expected physical damage whereas economic losses are given by vulnerability functions. The typical results of risk assessment comprise estimates of the potential physical damage and direct economic losses.

The main objective of this study was to develop a set of probability-based analytical methods and tools for efficient analysis of seismic vulnerability of stone masonry buildings with systematic treatment of respective uncertainties. The specific objectives were to: (1) develop fragility and vulnerability functions for stone masonry buildings; (2) quantify the uncertainties in the vulnerability modelling and (3) apply the developed tools to evaluate the seismic vulnerability and risk of stone masonry buildings and other buildings types in Old Quebec City.

A simplified probabilistic analytical methodology for vulnerability modelling of stone masonry building with systematic treatment of uncertainties that can be adapted to other building types was developed in this study and presented in Chapter 2. Old Québec City was selected as a study area representative for historical urban centers in Eastern Canada. The first step in the methodology consisted of inventory of the existing stone masonry buildings and characterization of representative typology. Respective building capacity model was developed using a simplified mechanical model. Displacement based procedure was then

used to develop damage state fragility functions, based on drift thresholds of stone masonry walls, assigned based on literature experimental data. A simplified probabilistic seismic demand analysis was proposed to capture the combined uncertainty in capacity and demand on the fragility curves. The generated displacement fragility functions were determined for low-rise stone masonry buildings as functions of spectral displacement. The proposed methodology can easily be applied to other building types provided that damage state drift thresholds and material properties are available.

A robust analytical procedure for the development of seismic hazard compatible fragility and vulnerability functions of stone masonry buildings was presented in Chapter 3. The two main outputs that were developed in Chapter 2; the capacity curves and the displacement based fragility functions; were convolved with response spectra to estimate the structural damage to buildings for a series of earthquake magnitude-distance combinations in order to develop seismic hazard compatible fragility and vulnerability functions in terms of a structure-independent intensity measure (spectral acceleration). These functions can be directly used with results of a seismic hazard analysis output that is typically presented in terms of structure-independent intensity measure (IM). The procedure revealed to be effective for conducting rapid vulnerability assessment of building classes by considerably reducing the computational time. For a given building type, the developed procedure comprised the following steps: (1) seismic hazard definition in terms of response spectra defined by structure-independent intensity measures (e.g. spectral acceleration at a particular period); (2) structural analysis on the pre-developed capacity curves to estimate the seismic demand; (3) damage analysis using the pre-developed displacement based fragility functions for the estimated seismic response and (4) loss analysis in terms of the mean damage factor (MDF) which is obtained as a sum of the probabilities of being in each damage state obtained from the fragility functions, multiplied by a damage factor (DF) that reflects the expected repair to replacement cost ratio for a building experiencing a specific damage state.

Sensitivity analysis of uncertainties in analytical vulnerability modelling of stone masonry buildings is presented in Chapter 4. The following parameters were varied: structural parameters (capacity curves yield acceleration, elastic damping ratios, degradation factors), damage parameters (displacement fragility functions median and standard deviation), and loss parameters (repair cost ratio). For each parameter, a set of increments was considered. First the vulnerability functions were developed for the base-case scenario. Then, the vulnerability functions were developed by varying the considered parameter only and keeping the remaining parameters constant. The sensitivity was determined comparing deviations from the base-case scenario using tornado diagrams for different levels of seismic intensity. The conducted sensitivity study revealed that largest part of MDF sensitivity is due to the uncertainty in displacement fragility functions medians and the yield acceleration of the capacity curve.

The proposed methodology was validated by conducting a scenario-based seismic risk assessment of existing buildings in Old Québec City. The validation study is presented in Chapter 5. The procedure for hazard compatible vulnerability modelling presented in Chapter 3 was used to develop seismic fragility functions in terms of spectral acceleration of existing buildings inventory in Old Quebec City. The inventory consisted of 1220 buildings classified according to their material type, height, and seismic design level. Many of these buildings were built before the introduction of seismic provisions. The assessment was performed for a scenario event of magnitude 6.2 at distance 15km with a probability of exceedance of 2% in 50 years. The study showed that most of the damage is expected to be concentrated in the old brick and stone masonry buildings, with 33% and 39% of damaged buildings in the respective classes. The damage results are almost identical with those obtained by applying the Hazus software for the same input parameters.

Conclusions

A simplified probabilistic analytical methodology for vulnerability modelling of stone masonry building with systematic treatment of uncertainties was developed in this study. Respective building capacity model was developed using a simplified mechanical model. Displacement based procedure was then used to develop damage state fragility functions, based on drift thresholds of stone masonry walls, assigned based on literature experimental data.

The proposed methodology can easily be applied to other building types provided that damage state drift thresholds and material properties are available. It has several advantages, first of all in the use of simplified mechanical models for generation of capacity curves which proved particularly effective for carrying out analyses of uncertainties with significantly reduced computational time. The second advantage is represented in the use of experimental displacement based damage criteria instead of relying on expert opinion. Based on the analysis of experimental drift data, increased uncertainties were observed in the identification of the complete damage state. This is generally attributed to the rapid degradation of the stone walls after reaching peak strength. This issue should be taken into consideration.

A comparison of the developed displacement fragility functions was made with those implicit in the existing seismic risk assessment tools Hazus and ELER. Significant differences have been observed. These differences were replicated in comparatively significant disparities among the probability estimates for different damages states. Hazus showed highest probability of occurring no to slight damage due to the assumed higher deformation capacity, whereas the highest probabilities of extensive and complete damage were predicted with ELER due to the assumed lower deformation capacity representative of older stone masonry structures in Italy. This comparative example showed the importance of the development of specific fragility functions that reflect the specific construction characteristics for the considered study area and emphasized the need of critical use of existing risk assessment tools and the results they generate.

A robust analytical procedure for the development of seismic hazard compatible fragility and vulnerability functions of stone masonry buildings was presented in the second part. The results are given as sets of seismic hazard compatible functions that can be directly integrated along with the results of a seismic hazard analysis typically presented in terms of structure-independent intensity measure (IM). The procedure was used to develop fragility functions, describing the damage states, and vulnerability functions describing the economic losses for stone masonry buildings. It was validated through damage assessment for several earthquake scenarios. The procedure revealed to be effective for conducting rapid vulnerability assessment of the building types for the assessment of the potential physical damage and direct economic losses for a given earthquake scenario. Moreover, the procedure led to a considerable reduction of the computational time, which is particularly useful for the conducted sensitivity analysis of the vulnerability assessment.

The sensitivity study of the seismic vulnerability modelling of stone masonry buildings revealed the dominant role of the uncertainties related to the medians of the displacement fragility functions, and the yield acceleration of the capacity curve. These uncertainties are of epistemic nature and may be further reduced with additional knowledge of the median threshold values for stone masonry buildings and the mechanical properties that affects the capacity curve (e.g., the shear strength of masonry). Therefore, more attention should be given to these parameters. The sensitivity of the mean damage factor (MDF) to uncertainties in the standard deviation of the displacement fragility functions and the DFs corresponding to each of the damage states is due first of all to the intensity of the considered ground motion. The MDF appears moderately sensitive to the elastic damping and the degradation parameter.

Recommendations for future research

Based on the above conclusions, it is suggested to extend the future research in the following areas:

- Experimental investigations should be conducted to characterise the nonlinear deformation behaviour, drift thresholds and material strength parameters of stone and brick masonry walls representative of those existing in Eastern Canadian urban centers. These investigations should also consider the effect of potential seismic retrofit schemes;
- an updated database of experimental drift thresholds and capacity curves can be compiled for other representative buildings types in Eastern Canada including concrete, steel and wood buildings in order to provide future users with the option to apply site specific fragility functions and implemented in the proposed vulnerability methodology;
- the developed methodology can also be extended to take into account possible out-of-plane failure mechanisms of masonry walls that might occur in case where poor connection between floor and wall exists;
- in order to evaluate different mitigation strategies, the proposed methodology can be used to develop fragility functions for various seismic retrofit schemes;
- the procedure can be extended to include the higher modes that can affect the response of high-rise buildings.
- the methodology can be extended to develop simplified vulnerability functions for social losses such as the expected casualties assigned to the predicted damage states, mainly extensive and complete damage states.

APPENDIX I

DISPLACEMENT BASED FRAGILITY ANALYSIS RESULTS

This section presents the results for the displacement based fragility analysis for one story and three stories stone masonry buildings typologies in Old Quebec City (Figure 2.2, Chapter 2). Table-A I-1 shows the results for the median and dispersion of the spectral displacement thresholds for different damage states for one story stone masonry buildings. The median and dispersion of the yield acceleration of the capacity curves and the fundamental period of vibrations are also given in this table. Table-A- I-2 shows similar results for three stories stone masonry buildings. The displacement based procedure presented in (section 2.4, Chapter 2) was applied to obtain the displacement based fragility functions. The mechanics based model for the development of capacity curves was used to develop the capacity curve parameters (section 2.5, Chapter 2).

Table-A I-1 Fragility analysis results for one story stone masonry buildings

Displacement based fragility functions parameters		
Damage state	Median S_d [m]	Dispersion β
DS1 [Slight]	0.003	0.20
DS2 [Moderate]	0.008	0.38
DS3 [Extensive]	0.017	0.40
DS4 [Complete]	0.026	0.50
Capacity curve parameters		
	Median	Dispersion β
Yield acceleration S_{ay} [g]	0.33	0.18
Fundamental period of vibration T [sec]	0.12	0.33

Table-A I-2 Fragility analysis results for three stories stone masonry buildings

Displacement based fragility functions parameters		
Damage state	Median S_d [m]	Dispersion β
DS1 [Slight]	0.008	0.20
DS2 [Moderate]	0.014	0.38
DS3 [Extensive]	0.025	0.40
DS4 [Complete]	0.033	0.50
Capacity curve parameters		
	Median	Dispersion β
Yield acceleration S_{ay} [g]	0.24	0.40
Fundamental period of vibration T [sec]	0.35	0.35

APPENDIX II

COMPUTATIONS FOR THE SEISMIC HAZARD COMPATIBLE VULNERABILITY MODELLING

In this section, the detailed computations for the methodology of development seismic hazard compatible fragility and vulnerability functions are presented. In order to avoid computationally costly iterations to find the structural displacement response (i.e. the performance point) in the CSM procedure, the procedure is amended according to the procedure proposed by (Porter, 2009). A spreadsheet calculation algorithm was built using Microsoft Excel. The structure of the algorithm is shown in Figure-A II-1.

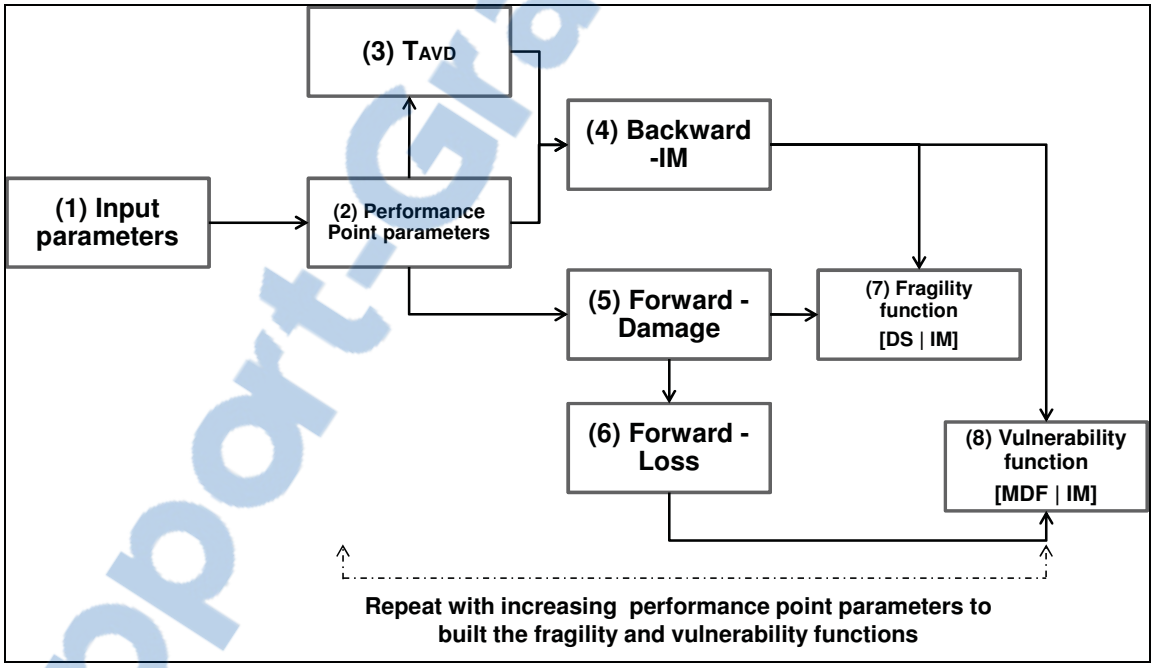

Figure-A II-1 Algorithm structure in Excel for the development of seismic hazard compatible fragility and vulnerability functions.

Step-1: Input parameters:

For each building type, the required input parameters are summarized in Table-A II-1.

Table-A II-1 Input parameters

Capacity Curve parameters:	Yield Displacement D_y(m)
	Yield Acceleration A_y (g)
	Ultimate Displacement D_u (m)
	Ultimate Acceleration A_u (g)
	Elastic damping ratio ξ_e
	Degradation factor κ
Displacement Fragility Functions parameters:	Slight damage median λ_1 (m)
	Slight damage log-Standard deviation β_1
	Moderate damage median λ_2 (m)
	Moderate damage log-Standard deviation β_2
	Extensive damage median λ_3 (m)
	Extensive damage log-Standard deviation β_3
	Complete damage median λ_4 (m)
	Complete damage log-Standard deviation β_4
Seismic setting parameters:	
	A ground motion prediction equation (GMPE).
	Site class : A (Hard rock), B(Rock), C(Very Dense soils), D(Stiff soils), E(Soft soils)
	Magnitude (M)
	Distance, R (km)

Step-2: Performance point parameters:

This is the central step of the procedure from which calculations are carried out backward to evaluate the structure-independent intensity measure IM and forward to damage and loss analysis. The performance point is defined as the intersection of the capacity curve and the demand spectrum (over-damped spectrum) with known values of (S_d ,S_a, T, ξ_{eff}). T denote the effective period at the performance point. The procedure starts with assuming a value of S_d, calculate S_a of the performance point from the capacity curve, calculate effective damping and period which is illustrated in Figure-A II-2.

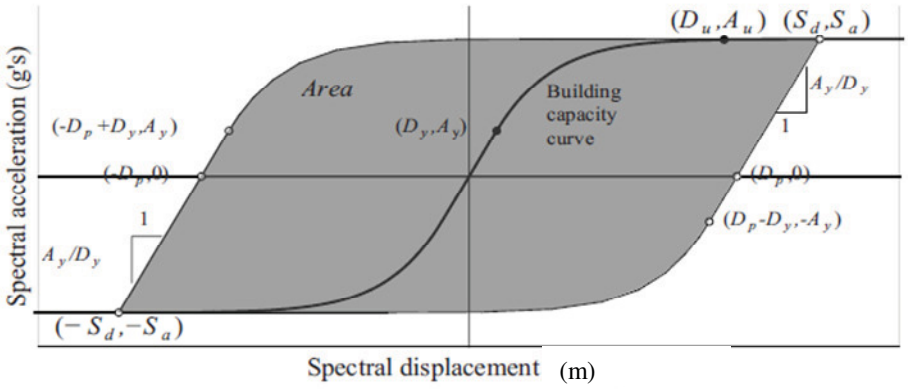

Calculate Sa

$$S_a = S_d A_y / D_y \qquad S_d < D_y$$

$$= A_0 + b\sqrt{1 - \frac{(S_d - D_u)^2}{a^2}} \qquad D_y \le S_d < D_u$$

$$= A_u \qquad D_u \le S_d$$

$$b = \frac{D_y(A_y - A_u)^2 - (D_y - D_u)A_y(A_y - A_u)}{(D_y - D_u)A_y - 2D_y(A - A_u)}$$

$$a = \sqrt{\frac{-D_y(A_y - A_u)b^2}{A_y(A_y - A_u + b)}}$$

$$A_0 = A_u - b$$

Calculate ξ_{eff}

$$\xi_{eff} = \xi_e + k\left(\frac{Area}{2\pi S_d S_a}\right)$$

$$Area = 4S_a\left(S_d - \frac{S_a}{A_y / D_y}\right)$$

Calculate T

$$T = 2\pi\sqrt{\frac{S_d}{S_a \cdot g}}$$

Figure-A II-2 Calculations of the performance point parameters.

Step-3: Evaluation of T_{AVD}:

T_{AVD} is the period at the intersection of the constant-acceleration and constant-velocity portions of the demand spectrum that correspond to the performance point in step-2. T_{AVD} is used to decide whether the performance point falls on the constant acceleration portion or the constant velocity portion of the demand spectrum. Figure-A II-3 illustrates the procedure to calculate T_{AVD} for a given magnitude, distance, site class, and effective damping ratio.

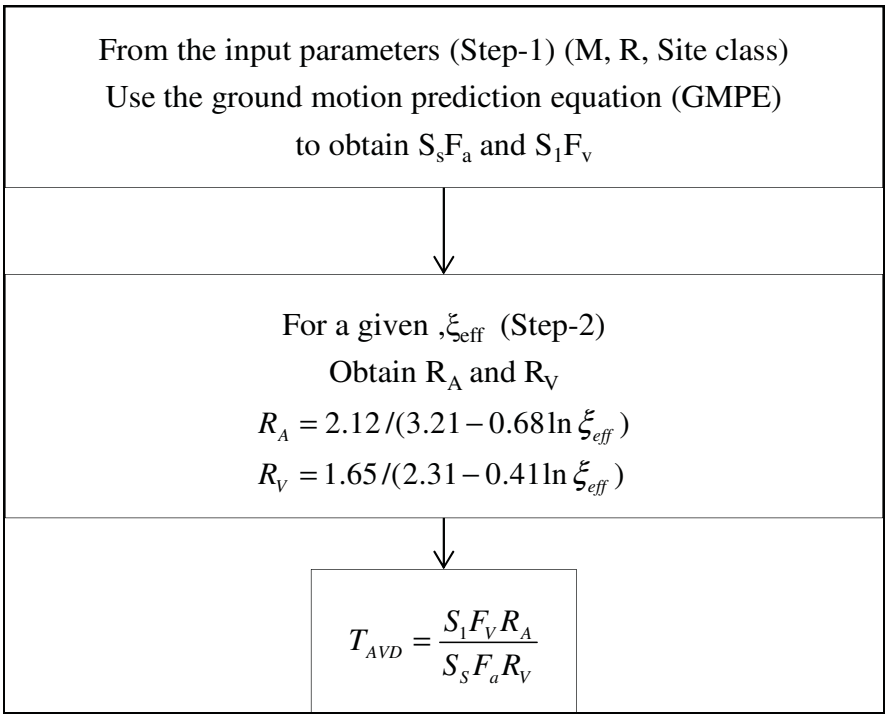

Figure-A II-3 Calculations of the T_{AVD}.

The GMPE is used to predict the site-soil 5% damped elastic response spectrum defined by the control point S_sF_a = (Sa0.3sec,5%) and S_1F_v = (Sa1.0sec,5%) for the given M,R. S_s and S_1 are the site class B accelerations for the constant acceleration and velocity portions of the spectrum, respectively. S_sF_a is the soil-site adjusted spectral acceleration for 5% damping at 0.3sec and S_1F_v is the soil-site adjusted spectral acceleration for 5% damping at 1.0sec. F_a and F_v are the soil-site amplification factors other than site-class B for constant-acceleration

portion and constant-velocity portion of the spectrum, respectively (Table-A II-2). R_A and R_V are the damping reduction factor for damping ratios more than 5% for constant-acceleration portion and constant-velocity portion of the spectrum, respectively. It should be noted that the NBCC (2010) applies equivalent amplification factors to the FEMA (2003) with a reference site class C. The application of the FEMA (2003) site-amplification factors is adopted in order to be compatible with the values implemented in Hazus where site-class B is used as the reference site in the GMPE.

Table-A II-2 Site amplification factors (FEMA, 2003).

	Site class				
	A	B	C	D	E
S_s (g)	F_a				
<0.25	0.8	1.0	1.2	1.6	2.5
0.5	0.8	1.0	1.2	1.4	1.7
0.75	0.8	1.0	1.1	1.2	1.2
1.0	0.8	1.0	1.0	1.1	0.9
>1.25	0.8	1.0	1.0	1.0	0.8
S_1 (g)	F_v				
<0.1	0.8	1.0	1.7	2.4	3.5
0.2	0.8	1.0	1.6	2.0	3.2
0.3	0.8	1.0	1.5	1.8	2.8
0.4	0.8	1.0	1.4	1.6	2.4
>0.5	0.8	1.0	1.3	1.5	2.0

Step-4: Backward IM:

In the previous step, an estimate of T_{AVD} for a given combination of magnitude, distance, site class and damping ratio was obtained. In this step, calculating backwards from the performance point to the parameters of the input spectrum is conducted. It is desirable to infer the "control points" of the index spectrum given a point on the demand spectrum (the performance point), magnitude, distance, and site class. Control points here mean S_sF_a = (Sa0.3sec,5%) and S_1F_v = (Sa1.0sec,5%) of the index spectrum. The control points values depend on whether the performance point falls on the constant acceleration portion ($T < T_{AVD}$) or the constant velocity portion of the demand spectrum ($T > T_{AVD}$). Figure-A II-4 illustrates the calculations.

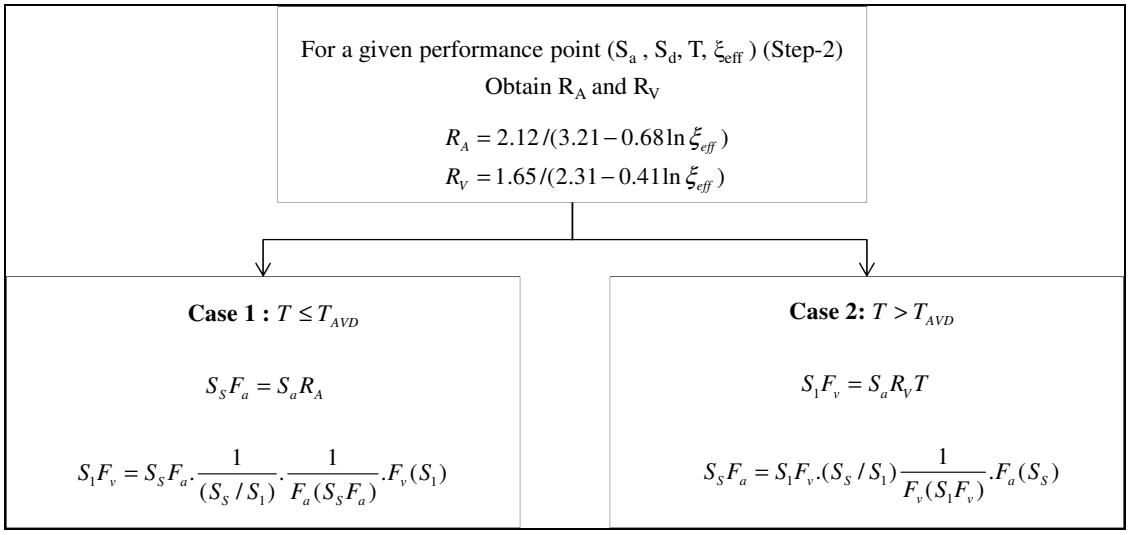

Figure-A II-4 Calculations of the control points of the index spectrum.

(S_S / S_1) is the spectral acceleration response factor that can be derived from step-3 for the T_{AVD} of site class B and 5% damping. $F_a(S_S)$ and $F_v(S_1)$ are the site amplification factors given in Table-A II-2. = (Sa0.3sec,5%). $F_a(S_S F_a)$ is the site amplification factor F_a expressed as a function $S_S F_a$ (Table-A II-3) and $F_v(S_1 F_v)$ is the site amplification factor F_v expressed as a function $S_1 F_v$ (Table-A II-4). These factors provide a mapping from site-amplified shaking to rock shaking.

Table-A II-3 Inferring F_a from S_S F_a and site class.

Site class	**S_S F_a (g)**						
	0.1	0.2	0.4	0.6	0.8	1	1.25
A	0.8	0.8	0.8	0.8	0.8	0.8	0.8
B	1	1	1	1	1	1	1
C	1.2	1.2	1.2	1.2	1.11	1	1
D	1.6	1.6	1.6	1.47	1.3	1.15	1
E	2.5	2.5	2.5	2.5	1.88	0.9	0.9

Table-A II-4 Inferring F_v from S_1 F_v and site class.

Site class	**S_1 F_v (g)**						
	0.1	0.2	0.4	0.6	0.8	1	1.2
A	0.8	0.8	0.8	0.8	0.8	0.8	0.8
B	1	1	1	1	1	1	1
C	1.7	1.68	1.54	1.36	1.3	1.3	1.3
D	2.4	2.4	2	1.68	1.5	1.5	1.5
E	3.5	3.5	3.45	3.24	2.88	2.4	2.4

Step-5: Forward damage:

In this step, we work forward from the performance point (step-2) into a set of displacement based fragility functions, to determine the probability of damage state. The obtained probabilities are tabulated conditioned to the computed IM obtained from step-4. This is illustrated in Figure-A II-5.

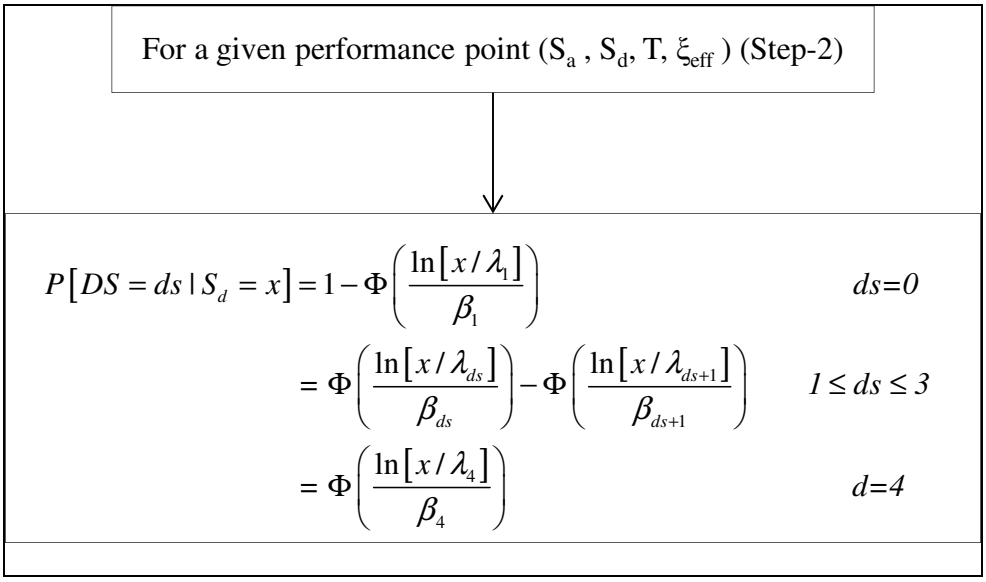

Figure-A II-5 Calculations of damage states probabilities for a given performance point.

Where $P[DS = ds \mid S_d = x]$ denotes the probability of structural damage state ds given that S_d takes on some particular value x, and Φ denotes the cumulative standard normal distribution. The parameters λ_{ds} , β_{ds} denote, respectively, the median and logarithmic standard deviation values of the fragility function to resist damage state *ds* from 0 as no damage, 1 as slight damage, 2 as moderate damage, 3 as extensive damage and 4 as complete damage.

Step-6: Forward loss:

Finally, the integration of the loss conditioned on the probability of being in each damage state was conducted to determine the MDF at the computed IM (step-4). The MDF is computed as follows

$$MDF = \sum_{dsi=1}^{4} P[DS = ds_i \mid S_d = x].DF_{dsi}$$

The DF, central value in a range of damage factors, used to predict the MDF was assumed to be: 2% of the building structural system replacement cost for slight structural damage, 10% for moderate damage, 50% for extensive damage, and 100% for complete damage (Kircher et al., 1997b).

Step-7 and 8: Hazard compatible fragility and vulnerability functions:

To establish the fragility and vulnerability functions in terms of structure-independent IMs, the procedure is repeated for increasing values of the performance points (step-2). The computed probabilistic damage states and mean damage factor are given in tabular format for respective structure-independent IM. The data are then fitted to provide suitable hazard compatible seismic fragility (Figure-A II-6) and vulnerability functions (Figure-A II-7) as a lognormal cumulative distribution functions.

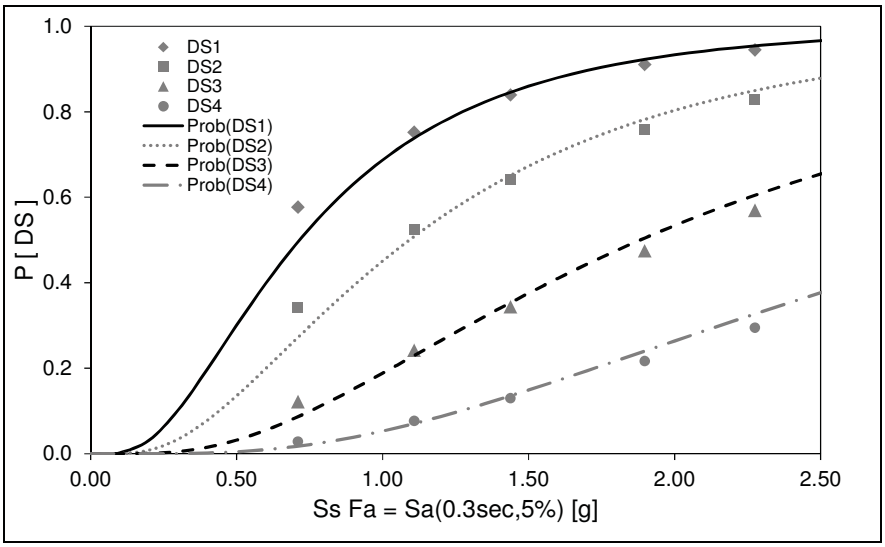

Figure-A II-6 Illustration of the fitted lognormal distribution for the hazard compatible fragility functions.

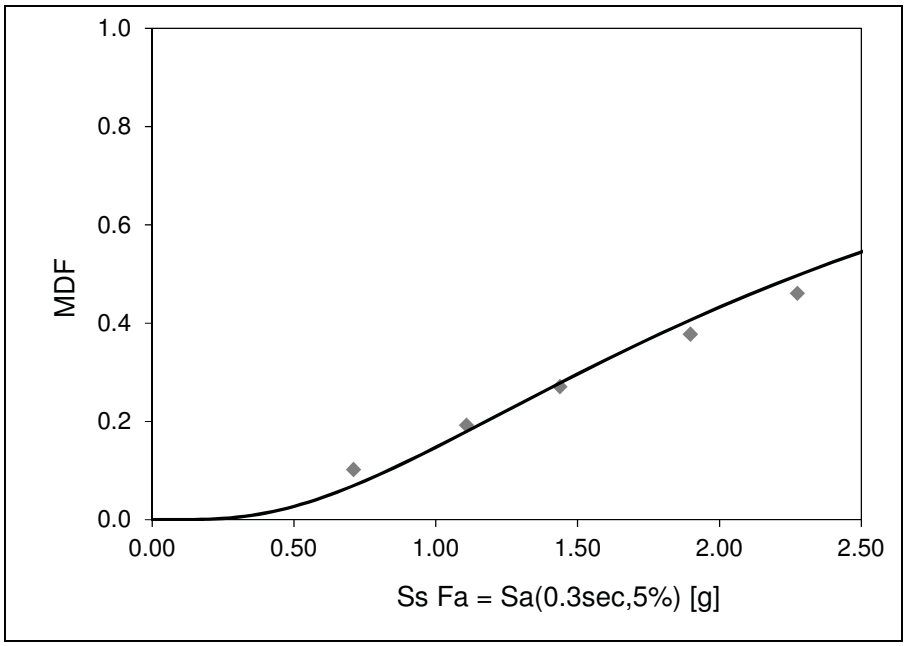

Figure-A II-7 Illustration of the fitted lognormal distribution for the hazard compatible vulnerability functions.

APPENDIX III

HAZARD COMPATIBLE FRAGILITY FUNCTIONS FOR BUILDING TYPES IN OLD QUEBEC CITY

Table-A III-1 Capacity curves input parameters (FEMA, 2003)

Building Type	**D_y(m)**	**A_y (g)**	**D_u (m)**	**A_u (g)**	**ξ_e**	**κ**
W1L-precode	0.006	0.2	0.110	0.6	15%	0.3
W1L-midcode	0.009	0.3	0.165	0.9	15%	0.6
S1L-precode	0.004	0.062	0.070	0.187	5%	0.2
S1L-midcode	0.008	0.125	0.140	0.375	5%	0.4
S1M-precode	0.011	0.039	0.135	0.117	5%	0.2
S2L-precode	0.004	0.1	0.048	0.2	5%	0.2
S2L-midcode	0.008	0.2	0.096	0.4	5%	0.4
S2M-precode	0.015	0.083	0.123	0.167	5%	0.2
S5L-precode	0.003	0.1	0.030	0.2	5%	0.2
C1M-midcode	0.015	0.104	0.176	0.312	7%	0.4
URML-precode	0.006	0.2	0.061	0.4	10%	0.2
URMM-precode	0.007	0.11	0.046	0.222	10%	0.2

Table-A III-2 Displacement fragility functions input parameters (FEMA, 2003)

Building Type	**S_d (m)**							
	Slight		**Moderate**		**Extensive**		**Complete**	
	λ_1	β_1	λ_2	β_2	λ_3	β_3	λ_4	β_4
W1L-precode	0.010	1.01	0.025	1.05	0.078	1.07	0.192	1.06
W1L-midcode	0.013	0.84	0.032	0.86	0.098	0.89	0.240	1.04
S1L-precode	0.026	0.85	0.042	0.82	0.089	0.80	0.219	0.95
S1L-midcode	0.033	0.80	0.057	0.75	0.129	0.74	0.329	0.88
S1M-precode	0.044	0.70	0.070	0.75	0.148	0.81	0.366	0.98
S2L-precode	0.022	1.01	0.035	0.96	0.088	0.88	0.219	0.98
S2L-midcode	0.027	0.93	0.047	0.92	0.128	0.93	0.329	0.93
S2M-precode	0.037	0.73	0.058	0.75	0.146	0.80	0.366	0.98
S5L-precode	0.013	1.20	0.026	1.11	0.066	1.08	0.154	0.95
C1M-midcode	0.038	0.70	0.066	0.70	0.178	0.70	0.457	0.89
URML-precode	0.008	1.15	0.017	1.19	0.041	1.20	0.096	1.18
URMM-precode	0.013	0.99	0.026	0.97	0.064	0.90	0.149	0.88

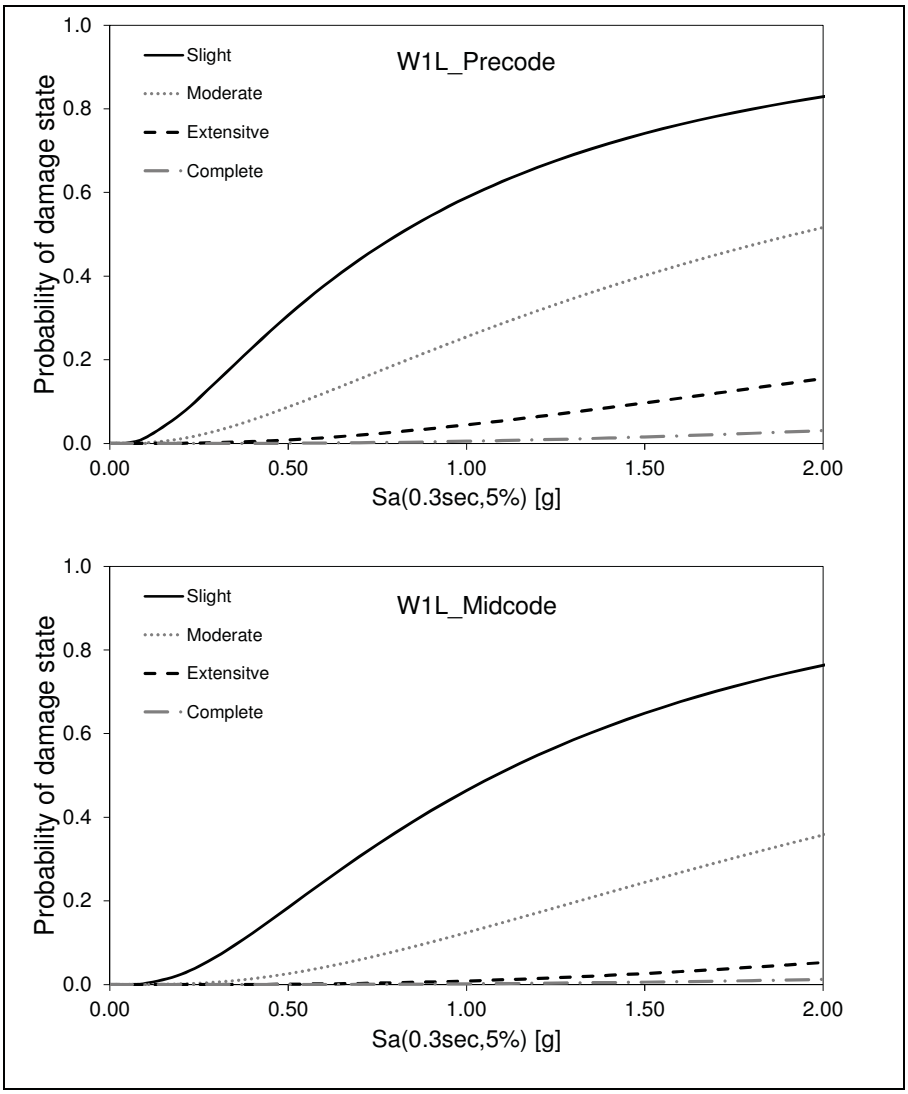

Figure-A III-1 Seismic hazard compatible fragility for building types in Old Quebec City.

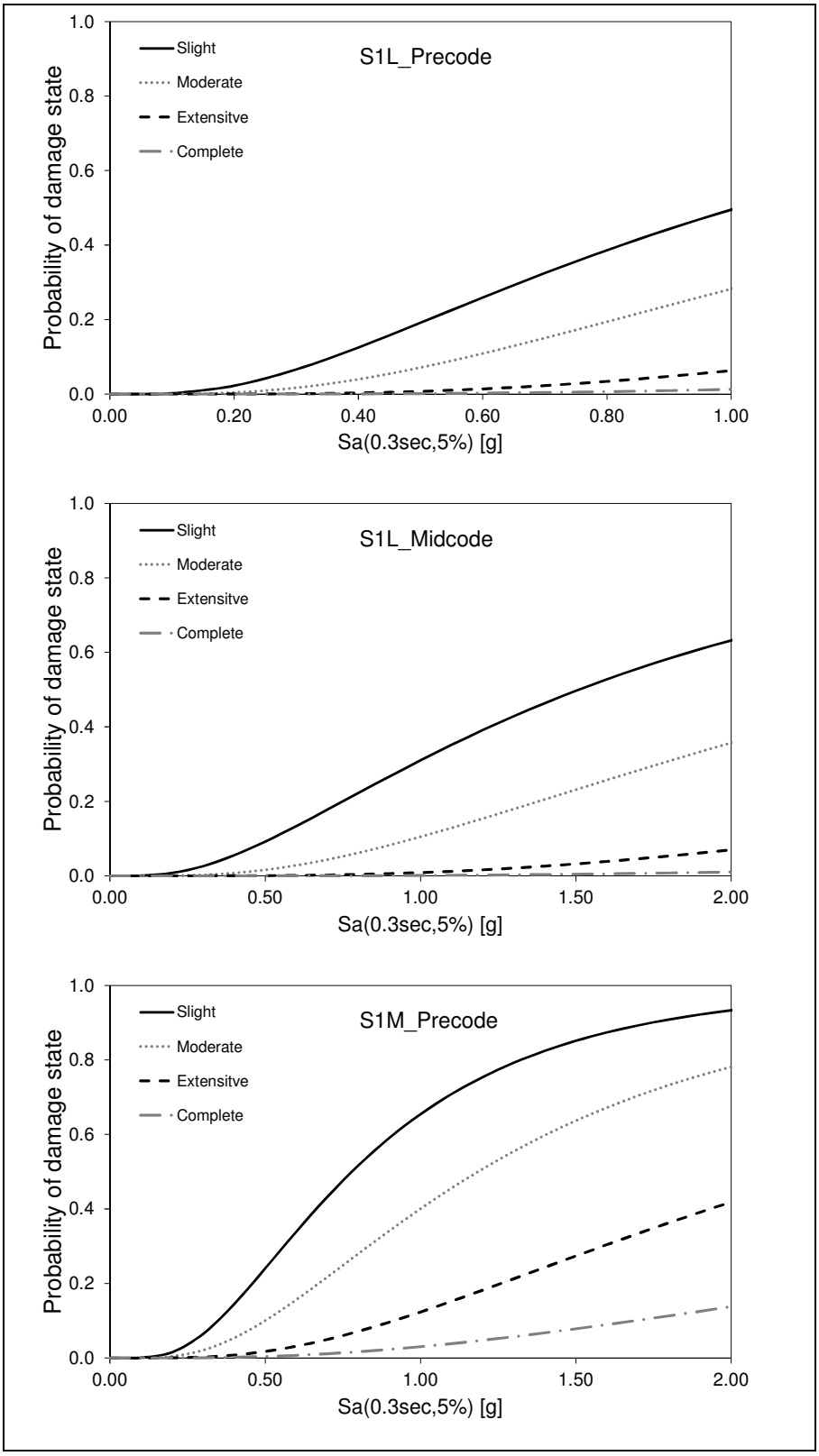

Figure-A III-1 Continued.

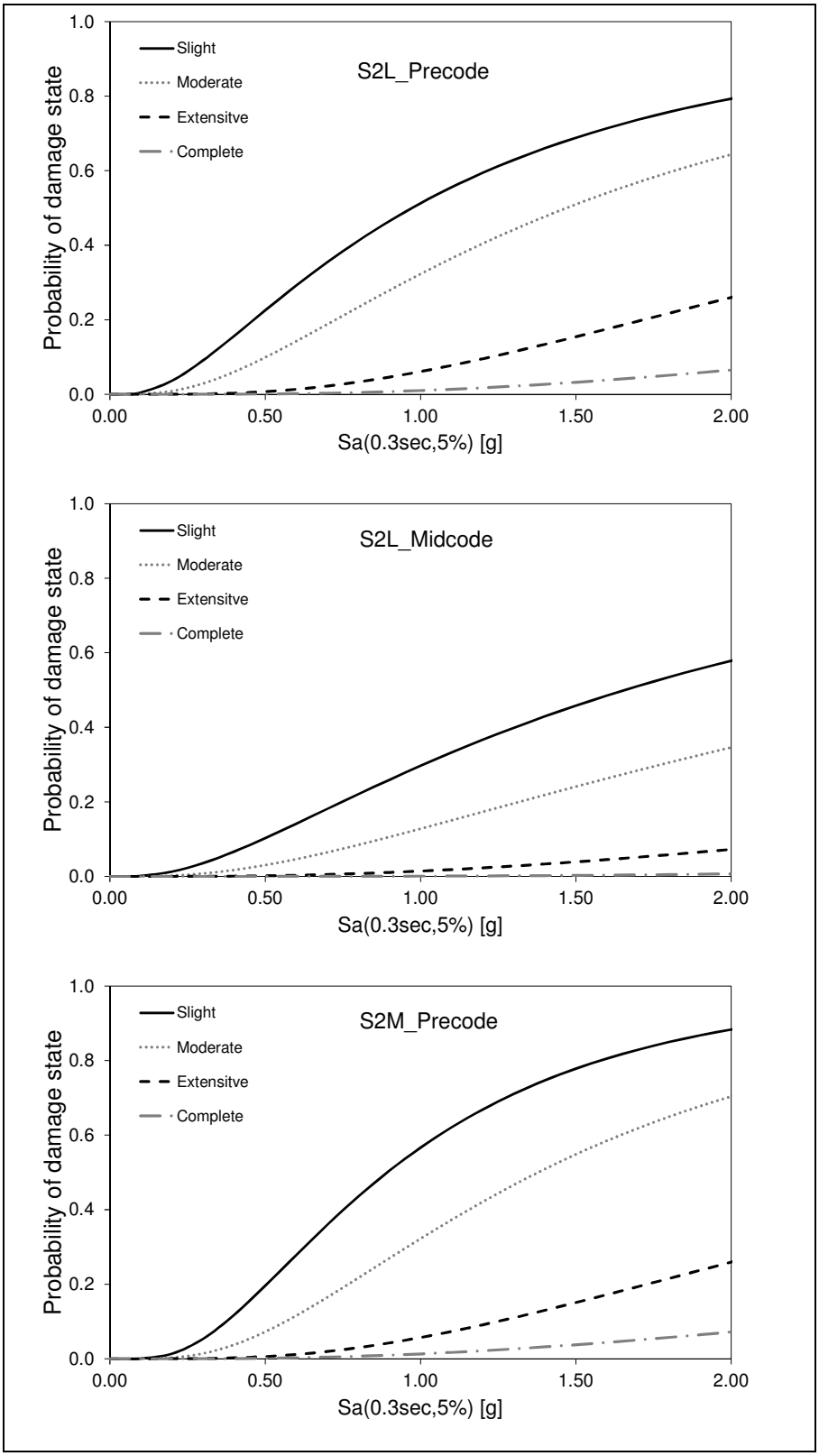

Figure-A III-1 Continued.

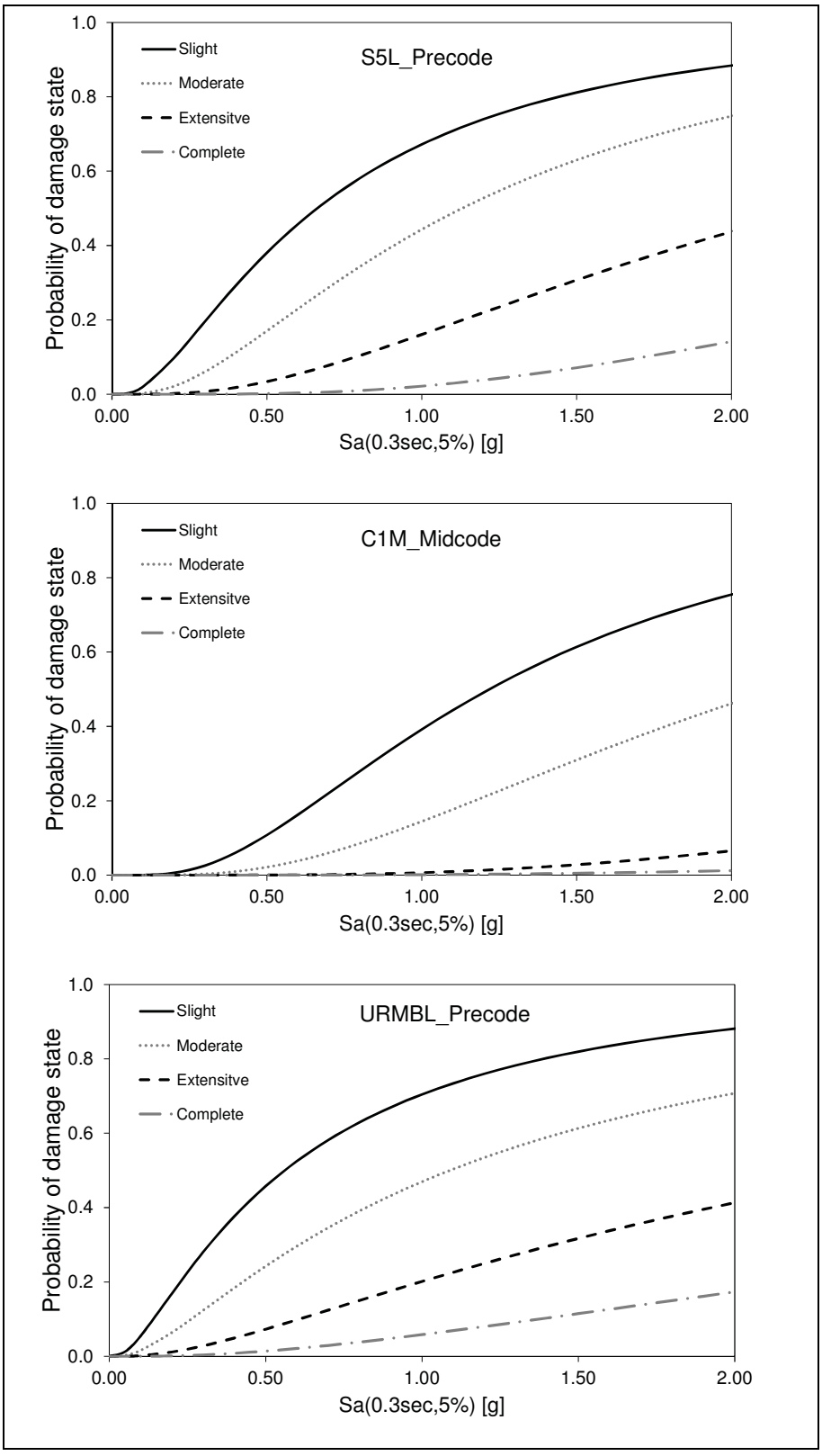

Figure-A III-1 Continued.

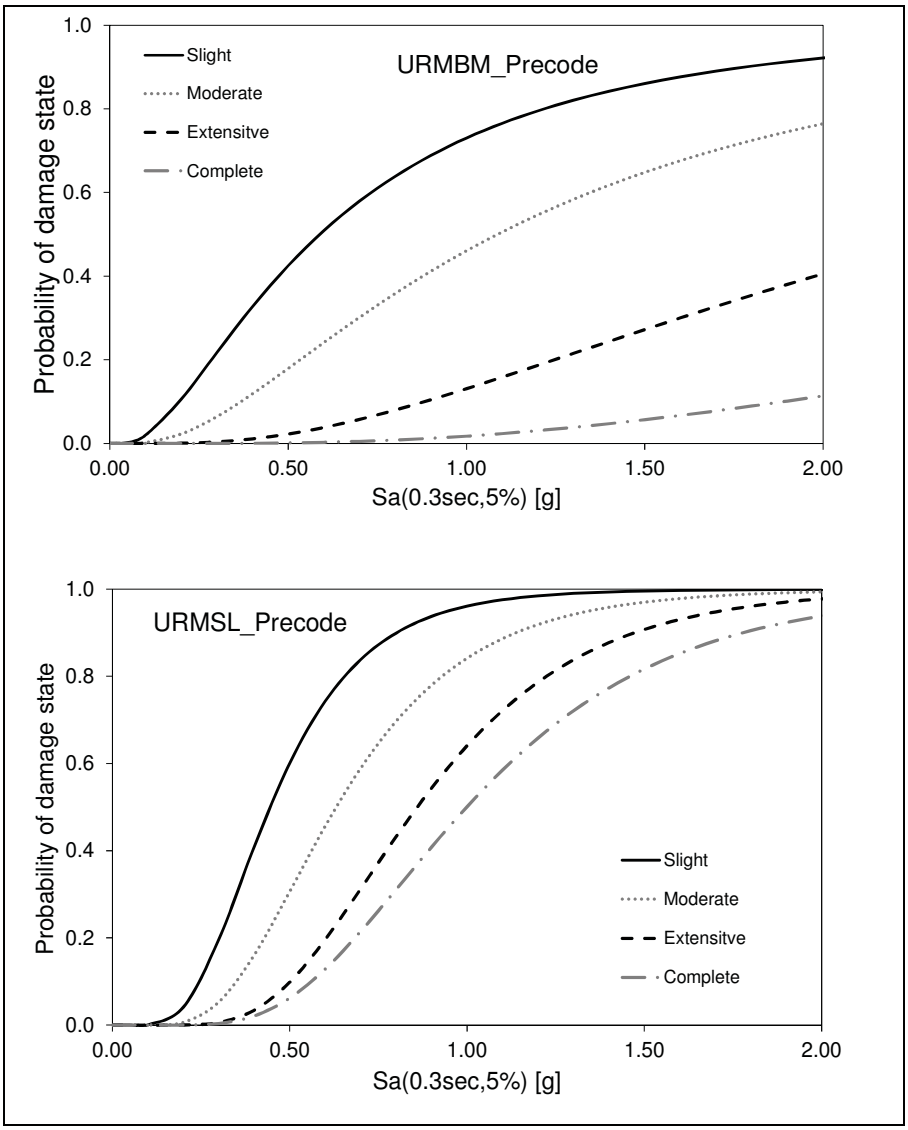

Figure-A III-1(continued).

APPENDIX IV

ATKINSON AND BOORE (2006) GROUND MOTION PREDICTION EQUATION FOR EASTREN NORTH AMERICA

Atkinson and Boore (2006) ground motion prediction equation to estimate the spectral acceleration at a particular period for a Magnitude (M) at distance from fault rupture (R) takes the following form:

$$Log[S_a(T)] = c_1 + c_2M + c_3M^2 + (c_4 + c_5M)f_1 + (c_6 + c_7M)f_2 + (c_8 + c_9M)f_0 + c_{10}R + S$$

Where:

f_0 = max (log (R_0/R), 0); f_1 = min (log R, log R_1); f_2 = max (log (R/R_2), 0); R_0 =10; R_1 = 70; R_2 = 140 and S is the soil site parameter that takes the form:

$$S = \log\left\{\exp\left[b_{lin}\ln(V_{30}/V_{ref}) + b_{nl}\ln(60/100)\right]\right\} \quad \text{for pgaBC} \le 60\text{cm/s}^2$$

$$S = \log\left\{\exp\left[b_{lin}\ln(V_{30}/V_{ref}) + b_{nl}(pgaBC/100)\right]\right\} \quad \text{for pgaBC} > 60\text{cm/s}^2$$

$$\begin{aligned}
b_{nl} &= b_1 && \text{for } V_{30} \le \upsilon_1 \\
b_{nl} &= (b_1\text{-}b_2)\ln(V_{30}/\upsilon_2)/\ln(\upsilon_1/\upsilon_2) + b_2 && \text{for } \upsilon_1 < V_{30} < \upsilon_2 \\
b_{nl} &= b_2\ln(V_{30}/V_{ref})/\ln(\upsilon_2/V_{ref}) && \text{for } \upsilon_2 < V_{30} < V_{ref} \\
b_{nl} &= 0.0 && \text{for } V_{30} > V_{ref}
\end{aligned}$$

Where :

V_{30} is the soil shear-wave velocity in the upper 30m; pgaBC is the predicted value of PGA for V_{30} = 760m/sec; and V_{ref} = 760 m/sec (limit between site-class B and C), υ_2 = 300 m/sec (limit for site-class D) and υ_1 = 180 m/sec (limit for site-class E).

Table-A IV-1 Coefficients of for the equation for predicting ground motion acceleration at a particular period for (V_{30} = 760 m/sec) at 5% damping.

Period	c_1	c_2	c_3	c_4	c_5
(sec)					
5.00	-4.58E+00	1.58E+00	-8.07E-02	-2.53E+00	2.22E-01
4.00	-5.26E+00	1.79E+00	-9.79E-02	-2.44E+00	2.07E-01
3.13	-5.59E+00	1.97E+00	-1.14E-01	-2.33E+00	1.91E-01
2.50	-5.80E+00	2.13E+00	-1.28E-01	-2.26E+00	1.79E-01
2.00	-5.85E+00	2.23E+00	-1.39E-01	-2.20E+00	1.69E-01
1.59	-5.75E+00	2.29E+00	-1.45E-01	-2.13E+00	1.58E-01
1.25	-5.49E+00	2.29E+00	-1.48E-01	-2.08E+00	1.50E-01
1.00	-5.06E+00	2.23E+00	-1.45E-01	-2.03E+00	1.41E-01
0.794	-4.45E+00	2.12E+00	-1.39E-01	-2.01E+00	1.36E-01
0.629	-3.75E+00	1.97E+00	-1.29E-01	-2.00E+00	1.31E-01
0.500	-3.01E+00	1.80E+00	-1.18E-01	-1.98E+00	1.27E-01
0.397	-2.28E+00	1.63E+00	-1.05E-01	-1.97E+00	1.23E-01
0.315	-1.56E+00	1.46E+00	-9.31E-02	-1.98E+00	1.21E-01
0.251	-8.76E-01	1.29E+00	-8.19E-02	-2.01E+00	1.23E-01
0.199	-3.06E-01	1.16E+00	-7.21E-02	-2.04E+00	1.22E-01
0.158	1.19E-01	1.06E+00	-6.47E-02	-2.05E+00	1.19E-01
0.125	5.36E-01	9.65E-01	-5.84E-02	-2.11E+00	1.21E-01
0.100	7.82E-01	9.24E-01	-5.56E-02	-2.17E+00	1.19E-01
0.079	9.67E-01	9.03E-01	-5.48E-02	-2.25E+00	1.22E-01
0.063	1.11E+00	8.88E-01	-5.39E-02	-2.33E+00	1.23E-01
0.050	1.21E+00	8.83E-01	-5.44E-02	-2.44E+00	1.30E-01
0.040	1.26E+00	8.79E-01	-5.52E-02	-2.54E+00	1.39E-01
0.031	1.19E+00	8.88E-01	-5.64E-02	-2.58E+00	1.45E-01
0.025	1.05E+00	9.03E-01	-5.77E-02	-2.57E+00	1.48E-01
PGA	5.23E-01	9.69E-01	-6.20E-02	-2.44E+00	1.47E-01

Table-A IV-1 Continued.

Period	c_6	c_7	c_8	c_9	c_{10}
(sec)					
5.00	-1.43E+00	1.36E-01	6.34E-01	-1.41E-01	-1.61E-04
4.00	-1.31E+00	1.21E-01	7.34E-01	-1.56E-01	-1.96E-04
3.13	-1.20E+00	1.10E-01	8.45E-01	-1.72E-01	-2.45E-04
2.50	-1.12E+00	9.54E-02	8.91E-01	-1.80E-01	-2.60E-04
2.00	-1.04E+00	8.00E-02	8.67E-01	-1.79E-01	-2.86E-04
1.59	-9.57E-01	6.76E-02	8.67E-01	-1.79E-01	-3.43E-04
1.25	-9.00E-01	5.79E-02	8.21E-01	-1.72E-01	-4.07E-04
1.00	-8.74E-01	5.41E-02	7.92E-01	-1.70E-01	-4.89E-04
0.794	-8.58E-01	4.98E-02	7.08E-01	-1.59E-01	-5.75E-04
0.629	-8.42E-01	4.82E-02	6.77E-01	-1.56E-01	-6.76E-04
0.500	-8.47E-01	4.70E-02	6.67E-01	-1.55E-01	-7.68E-04
0.397	-8.88E-01	5.03E-02	6.84E-01	-1.58E-01	-8.59E-04
0.315	-9.47E-01	5.58E-02	6.50E-01	-1.56E-01	-9.55E-04
0.251	-1.03E+00	6.34E-02	5.81E-01	-1.49E-01	-1.05E-03
0.199	-1.15E+00	7.38E-02	5.08E-01	-1.43E-01	-1.14E-03
0.158	-1.36E+00	9.16E-02	5.16E-01	-1.50E-01	-1.18E-03
0.125	-1.67E+00	1.16E-01	3.43E-01	-1.32E-01	-1.13E-03
0.100	-2.10E+00	1.48E-01	2.85E-01	-1.32E-01	-9.90E-04
0.079	-2.53E+00	1.78E-01	1.00E-01	-1.15E-01	-7.72E-04
0.063	-2.88E+00	2.01E-01	-3.19E-02	-1.07E-01	-5.48E-04
0.050	-3.04E+00	2.13E-01	-2.10E-01	-9.00E-02	-4.15E-04
0.040	-2.99E+00	2.16E-01	-3.91E-01	-6.75E-02	-3.88E-04
0.031	-2.84E+00	2.12E-01	-4.37E-01	-5.87E-02	-4.33E-05
0.025	-2.65E+00	2.07E-01	-4.08E-01	-5.77E-02	-5.12E-05
PGA	-2.34E+00	1.91E-01	-8.70E-02	-8.29E-02	-6.30E-04

Table-A IV-2 Coefficients of site response.

Period	$\mathbf{b_{lin}}$	$\mathbf{b_1}$	$\mathbf{b_2}$
(sec)			
5.00	-0.752	-0.300	0.000
4.00	-0.745	-0.310	0.000
3.13	-0.740	-0.330	0.000
2.50	-0.735	-0.357	0.000
2.00	-0.730	-0.375	0.000
1.59	-0.726	-0.395	0.000
1.25	-0.738	-0.420	0.000
1.00	-0.700	-0.440	0.000
0.794	-0.690	-0.465	-0.002
0.629	-0.670	-0.480	-0.031
0.500	-0.600	-0.495	-0.060
0.397	-0.500	-0.508	-0.095
0.315	-0.445	-0.513	-0.130
0.251	-0.390	-0.518	-0.160
0.199	-0.306	-0.521	-0.185
0.158	-0.280	-0.528	-0.185
0.125	-0.260	-0.560	-0.140
0.100	-0.250	-0.595	-0.132
0.079	-0.232	-0.637	-0.117
0.063	-0.249	-0.642	-0.105
0.050	-0.286	-0.643	-0.105
0.040	-0.314	-0.609	-0.105
0.031	-0.322	-0.618	-0.108
0.025	-0.330	-0.624	-0.115
PGA	-0.361	-0.641	-0.144

APPENDIX V

COMPARISON WITH HAZUS SOFTWARE

The procedure presented in APPENDIX-I showed similar results when compared to the procedure implemented in HAZUS software tool for a ground motion input of Sa(0.3s)=0.38g and Sa(1.0s)=0.07g. The comparison of probability of structural damage is conducted for four building classes: URML_Precode, S2L_Precode, W1L_Precode and S1L_Precode. The results are summarized in Table-A V-1. Figures A-V-1 to A-V-8 presents the damage prediction using the fragility functions developed using the procedure proposed in this study and the results from HAZUS software.

Table-A V-1 Comparison of probability of damage with HAZUS software.

	URMBL_Precode		**S2L_Precode**		**W1L_Precode**		**S1L_Precode**	
Probability [%]	Fragility functions	HAZUS software	Fragility functions	HAZUS software	Fragility functions	HAZUS software	Fragility functions	HAZUS software
None	64	66	86	87	79	79	89	84
Slight	19	18	9	9	16	16	8	13
Moderate	13	12	5	5	5	4	3	3
Extensive	4	3	0	0	0	0	0	0
Complete	1	1	0	0	0	0	0	0

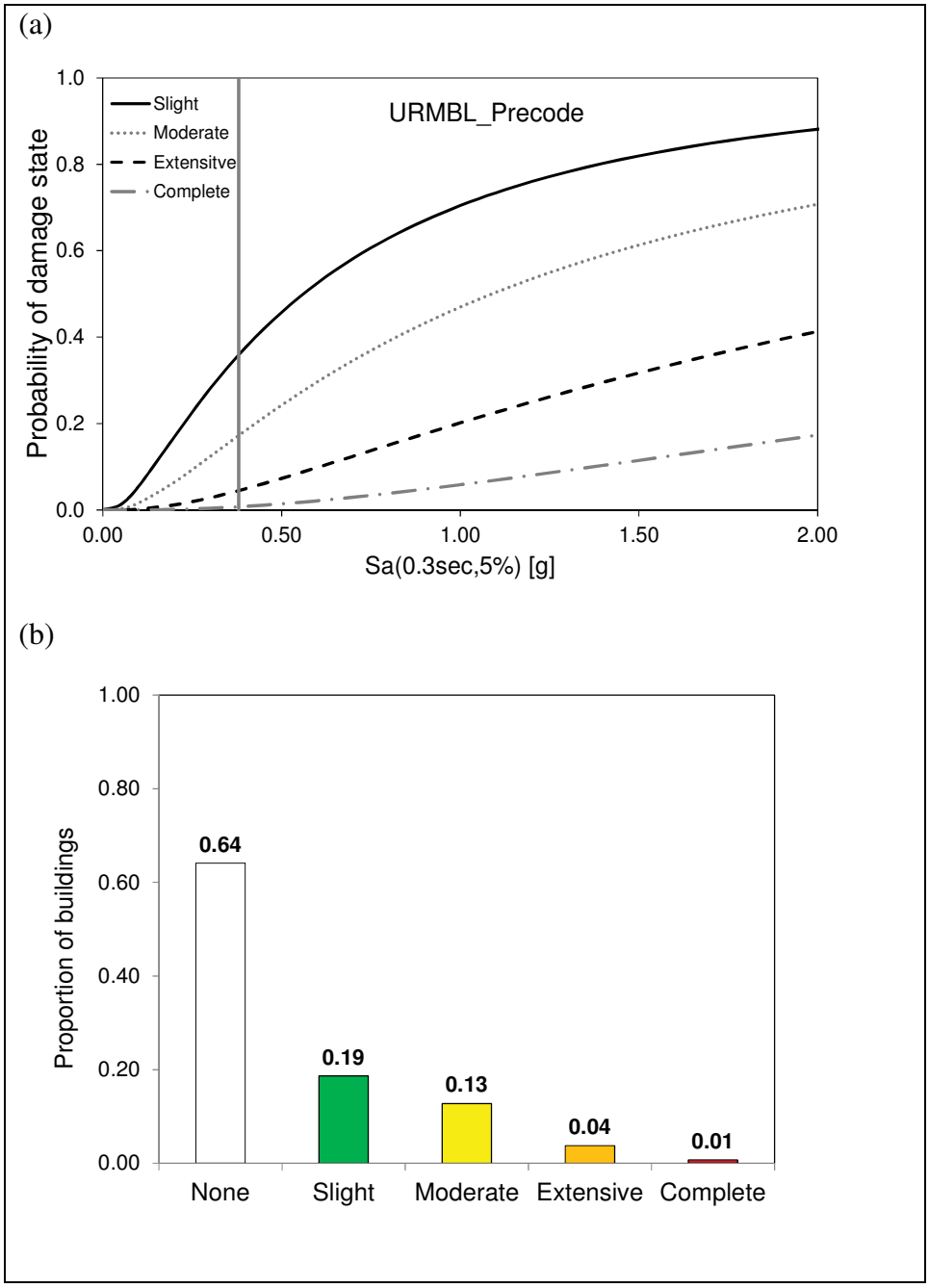

Figure-A V-1 Illustration of damage assessment using the procedure in this study: (a) fragility functions for URMBL-Precode building class and (b) the predicted damage proportions at Sa(0.3sec,5%)=0.38g.

HAZUS AEBM- Individual Building Report

7/20/2012

Building Information

Id Number:	US000014
Building Name:	24041001085_4_RES1_URML
Address:	Address
Latitude / Longitude:	45.61/-71.32
Building Profile:	4_RES1_URML_PC

Ground Motion

SA @ 0.3 seconds (g) :	0.38
SA @ 1.0 seconds (g) :	0.07
PGA (g) :	1.00
Soil Type :	Very Dense Soil and Soft Rock

Building Intersection Points

Displacement (in) :	0.20
Acceleration (g) :	0.58

Building Damage

Damage State	Damage State Probabilities (%)		
	Structural	Non-Structural Drift	Non-Structural Acceleration
None	66.0	79.0	6.0
Slight	18.0	12.0	22
Moderate	12.0	7.0	41
Extensive	3.0	1.0	25
Complete	1.0	1.0	6

Figure-A V-2 HAZUS software damage prediction at Sa(0.3sec,5%)=0.38g for the URML_Precode building class.

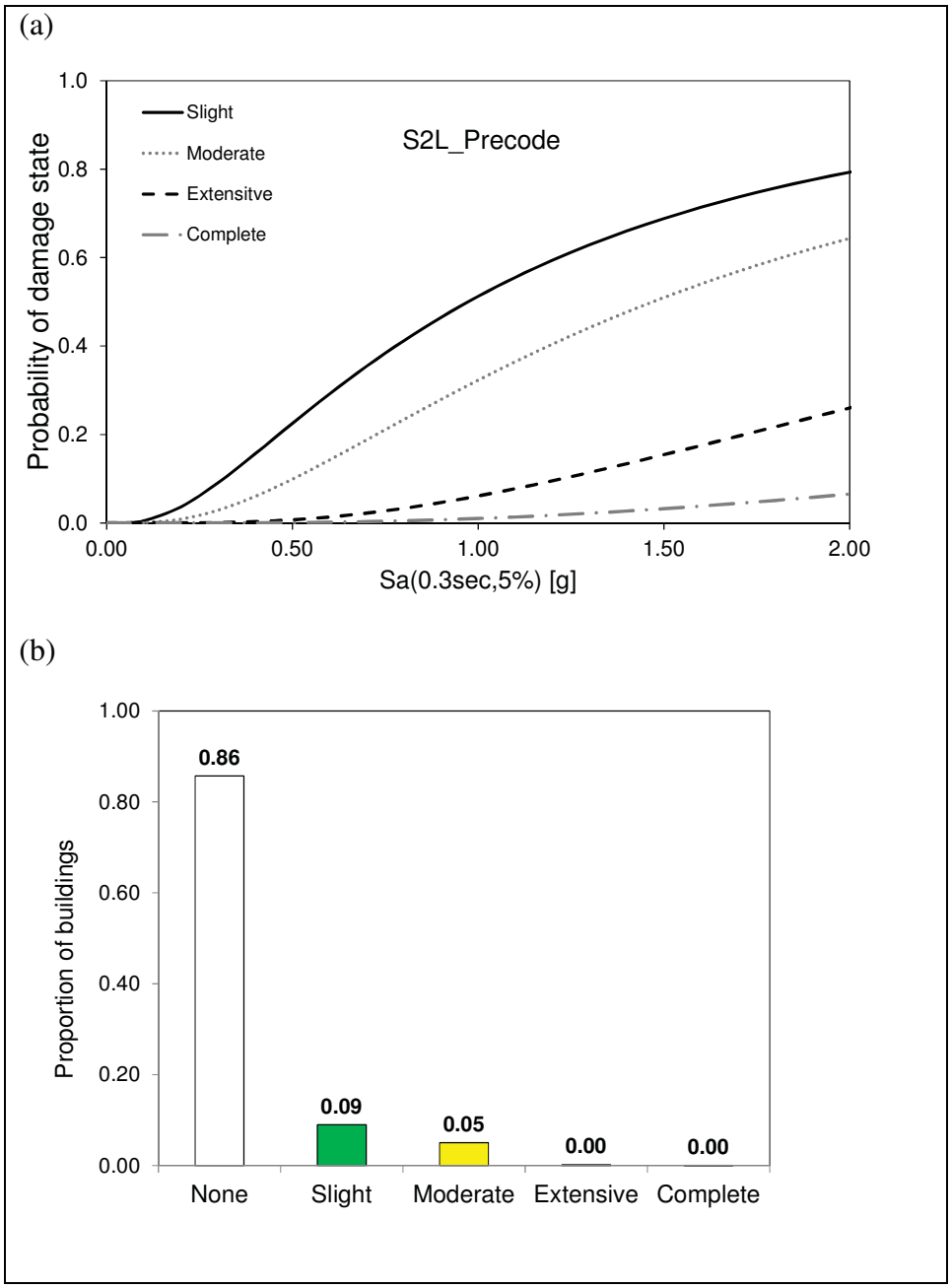

Figure-A V-3 Illustration of damage assessment using the procedure in this study: (a) fragility functions for S2L-Precode building class and (b) the predicted damage proportions at Sa(0.3sec,5%)=0.38g.

HAZUS AEBM- Individual Building Report

7/20/2012

Building Information

Id Number:	US000026
Building Name:	24041001085_7_RES1_S2L_F
Address:	Address
Latitude / Longitude:	45.61/-71.32
Building Profile:	7_RES1_S2L_PC

Ground Motion

SA @ 0.3 seconds (g) :	0.38
SA @ 1.0 seconds (g) :	0.07
PGA (g) :	1.00
Soil Type :	Very Dense Soil and Soft Rock

Building Intersection Points

Displacement (in) :	0.28
Acceleration (g) :	0.57

Building Damage

Damage State	Damage State Probabilities (%)		
	Structural	Non-Structural Drift	Non-Structural Acceleration
None	87.0	86.0	5.0
Slight	9.0	11.0	25
Moderate	5.0	3.0	39
Extensive	0.0	0.0	24
Complete	0.0	0.0	6

Figure-A V-4 HAZUS software damage prediction at Sa(0.3sec,5%)=0.38g for the S2L_Precode building class.

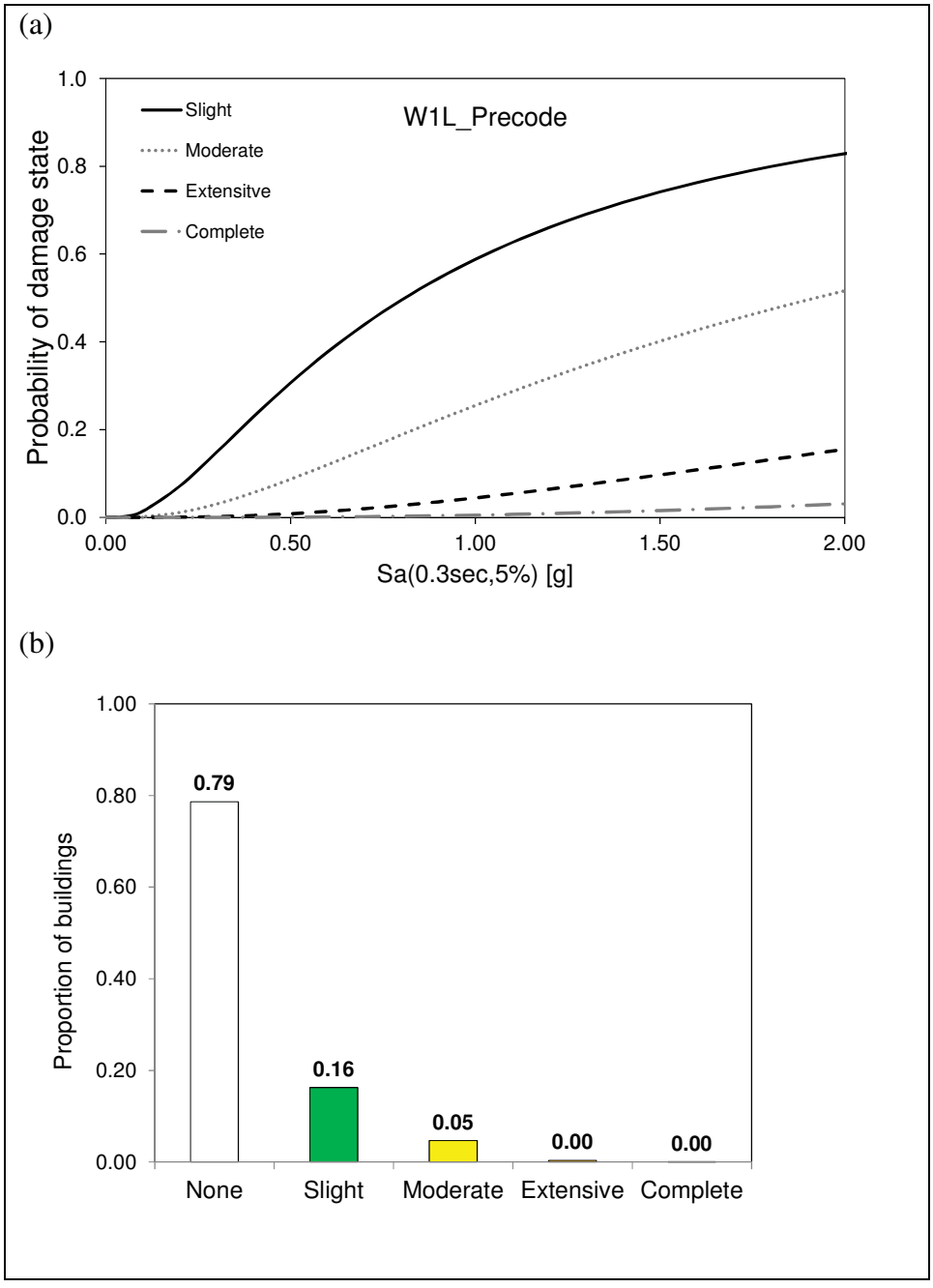

Figure-A V-5 Illustration of damage assessment using the procedure in this study: (a) fragility functions for W1L-Precode building class and (b) the predicted damage proportions at Sa(0.3sec,5%)=0.38g.

HAZUS AEBM- Individual Building Report

7/20/2012

Building Information

Id Number:	US000017
Building Name:	24041001085_5_RES1_W1_P
Address:	Address
Latitude / Longitude:	45.61/-71.32
Building Profile:	5_RES1_W1_PC

Ground Motion

SA @ 0.3 seconds (g) :	0.38
SA @ 1.0 seconds (g) :	0.07
PGA (g) :	1.00
Soil Type :	Very Dense Soil and Soft Rock

Building Intersection Points

Displacement (in) :	0.17
Acceleration (g) :	0.57

Building Damage

Damage State	Damage State Probabilities (%)		
	Structural	Non-Structural Drift	Non-Structural Acceleration
None	79.0	84.0	7.0
Slight	16.0	11.0	23
Moderate	4.0	5.0	39
Extensive	0.0	0.0	25
Complete	0.0	0.0	6

Figure-A V-6 HAZUS software damage prediction at Sa(0.3sec,5%)=0.38g for the W1L_Precode building class.

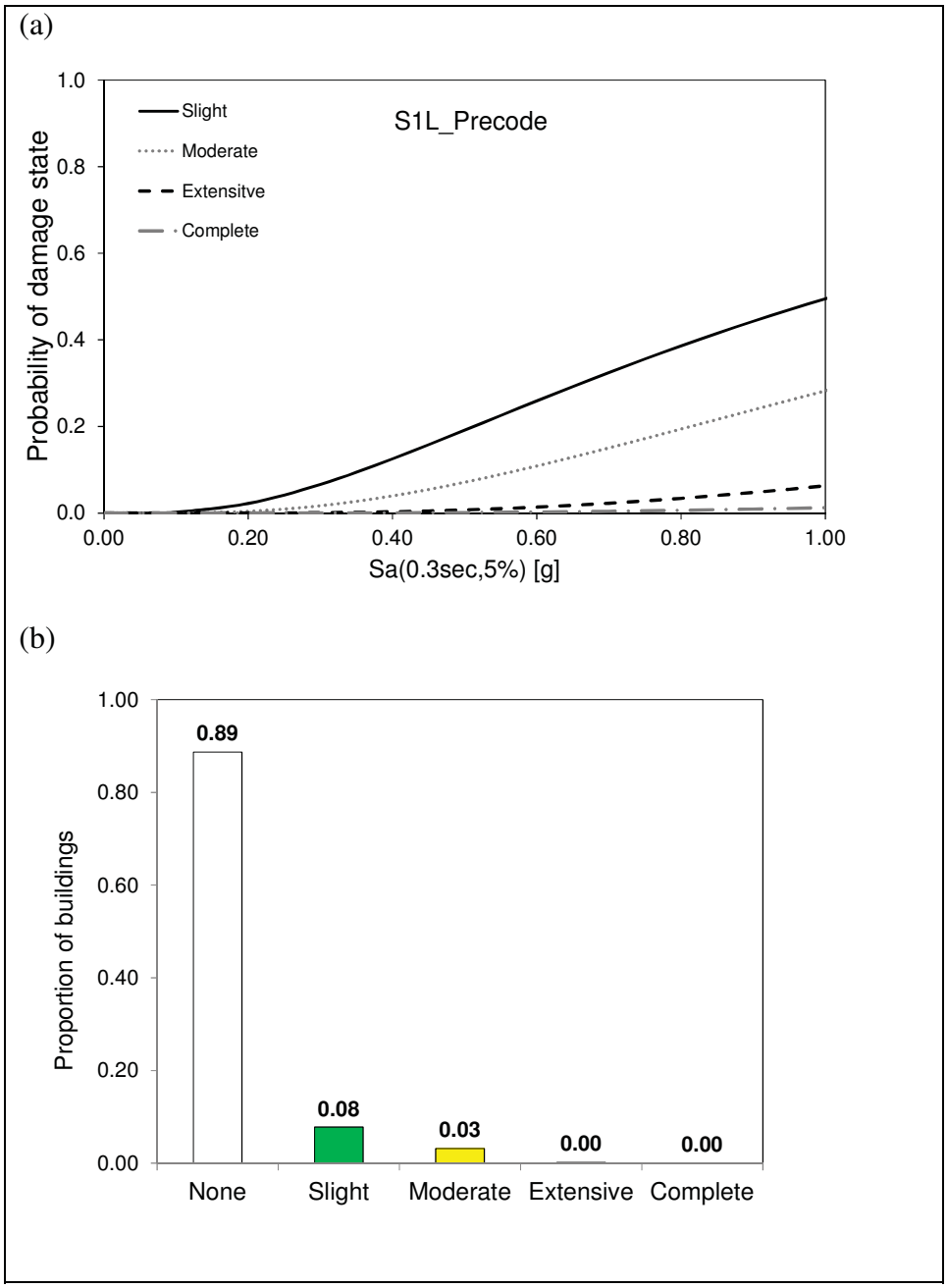

Figure-A V-7 Illustration of damage assessment using the procedure in this study: (a) fragility functions for S1L-Precode building class and (b) the predicted damage proportions at Sa(0.3sec,5%)=0.38g.

HAZUS AEBM- Individual Building Report

7/20/2012

Building Information

Id Number:	US000022
Building Name:	24041001085_6_RES1_S1L_P
Address:	Address
Latitude / Longitude:	45.61/-71.32
Building Profile:	6_RES1_S1L_PC

Ground Motion

SA @ 0.3 seconds (g) :	0.38
SA @ 1.0 seconds (g) :	0.07
PGA (g) :	1.00
Soil Type :	Very Dense Soil and Soft Rock

Building Intersection Points

Displacement (in) :	0.36
Acceleration (g) :	0.55

Building Damage

Damage State	Damage State Probabilities (%)		
	Structural	Non-Structural Drift	Non-Structural Acceleration
None	90.0	84.0	6.0
Slight	7.0	13.0	26
Moderate	3.0	3.0	39
Extensive	0.0	0.0	23
Complete	0.0	0.0	6

Figure-A V-8 HAZUS software damage prediction at Sa(0.3sec,5%)=0.38g for the S1L_Precode building class.

LIST OF BIBLIOGRAPHICAL REFERENCES

Abo-El-Ezz A., M.J. Nollet and M. Nastev. 2011a. « Analytical displacement-based seismic fragility analysis of stone masonry buildings». *Proceedings of the 3rd International Conference on Computational Methods in Structural Dynamics and Earthquake Engineering,* Corfu, Greece*., Paper No.679.*

Abo-El-Ezz A., M.J. Nollet and M. Nastev. 2011b. « Characterization of historic stone masonry buildings for seismic risk assessment: a case study at Old Quebec City ». *Proceedings of the Canadian Society of Civil Engineering General Conference,* Ottawa, Canada. Paper No. GC-223.

Abo-El-Ezz A., M.J. Nollet and M. Nastev. 2012a. « Development of seismic hazard compatible vulnerability functions for stone masonry buildings». *Proceedings of the Canadian Society of Civil Engineering 3rd Structural Specialty Conference,* Edmonton, Canada., Paper No. STR-1030.

Abo-El-Ezz A., M.J. Nollet and M. Nastev. 2012b. « Regional seismic risk assessment of existing building at Old Quebec City, Canada ». *Proceedings of the 15th World Conference on Earthquake Engineering,* Lisbon, Portugal, Paper No. 1543.

Abo-El-Ezz A., M.J. Nollet and M. Nastev. 2013a. « Seismic fragility assessment of low-rise stone masonry buildings ». *Journal of Earthquake Engineering and Engineering Vibrations*,Vol.12 No.1, 2013

Abo-El-Ezz A., M.J. Nollet and M. Nastev. 2013b. « A methodology for rapid earthquake damage assessment of existing buildings ». Accepted for publication in the proceedings of the *3rd Specialty Conference on Disaster Prevention and Mitigation*, *CSCE*, Montreal, Paper. No. DIS-16.

Adams, J., and S. Halchuk. 2003. *Fourth generation seismic hazard maps of Canada: Values for over 650* Canadian *localities intended for the 2005 National Building Code of Canada.* Geological Survey of Canada Open File, vol. 4459, p. 1-155.

Akkar, S., H. Sucuoğlu and A. Yakut. 2005. « Displacement-based fragility functions for low-and mid-rise ordinary concrete buildings ». *Earthquake Spectra,* vol. 21, p. 901.

ASCE. 2007. *Seismic rehabilitation of existing building*. ASCE Standard no. ASCE/SEI 41-06, American Society of Civil Engineers, USA.

ATC. 1996. *ATC-20, Procedures for Post-earthquake Safety Evaluation of Buildings*. Applied Technology Council, Redwood City, CA, USA.

ATC. 1996. *ATC-40, Seismic evaluation and retrofit of concrete buildings*, Vol. 1, Applied Technology Council, Redwood City, CA, USA.

Atkinson, G. M., and D. M. Boore. 2006. « Earthquake ground-motion prediction equations for eastern North America ». *Bulletin of the Seismological Society of America,* vol. 96, n° 6, p. 2181-205.

Barron-Corverra R. 2000. « Spectral Evaluation of Seismic Fragility in Structures » PhD Thesis, University at Buffalo, The State University of New York, Buffalo, USA.

Benedetti, D., P. Carydis and P. Pezzoli. 1998. « Shaking table tests on 24 simple masonry buildings ». *Earthquake engineering & structural dynamics,* vol. 27, n° 1, p. 67-90.

Borzi, B., H. Crowley and R. Pinho. 2008. « Simplified pushover-based earthquake loss assessment (SP-BELA) method for masonry buildings ». *International Journal of Architectural Heritage,* vol. 2, n° 4, p. 353-376.

Bosiljkov, V., AW Page, V. Bokan-Bosiljkov and R. Žarnić. 2010. « Evaluation of the seismic performance of brick masonry walls ». *Structural Control and Health Monitoring,* vol. 17, n° 1, p. 100-118.

Bruneau, M. 1994. « State-of-the-art report on seismic performance of unreinforced masonry buildings ». *Journal of Structural Engineering,* vol. 120, n° 1, p. 230-251.

Calderini, C., S. Cattari and S. Lagomarsino. 2009. « In-plane strength of unreinforced masonry piers ». *Earthquake engineering & structural dynamics,* vol. 38, n° 2, p. 243-267.

Calvi, G.M. 1999. « A displacement-based approach for vulnerability evaluation of classes of buildings ». *Journal of Earthquake Engineering,* vol. 3, n° 3, p. 411-438.

Chidiac, SE, S. Foo and MS Cheung. 2000. « Seismic guidelines for stone-masonry components and structures ». In *International Conference on Seismic Performance of Traditional Buildings*. (Turkey), p. 13.

Chopra, A.K., and R.K. Goel. 1999. « Capacity-demand-diagram methods based on inelastic design spectrum ». *Earthquake Spectra,* vol. 15, n° 4, p. 637-656.

Choun, Y.S., and A.S. Elnashai. 2010. « A simplified framework for probabilistic earthquake loss estimation ». *Probabilistic Engineering Mechanics,* vol. 25, n° 4, p. 355-364.

Coburn, A. and R. Spence. 2002. *Earthquake Protection,* 2nd Chichester: John Wiley and Sons.

Crowley, H., J. Bommer, J. Pinho and J. Bird. 2005. « The impact of epistemic uncertainty on an earthquake loss model ». *Earthquake Engineering and Structural Dynamics,* vol. 34, p. 1653–1685.

Crowley, H., R. Pinho and J.J. Bommer. 2004. « A probabilistic displacement-based vulnerability assessment procedure for earthquake loss estimation ». *Bulletin of Earthquake Engineering,* vol. 2, n° 2, p. 173-219.

Elmenshawi, A.E.A., M.S.M. Sorour, A.M.A. Mufti, L.G.J.L.G. Jaeger and N.S.N. Shrive. 2010. « In-plane seismic behaviour of historic stone masonry ». *Canadian Journal of Civil Engineering,* vol. 37, n° 3, p. 465-476.

Erberik, M.A. 2008. « Generation of fragility curves for Turkish masonry buildings considering in-plane failure modes ». *Earthquake engineering & structural dynamics,* vol. 37, n° 3, p. 387-405.

Erberik, M.A., and A.S. Elnashai. 2004. « Fragility analysis of flat-slab structures ». *Engineering Structures,* vol. 26, n° 7, p. 937-948.

Erdik, M., K. Sesetyan, M. Demircioglu, U. Hancilar, C. Zulfikar, E. Cakti, Y. Kamer, C. Yenidogan, C. Tuzun and Z. Cagnan. 2010. « Rapid earthquake hazard and loss assessment for Euro-Mediterranean region ». *Acta Geophysica,* vol. 58, p. 855-892

Fajfar, P. 1999. « Capacity spectrum method based on inelastic demand spectra ». *Earthquake Engineering and Structural Dynamics,* vol. 28, n° 9, p. 979-994.

Fajfar, P. 2000. « A nonlinear analysis method for performance-based seismic design ». *Earthquake Spectra,* vol. 16, n° 3, p. 573-592.

FEMA. 2000. *FEMA 356 Prestandard and Commentary for the Seismic Rehabilitation of Buildings*. United States Federal Emergency Management Agency, Washington, D.C., USA.

FEMA. 2003. *HAZUS-MH MR4: Multi-hazard Loss Estimation Methodology Earthquake Model Technical manual*. Federal Emergency Management Agency, National Institute of Building Science, Washington, D.C, USA.

FEMA. 2005. *Improvement of nonlinear static seismic analysis procedures, Report Number 440.* Federal Emergency Management Agency, Applied Technology Council, Washington D.C., USA.

Frankie T. 2010. « Simulation-based fragility relationships for unreinforced masonry buildings ». Master Thesis, University of Illinois at Urbana Champaign, USA.

Gencturk, Bora, Amr S. Elnashai and Junho Song. 2008. « Fragility Relationships for Populations of Woodframe Structures Based on Inelastic Response ». *Journal of Earthquake Engineering,* vol. 12, n° sup2, p. 119-128.

Giovinazzi S. 2005. «The vulnerability assessment and the damage scenario in seismic risk analysis». PhD Thesis, University of Florence, Italy and Technical University of Braunschweig, Germany.

Goel, R.K. 2011. « Variability and accuracy of target displacement from nonlinear static procedures ». *International Scholarly Research Network Civil Engineering,* Article ID 582426, vol. 2011.

Ingham, J., and M. Griffith. 2011. « Performance of unreinforced masonry buildings during the 2010 Darfield (Christchurch, NZ) earthquake ». *Australian Journal of Structural Engineering,* vol. 11, n° 3, p. 207.

Jeong, S.H., and A.S. Elnashai. 2007. « Probabilistic fragility analysis parameterized by fundamental response quantities ». *Engineering Structures,* vol. 29, n° 6, p. 1238-1251.

Kircher, C.A., A.A. Nassar, O. Kustu and W.T. Holmes. 1997a. « Development of building damage functions for earthquake loss estimation ». *Earthquake Spectra,* vol. 13, n° 4, p. 663-682.

Kircher, C.A., R.K. Reitherman, R.V. Whitman and C. Arnold. 1997b. « Estimation of earthquake losses to buildings ». *Earthquake Spectra,* vol. 13, n° 4, p. 703-720.

Lang, K. 2002. «Seismic Vulnerability of Existing Buildings», Institute of Structural Engineering (IBK), Swiss Federal Institute of technology ETH-Zurich, Report No. 273, Zurich.

Lefebvre, K. 2004. « Caractérisation structurale et évaluation de la vulnérabilité sismique des bâtiments historiques en maçonnerie du Vieux-Montréal». Masters of Science Thesis, Monreal, Ecole de Technologie Superieure.

Lutman and Tomazevic. 2002. World Housing Encyclopedia, housing report, stone masonry house, *Earthquake Engineering Research Institute (EERI) and International Association for Earthquake Engineering (IAEE)*, website: http://www.world-housing.net/whereport1view.php?id=100025.

Magenes, G., and G. M. Calvi. 1997. « In-plane seismic response of brick masonry walls ». *Earthquake engineering & structural dynamics,* vol. 26, n° 11, p. 1091-1112.

Magenes,G., A. Penna, A. Galasco, M. Da Parè. 2010. « In-plane cyclic shear tests of double-leaf stone masonry panels». Proceedings of the *8th International Masonry Conference,* Dresden, Germany.

Mahaney, J.A., T.F. Paret, B.E. Kehoe and S.A. Freeman. 1993. « The capacity spectrum method for evaluating structural response during the Loma Prieta earthquake ». *Proceedings of the 1993 United States National Earthquake Conference*, Memphis, Tennessee. Vol. 2, 501-510.

Mazzon N. 2010. «Influence of grout injection on the dynamic behaviour of stone masonry buildings». PhD Thesis, University of Padova, Italy.

Nollet M.J, Désilets C., Abo-El-Ezz A., and Nastev M., .2012. *Approche méthodologique d'inventaire de bâtiments pour les études de risque sismique en milieu urbain*. Open File, No. 7260, Geological Survey of Canada, Canada.

NRCC. 2010. *National Building Code of Canada 2010,* NBCC 2010. Ottawa, NRCC 47666:

Oropeza, M.C. Michel and P. Lestuzzi. 2010. «Fragility functions for seismic risk in regions with moderate seismicity». *Ninth U.S. National and Tenth Canadian Conference on Earthquake Engineering*, Toronto, Ontario, Canada.

Padgett, J. E., R. Desroches and E. Nilsson. 2010. « Regional Seismic Risk Assessment of Bridge Network in Charleston, South Carolina ». *Journal of Earthquake Engineering,* vol. 14, n^{o} 6, p. 918-933.

Park, J., P. Towashiraporn, J.I. Craig and B.J. Goodno. 2009. « Seismic fragility analysis of low-rise unreinforced masonry structures ». *Engineering Structures,* vol. 31, n^{o} 1, p. 125-137.

Porter, K. 2009. « Cracking an Open Safe: HAZUS Vulnerability Functions in Terms of Structure-Independent Spectral Acceleration ». *Earthquake Spectra,* vol. 25, n^{o} 2, p. 361-378.

Porter, K.A., 2002. Seismic vulnerability. Chapter 21, *Handbook of Earthquake Engineering*, W.F. Chen and C.R. Scawthorn, eds., CRC Press, Boca Raton, FL.

Powell, G. H. 2006. « Static Pushover Methods - Explanation, Comparison and Implementation ». In Proceeding of the 8th U.S. National Conference on Earthquake Engineering. San Francisco, California, USA, Paper No. 1608.

Restrepo-Vélez, LF .2003. «A simplified mechanics-based procedure for the seismic risk assessment of unreinforced masonry buildings». *Individual Study, European School for Advanced Studies in Reduction of Seismic Risk*, University of Pavia, Italy.

Rossetto, T., and A. Elnashai. 2005. « A new analytical procedure for the derivation of displacement-based vulnerability curves for populations of RC structures». *Engineering Structures,* vol. 27, n^{o} 3, p. 397-409.

Rota, M., A. Penna and G. Magenes. 2010. « A methodology for deriving analytical fragility curves for masonry buildings based on stochastic nonlinear analyses ». *Engineering Structures,* vol. 32, n^{o} 5, p. 1312-1323.

Ruiz-Garcia, J., and M. Negrete. 2009. « Drift-based fragility assessment of confined masonry walls in seismic zones ». *Engineering Structures,* vol. 31, n^{o} 1, p. 170-181.

Ruiz-Garcia, J., and E. Miranda. 2007. « Probabilistic estimation of maximum inelastic displacement demands for performance-based design ». *Earthquake engineering & structural dynamics,* vol. 36, n^{o} 9, p. 1235-1254.

Tomaževic, M. 1999. *Earthquake-Resistant Design of Masonry Buildings.* Innovation in Structures and Construction Vol. 1, Imperial College Press, London, UK.

Tomaževič, M., and M. Lutman. 2007. « Heritage Masonry Buildings in Urban Settlements and the Requirements of Eurocodes: Experience of Slovenia ». *International Journal of Architectural Heritage,* vol. 1, n° 1, p. 108-130.

Tomazevic, M., and P. Weiss. 2010. « Displacement capacity of masonry buildings as a basis for the assessment of behavior factor: an experimental study ». *Bulletin of Earthquake Engineering,* vol. 8, n° 6, p. 1267-1294.

Turnsek, V., and F. Cacovic. 1970. « Some experimental results on the strength of brick masonry walls ». In *Proceeding of the 2nd International Brick Masonry Conference*. (Stoke-on-Trent), p. 149–156.

Vallieres, A. 1999. « Processus de transformation typologique du bâti résidentiel dans l'arrondissement historique du Vieux-Québec». Master Thesis. Université Laval, École d'architecture.

Vasconcelos G .2005. « Experimental investigations on the mechanics of stone masonry: Characterization and behaviour of ancient masonry shear walls». *PhD Thesis,* University of Minho, Portugal.

Vasconcelos, G., and PB Lourenço. 2009. « In-plane experimental behavior of stone masonry walls under cyclic loading ». *Journal of Structural Engineering,* vol. 135, p. 1269.

Wen YK, Ellingwood BR and Bracci J .2004. *Vulnerability function framework for consequence-based engineering*. *Project DS-4 Report*, Mid-America Earthquake Center, University of Illinois at Urbana-Champaign, Urbana, IL.

Yucemen, M.S. 2005. « Probabilistic assessment of earthquake insurance rates for Turkey ». *Natural Hazards,* vol. 35, n° 2, p. 291-313.